DRAFT REPORT

# Measurements of VOCs in the SoCAB: Chemical Characterization and Impacts on Potential Ozone and PM Formation

**Final Report Contract No. 20RD002**

**Prepared for the California Air Resources Board and the California Environmental Protection Agency**


Dr. Toshihiro Kuwayama
State of California Air Resources Board
Research Division
P.O. Box 2815
Sacramento, CA 95812
(279) 842-9873

***Principal Investigator:***
**Jessica B. Gilman**
Tropospheric Chemistry Division
NOAA Chemical Sciences Laboratory
325 Broadway R/CSL7
Boulder, CO 80305
Phone: 303-578-0423
E-mail: Jessica.Gilman@noaa.gov


***Prepared on:***
30 October 2023

## DISCLAIMER

The statements and conclusions in the Report are those of the contractor and not necessarily those of the California Air Resources Board. The mention of commercial products, their source, or their use in connection with material reporter herein is not to be construed as actual of implied endorsement of such products.

## ACKNOWLEDGEMENTS

We acknowledge Chelsea Stockwell, Aaron Lamplugh, Jeffery Peischl, Matthew Coggon, Carsten Warneke, Mike Robinson, Patrick Veres, Andy Neuman, Kristen Zuraski, Lu Xu, Brian McDonald, and Steven S. Brown from the NOAA Chemical Laboratory for their tireless work in the field to provide critical measurements presented here and for their feedback and contributions to this report.

We are incredibly grateful for the support from Paul Wennberg, John Seinfeld, John Crounse, Benjamin Schulze, Christopher Kenseth, and Ryan Ward at the California Institute of Technology for coordinating the setup and logistics for the Pasadena ground site, data management server, and measurements they provided. This project would not have been as successful without their incredible efforts.

Lastly, we would like to thank our collaborators at the California Air Resources Board, including Shang Liu and Toshihiro Kuwayama, for providing critical measurements used in this analysis and for helping oversee all aspects of this proposal and report.

This Report was submitted in fulfillment of CARB contract number **20RD002** "*Measurements of VOC in SoCAB: Chemical Characterization and Impacts on Potential Ozone and PM Formation*" under the partial sponsorship of the California Air Resources Board. Work was completed as of 2024-xx-xx.

# TABLE OF CONTENTS

# LIST OF FIGURES

# LIST OF TABLES

## ABSTRACT

Air quality in the South Coast Air Basin has greatly improved over the last few decades, but these gains have slowed over the last few years. As transportation emissions have declined, the relative importance of other emissions sources has increased. For example, Mc Donald et al. [2018] identified emissions of volatile organic compounds (VOCs) from volatile chemical product usage (paints, solvents, coatings, adhesives, cleaning and personal care products, etc.) as the largest source of petrochemical emissions in the Los Angeles Basin. VCPs were found to be a larger potential source of ozone and particle formation compared to other fossil sources. In summer 2021, NOAA's Chemical Sciences Laboratory and colleagues deployed a full complement of advanced scientific instrumentation in Pasadena, California as part of the Re-evaluating the Chemistry of Air Pollutants in California (RECAP-CA) campaign in an effort to characterize the chemical, temporal and spatial variability of emissions and chemistry across the basin.

Here we identify the anthropogenic VOC source signatures of emissions from VCPs, cooking, and natural gas usage; naturally occurring biogenic emissions; and the secondary production of oxygen- and nitrogen-containing VOCs and ozone. We have determined emission ratios of 70 species, which compared well with previous datasets collected in Pasadena in 2010 and 2020 during the COVID pandemic. This analysis highlights the large emissions of ethanol, methanol, and acetone consistent with VCP usage and an increased emission of ethane from natural gas sources. Oxygenated and biogenic VOCs are the largest contributors to potential ozone formation while aromatics were identified as the most likely contributors to secondary aerosol formation. Results from this project will help inform the development of effective regulatory policies for future State Implementation Plans (SIP) and $O_3$ and PM reduction strategies.

# EXECUTIVE SUMMARY

Air quality has greatly improved in the South Coast Air Basin (SoCAB) over the last half-century; however, gains in air quality improvement have slowed over the last decade as evidenced by a stagnation in ozone design values for the South Coast Air Basin that remain well above the National Ambient Air Quality Standard. Ozone and secondary organic aerosol, an important source of $PM_{2.5}$, are criteria pollutants that are formed in the atmosphere from reactions involving a complex mixture of organic gases, nitrogen oxides, and other oxidants often mediated by sunlight. It is important to identify and characterize modern emission sources of volatile organic compounds (VOCs) in order to effectively mitigate air pollution and safeguard human health.

Measurements made by NOAA's Chemical Sciences Laboratory and colleagues during the California Nexus on Air Quality and Climate (CalNex) campaign Pasadena in 2010 enabled critical evaluation of emissions inventories and improved our understanding of urban chemistry. From this seminal dataset, Mc Donald et al. [2018] identified volatile chemical products (VCPs, e.g., paints, coatings, fragrances, cleaning products, personal care products, etc.) as the largest petrochemical source of VOCs in Los Angeles. Advances in scientific instrumentation and our understanding of the role of VCPs in the urban atmosphere have greatly improved in the intervening years prompting a keen interest in revisiting Los Angeles nearly a decade later to better characterize modern urban emission sources.

Here we present detailed chemical measurements of a full suite of VOCs and trace gases in summer 2021 as part of the Re-evaluating the Chemistry of Air Pollutants in California (RECAP-CA) campaign in an effort to characterize the chemical, temporal and spatial variability of VOC emissions and chemistry across the basin. An array of state-of-the-art instruments installed at a Pasadena ground site provided unparalleled chemical speciation of a full suite of VOCs, methane, and inorganic gases necessary to measure emissions and chemistry downwind of the greater Los Angeles metropolitan area. We also utilized the NOAA Mobile Laboratory to conduct ten surveys across the basin in order to investigate the spatial distribution of VOC sources and to target specific emission-rich source sectors.

The objectives of this study were to evaluate all major VOC sources, including volatile chemical products (VCPs), cooking, natural gas usage, biogenic emissions and secondary products in order to fully characterize emission sources and atmospheric chemistry affecting photochemical ozone formation.

Analysis of diel profiles of over one hundred (100) different analytes were used to assess the relative importance of boundary layer dynamics, transport, primary emission source strength, and both the photochemical degradation of reactive precursors and the subsequent formation of secondary products. Overall, oxygenated VOCs were highly abundant and were associated with a wide array of primary and secondary sources. Ethanol and methanol continue to be the most abundant VOCs measured in Pasadena in both 2010 and 2021, and in other urban areas we have studied including New York City, NY, indicating the prevalence of substantial primary emission sources of these species in urban environments. They are not particularly reactive in the atmosphere and thus exempt from current regulatory actions, but they were significant contributors to the VOC reactivity (one metric used to assess the propensity to form ozone) due to their excessive concentrations.

VOCs that routinely had higher daytime mixing ratios (coincident with the hours of peak photochemical formation of ozone and organic aerosol) included natural emissions of isoprene from urban vegetation, and its oxidation products. Photochemical formation of formaldehyde, an air toxic, from reactive oxidation of reactive hydrocarbon precursors including biogenic isoprene and anthropogenic combustion sources dwarfed primary emissions at the Pasadena site. Collectively, these

species were the dominant contributors to OH-reactivity pointing to the outsize role that isoprene and its oxidation products will have on air quality in the Los Angeles Basin.

We have identified several tracers different VCP emission source sectors including, D5-siloxane, a tracer for personal care product usage; para-chlorobenzotrifluride (PCBTF), a useful VCP tracer for solvent-based coatings; and Texanol, a VCP marker for water-based coatings. Emissions of these species in Los Angeles were comparable to other urban areas that we have studied. We did not see evidence of a large source of anthropogenic monoterpenes associated with fragranced VCPs.

Octanal and nonanal were identified as useful tracers for cooking emissions and their correlations with carbon monoxide (CO, a combustion tracer) were leveraged to calculate emission rates in the Los Angeles Basin of 5.6 and 3.2 tons per day for octanal and nonanal, respectively, thus providing critical new information on a previously understudied emission source [Coggon et al., 2023b]. And lastly, benzenenitrile was useful to assess the influence of aged wildfire smoke mixed with urban emissions.

We observed a doubling of the ethane/CO emission ratio compared to CalNex 2010, which is consistent with increased ethane emissions from natural gas usage in the Los Angeles Basin [Wunch et al., 2016]. Mobile lab measurements during RECAP-CA and subsequent airborne measurements in 2023 show that ethane and propane are prevalent throughout the basin with prominent ethane sources occurring near the Port of Long Beach.

The RECAP-CA measurements were used to derive VOC/CO and VOC/ethyne emission ratios for 70 different chemical species. Overall, the RECAP-CA VOC/CO emission ratios were lower compared to 2010 values and were largely consistent with those from 2020 [de Gouw et al., 2017, 2018; Van Rooy et al., 2021]. Notable exceptions include ethane (discussed above), ethyne, and the C7+ alkanes. Ethyne/CO emission ratios were less than 2010, but greater than 2020 values [de Gouw et al., 2017, 2018; Van Rooy et al., 2021]. Van Rooy et al. [2021] posited that a shift from on-road to off-road combustion sources could explain a shift towards lower ethyne/CO emission ratios. Emission ratios for C7+ alkanes were higher compared to both previous datasets. The reason for this is unknown but could be related, in part, to higher ambient temperatures during RECAP-CA implicating an evaporative emission source.

This expansive new dataset will serve as the new foundation to assess emission inventories and chemical models used to understand and predict secondary ozone and aerosol formation in the Los Angeles Basin. Improved understanding of modern emission sources of VOCs and trace gases are critical for California to meet is air quality and climate goals. The results from this project will help inform the development of effective regulatory policies for future State Implementation Plans (SIP) and $O_3$ and PM reduction strategies.

# 1.0 INTRODUCTION

Air quality has greatly improved in the South Coast Air Basin (SoCAB) over the last half-century in spite of a growing population and more vehicle miles driven; however, approximately 55% of the SoCAB does not meet the National Ambient Air Quality Standard (NAAQS) for ozone ($O_3$) for 100 days of the year (*Figure 1*) [CARB, 2013]. $O_3$ and fine particulate matter ($PM_{2.5}$) are criteria air pollutants and are the primary ingredients of urban smog responsible for adverse health effects and diminished visibility. Both $O_3$ and secondary organic aerosol (SOA, a component of $PM_{2.5}$) can be formed in the atmosphere from the interaction of volatile organic compounds (VOCs) and nitrogen oxides ($NO_x$ = NO + $NO_2$) in the presence of oxidants often mediated by sunlight. It is critical to identify and characterize the most important anthropogenic VOC emissions to effectively mitigate air pollution and safeguard human health [McDonald et al. 2018].

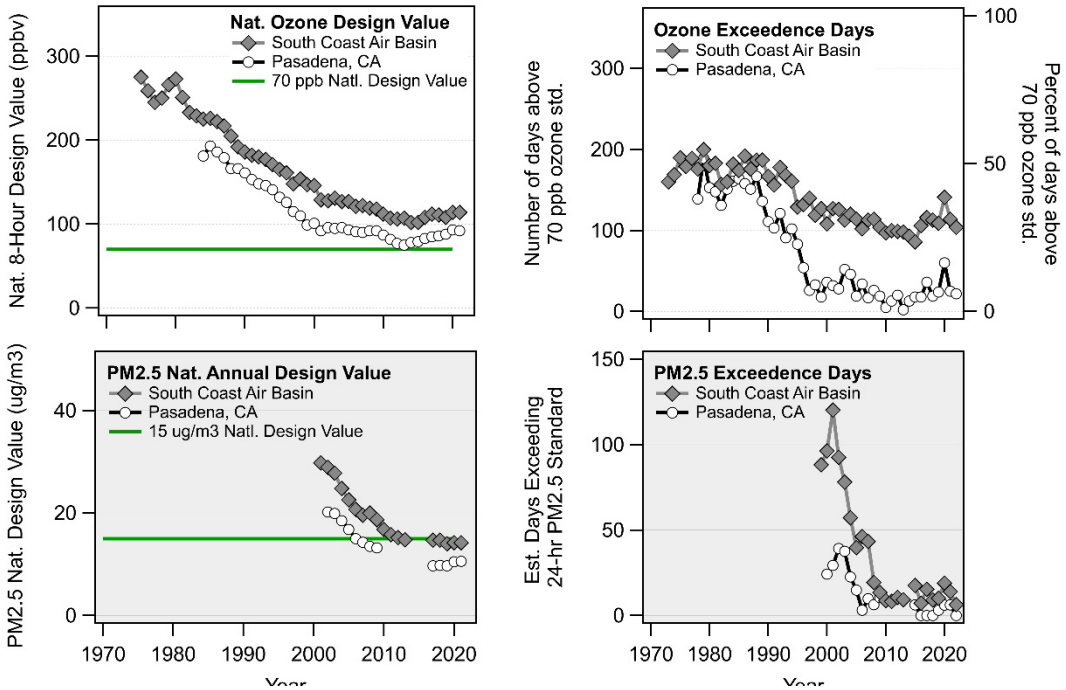


*Figure 1. Ozone and $PM_{2.5}$ trends in the South Coast Air Basin and Pasadena, California*

VOCs are an incredibly diverse chemical family composed of reactive and unreactive organic gases that are ubiquitous throughout Earth's atmosphere. VOCs are directly emitted from natural sources and anthropogenic activities, or they can be secondarily produced in the atmosphere through chemical reactions of precursor VOCs. Urban VOC emissions in megacities around the world, including Los Angeles, have traditionally been dominated by fossil fuel use associated with transportation-related sources [Molina and Molina 2004]. There has been a 50-fold reduction in VOC emissions in Los Angeles since 1960 as the result of advances in emission control technologies and targeted regulatory actions but more recent gains in emission reductions are diminishing [Bishop 2019; CARB 2013; Warneke et al. 2012]. Trends in US $NO_2$ columns observed from space indicate that $NO_x$ emissions were decreasing strongly from 2005-2009 but decreases have slowed from 2011-2015 [Jiang et al. 2018]. With slowing trends in ozone precursors, decreases in ozone design values may have slowed as well (*Figure 1*)[Parrish et al. 2017].

As mobile sources have become cleaner, new sources of pollution such as the use of volatile chemical products (VCPs) like personal care products, cleaning products, coatings, and adhesives are emerging in relative importance. McDonald et al. [2018] showed that VCP emissions in Los Angeles are larger than transportation VOC emissions and could be responsible for as much as half of the VOC reactivity with the hydroxyl radical (OH), a proxy for potential $O_3$ formation, and half of the mass associated with fossil-derived SOA formation - potentially contributing to urban air quality and associated human health effects in a significant way. Subsequent work by Coggon et al. [2021b, 2018b] and Gkatzelis et al. [2021a, 2021b] have identified unique chemical tracers for VCP emission source sectors and have shown that VCP emissions are ubiquitous in urban areas including Boulder, CO; Chicago, IL; New York City, NY; and Toronto, Canada. Modeling of the measured VCP emissions in New York City, shows that VCP emissions are as important to ozone production as fossil fuel VOCs [Coggon et al., 2021b].

McDonald et al. [2018] showed that aldehydes with 5 or more carbon atoms measured in Los Angeles could not be explained by emissions inventories that contain VCPS, fossil fuels, or biogenic sources. Cooking is a source of oxygenated VOCs including aldehydes, ketones, alcohols, and acids [Coggon et al., 2023b; Schauer et al., 1999b]. Numerous studies have shown that cooking is a ubiquitous and important component of aerosol in urban datasets [Hayes et al., 2015; Slowik et al., 2010], but fewer studies have identified the contribution of cooking to VOC emissions [Coggon et al., 2023b; Peng et al., 2022].

In summer 2021, the NOAA Chemical Sciences Laboratory and colleagues deployed a full complement of advanced scientific instrumentation as part of the Re-evaluating the Chemistry of Air Pollutants in California (RECAP-CA) campaign in an effort to characterize traditional and emerging sources of VOC emissions in the Los Angeles Basin in an effort to better understand how these sources will impact the photochemical formation of ozone and organic aerosol. Here we present a detailed analysis of variations in the chemical, temporal, and spatial distributions of VOCs observed at the RECAP-CA stationary site in Pasadena, CA, as well as from the NOAA Mobile Laboratory used to survey emissions and chemical transport across the basin and to target various source-specific sites including restaurant emissions. The results of this study are compared to measurements made during CalNex 2010 (California Nexus of Air Quality and Climate), LAAQS 2020 (Los Angeles Air Quality Study) which took place soon after the COVID-19 pandemic started, and from AEROMMA 2023 (Atmospheric Emissions and Reactions Observed from Megacities to Marine Areas) which included three flights over the Los Angeles Basin. Results from this project will help inform the development of effective regulatory policies for future State Implementation Plans (SIP) and $O_3$ and $PM_{2.5}$ reduction strategies.

# 2.0 MATERIALS AND METHODS

The RECAP-CA measurement intensive took place in Pasadena, California, in summer 2021. The measurement sites, measurement platforms, and instrumentation are described here. Since this work focuses on VOCs and their relation to carbon monoxide (CO), we include a detailed discussion of overall instrument performances, data reduction steps, and data quality assurance and control measures for the VOC and CO measurements.

## *2.1 MEASUREMENT SITES AND PLATFORMS*

Locations of the two RECAP-CA measurement sites on the California Institute of Technology (Caltech) campus in Pasadena, California are shown in *Figure 2.* The Pasadena ground site (34.1403 N, 118.1253 W) was centrally located on campus in a gated construction staging area. It is located on the southwest corner of East Del Mar Blvd and South Michigan Ave and is surrounded by small parking lots to the north, west, and south. A partner site at the Ronald and Maxine Linde Laboratory (34.1364 N, 118.1268 W) was located 0.6 km to the south-southwest. A South Coast Air Quality Management District measurement site (AQS ID 060372005, CARB #70088, 34.132 N, -118.127 W) is located 1 km to the south-southwest. This site monitors carbon monoxide (CO), nitrogen dioxide ($NO_2$), ozone ($O_3$), and particulate matter ($PM_{2.5}$). We will make comparisons to the VOC measurements NOAA conducted from May 15-June 15, 2010 as part of the California Research at the Nexus of Air Quality and Climate Change [Ryerson et al., 2013]. The 2010 CalNex measurement site (34.1406 N, 118.1224 W) was located 0.5 km to the east-northeast of the 2021 Pasadena site.

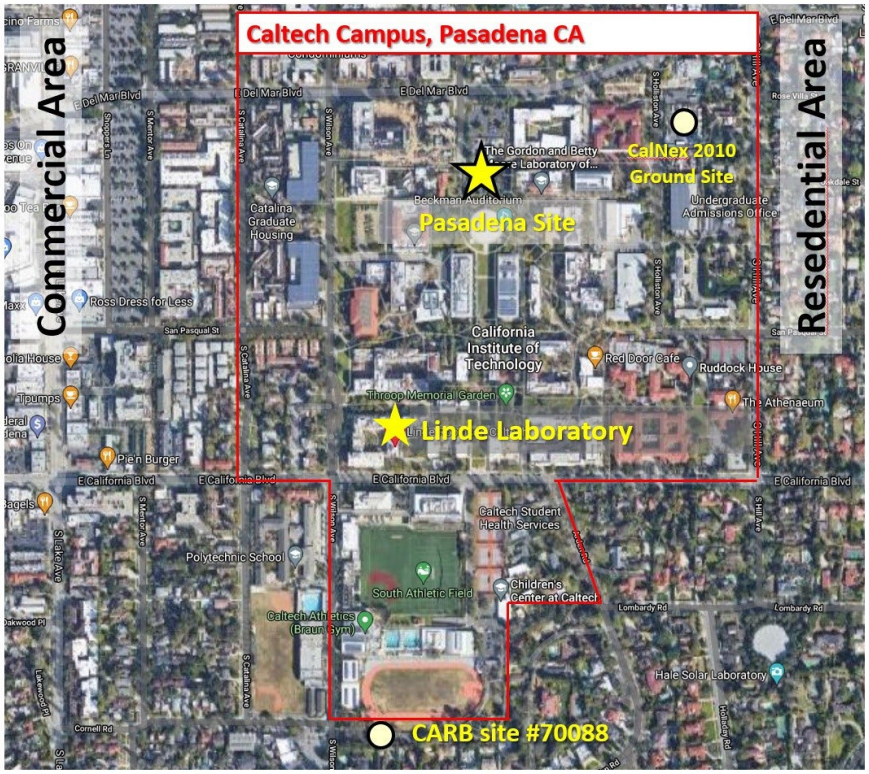


*Figure 2. Google Earth image of Caltech campus with the RECAP-CA measurement sites (stars) and CalNex 2010 and CARB Air Quality measurement sites (circles) for reference.*

Three instrumented trailers, two mobile laboratories, and a 10 m inlet tower were staged at the Pasadena ground site as shown in *Figure 3*.

- The University of California, Davis smog chamber was deployed at the Pasadena site from July 16 to October 31, 2021 in order to investigate ozone sensitivity to NOx and VOCs during RECAP-CA (CARB #19RD012) [Wu et al., *Submitted*].
- The NOAA trailer was installed August 2 to September 7, 2021. This trailer housed the majority of the gas-phase instruments deployed at the Pasadena site, including the NOAA GC-MS instrument.
- The NOAA mobile laboratory was used as both a stationary measurement platform and mobile laboratory. We conducted ten different air quality surveys across the L.A. Basin on August 3-6, 30-31, and September 1-3, 2021. The mobile drive measurements are useful to determine the spatial distribution of VOCs and NOx and to characterize a wide array of local emission sources.
- The CARB mobile laboratory was installed August 5-September 6, 2021 and remained stationary for the duration of the project.
- Two NOAA LIDAR systems were also deployed. These included the stationary Dalek 1 LIDAR (*Figure 3*) and a mobile Micro Doppler Lidar system (PUMAS, *not shown*) that surveyed the greater L.A. Basin.


*Figure 3. Measurement platforms staged at the Pasadena ground site.*

*Table 1. RECAP-CA Instrumentation*

**RECAP-CA ground site measurements at Caltech in Pasadena, CA**

| Instrument Name | Measurement Technique | Reported Species/Parameters | Time Resolution | Instrument PI(s) | Data Status |
|---|---|---|---|---|---|
| **NOAA GC-MS** | In-situ gas chromatography-mass spectrometry | Speciated measurements of VOCs | 4 minute sample preconcentration every 20 minutes | Jessica Gilman, Aaron Lamplugh | R0 |
| **NOAA iWAS** | Improved whole air sampling system with offline analysis by NOAA GC-MS | Speciated measurements of VOCs | 120 second samples filled on-demand | Jessica Gilman, Aaron Lamplugh | R0 |
| **NOAA PTR-ToF-MS** | Proton-transfer reaction high-resolution time-of-flight mass spectrometry | VOC masses | 1 Hz data average to 1-minute | Chelsea Stockwell, Matt Coggon, Carsten Warneke | R1 |
| **NOAA Picarro** | Picarro G2401 wavelength-scanned cavity ring down spectroscopy | CO2, CH4, CO, H2O | 1 Hz data average to 1-minute | Jeff Peischl | R0 |
| **NOAA LGR** | Los Gatos Research infared laser off-axis integrated-cavity-output spectrometry | CO, N2O, H2O | 1 Hz data average to 1-minute | Jeff Peischl | R0 |
| **NOAA Iodide CIMS** | Iodide ion chemical ionization time-of-flight mass spectrometry | ClNO2, HCOOH, HNO2, HNO3, N2O5, Organic Nitrates, PANs | 1 Hz data average to 1-minute | Michael Robinson, Andy Neuman, Patrick Veres | R0 |
| **NOAA NOxCaRD** | Nitrogen Oxides by Cavity Ring Down Spectroscopy | NO, NO2, NOx, NOy, O3, Ox | 1 Hz data average to 1-minute | Kristen Zuraski, Michael Robinson, Jeff Peischl, Steve Brown | R0 |
| **NOAA LIF** | Laser Induced Fluoresence Spectroscopy | NO, NO2 | 1 Hz data average to 1-minute | Andrew Rollins | R0 |
| **NOAA jNO2** | Filter radiometry | jNO2 photolysis rates | 1 Hz data average to 1-minute | Michael Robinson, Aaron Lamplugh | R0 |
| **NOAA LIDAR** | Leosphere 200S Doppler Lidar Dalek01 | Boundary layer height, cloud base height, vertically resolved wind speed and direction from 51-1983 m a.g.l. | 1 profile every 15 minutes | Alan Brewer | R0 |
| **NOAA Met** | Airmar Wx200 | Air Temperature, Relative Humidity, Pressure, surface level Wind Speed and Direction, GPS position | 1 Hz data average to 1-minute | Ken Aikin, Jeff Peischl, Andy Neuman | RA |
| **CARB Picarros** | Picarro G2401, G2307, and G2103 spectrometers | CO2, CH4, CO, H2O, HCHO, NH3 | 1 Hz data average to 1-minute | Shang Liu | RA |
| CARB Aethalometer | Magee Scientific Aethalometer AE33 filter-based optical scanner | Black carbon aerosol | 1 Hz data average to 1-minute | Shang Liu | RA |
| **CARB Met** | Airmar weather | Air Temperature, Relative Humidity, Pressure, Dew Point, surface-level Wind Speed and Direction | 1 Hz data average to 1-minute | Shang Liu | RA |
| Aerodyne HCl | Tuneable infared laser direct absorption spectroscopy | HCl | 1 Hz data average to 1-minute | Scott Herndon, Connor Daube | RA |
| UC Davis Smog Chamber | Three channel portable smog chamber to measure ozone sensitivity to VOC and NOx perurbations | VOC, NOx, O3, O3-sensitivity, Temperature, and RH measurements | 2-hr ambient air collection 10 a.m. to noon each day | Michael Kleeman | Unknown |

**RECAP-CA measurements at Linde Laboratory at Caltech in Pasadena, CA**

| Instrument Name | Measurement Technique | Reported Species | Time Resolution | Instrument PI(s) | Data Status |
|---|---|---|---|---|---|
| CIT AQS | Teledyne T640, T200U, M300EU2, T400, T500U spectrometers | NO, NO2, Noy, O3, CO, PM2.5, PM10, Temperature and Pressure | 1-minute | Paul Wennberg, John Counse | RA |
| **CIT Picarro** | Picarro G2401-m spectrometer | CO2, CO, CH4, H2O | 1-minute | John Seinfeld | RB |
| CIT HF-TOF-AMS | High-resolution time-of-flight aerosol mass spectrometer | submicron non-refractory aerosol composition (Organic, Sulfate, Ammonium, Nitrate, Chloride) | 1 Hz data average to 1-minute | John Seinfeld | R0 |
| CIT Met | Meterological measurements via Vaisala HMP60, Apogee SP-100, and Setra 270 sensors | Air Temperature, Relative Humidity, Pressure, Precipitation, Wind Speed and Direction | 1 Hz data average to 1-minute | Paul Wennberg, John Counse | RA |

## 2.2 MEASUREMENT OVERVIEW

A list of instruments deployed during RECAP-CA are shown in *Table 1*. In this report, we present a comprehensive analysis of the VOC measurements and trace gases including carbon monoxide (CO), carbon dioxide ($CO_2$), methane ($CH_4$), nitrogen oxide (NO), nitrogen dioxide ($NO_2$), and ozone ($O_3$) in order to fully characterize VOC emission sources and the photochemical formation of ozone.

A timeline of the active sampling times for the RECAP-CA measurements is shown in *Figure 4*. We had excellent data coverage for nearly all instruments. The NOAA LIF and Aerodyne HCl instruments were not deployed for the full measurement intensive as they were utilized in other experiments in addition to RECAP-CA. Each of the high-time-resolution measurements reported 1-min averaged data for the ground sites and 1-Hz data for the NOAA Mobile Lab data. The NOAA Lidar reported boundary layer heights every 15 minutes, and the NOAA GC-MS collected 4-minute samples every 20 minutes as described below.

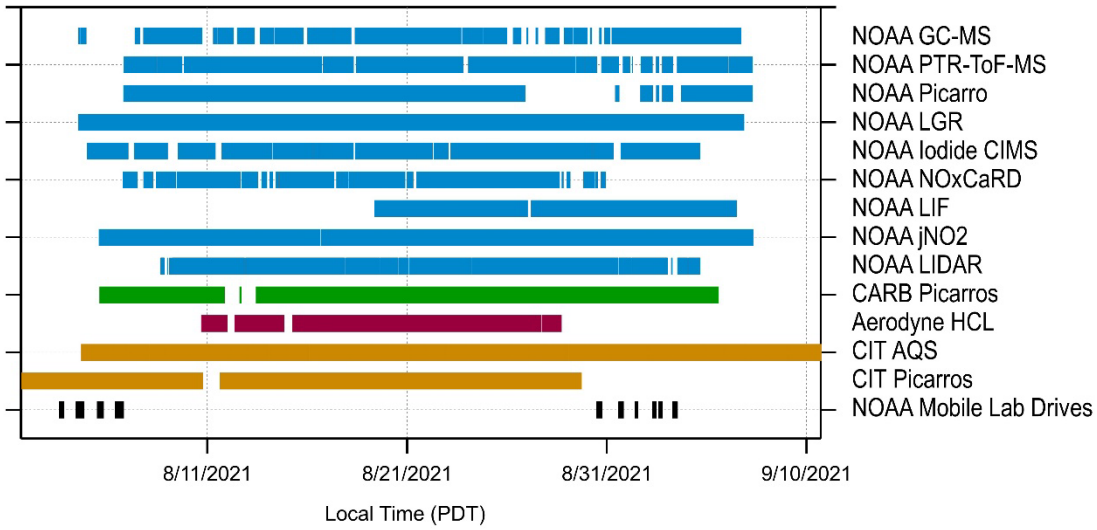


*Figure 4. Active sampling times for RECAP-CA instruments*

## 2.3 NOAA GC-MS

The NOAA GC-MS provides exact chemical speciation of $C_2$-$C_{10}$ hydrocarbons, relatively non-polar oxygenated VOCs, alkyl nitrates, and halocarbons [Lerner et al., 2017]. The instrument setup and performance during the RECAP-CA 2021 experiment is described here. A general instrument schematic is shown in *Figure 5*.

### 2.3.1 GC-MS SAMPLING AND ANALYSIS

A 6-port sample selector valve directs one of five different pressurized samples to the GC-MS sample traps. These sample types include: ambient air, whole air canister samples, a secondary standard used to characterize instrument response of a range of VOCs, ultra-high purity nitrogen to check the system for contamination, or helium carrier gas. This sixth port is capped and used to leak test the GC-MS system.

Ambient air samples:

The ambient air sample inlet was 12m (6.35 mm O.D., 3.96 mm I.D.) perfluoroalkoxy (PFA) polymer tubing. The inlet opening was at the top of a 10 m tower on the south side of the trailer. A Teflon-diaphragm

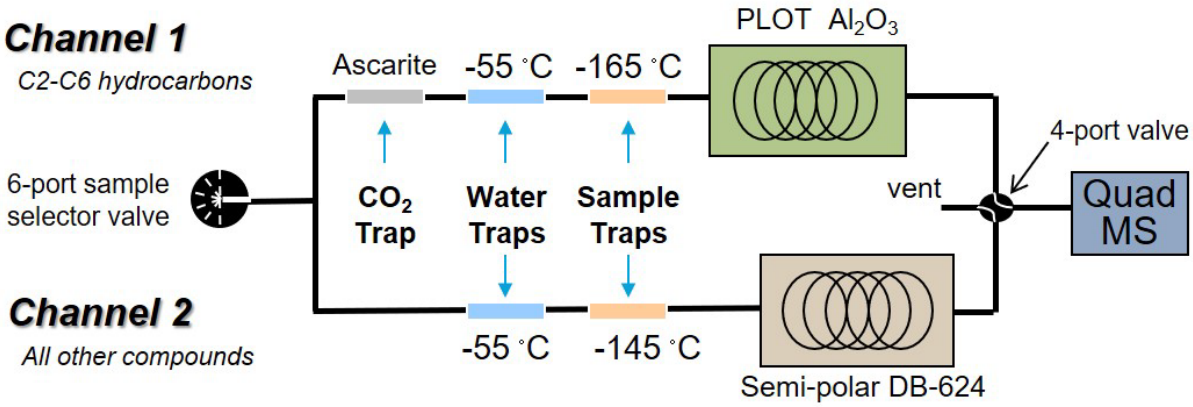


*Figure 5. NOAA GC-MS instrument schematic.*

pump continuously flushes ambient air through the inlet line at a rate of 7 SLPM (standard liters per minute) resulting in an inlet residence time of 5 seconds. A back-pressure regulator on the pump exhaust is used to pressurize the sample stream to 20 psia (0.29 hPa). From this high-volume, continuous flow, a small aliquot of 120 sccm of ambient air is sent through its individual port on the 6-channel sample selector valve to the GC-MS system for analysis. A total of 1845 in-situ ambient air samples were analyzed at the Pasadena ground site.

Whole air samples:

While the GC-MS was primarily set to measure ambient air in-situ at the Pasadena site. A total of 178 whole air samples were collected aboard the NOAA Mobile Laboratory as it drove around the greater Los Angeles Basin. The NOAA whole air samplers are custom-designed, electro-polished, 2.7 L stainless steel canisters that are evacuated and then filled with 10 torr (13.3 hPa) of water vapor as described in Lerner et al. (2017). The WAS inlet consisted of 3 m (1.65 mm I.D.) PFA tubing with an aft-facing inlet port on the roof of the mobile lab. A stainless-steel bellow compressor continuously flushes the inlet line and sampling manifold, which is pressurized to 50 psia (0.7 hPa) via a proportional relief valve upstream of the sample exhaust. The canister valves are electronically controlled by the mobile lab operator for instant, on-demand sampling. For the RECAP-CA experiment, we reduced the pump flow rate down to 3 SLPM in order to purposefully increase the fill time to 50 ± 10 seconds in order to get better overlap with the real-time instruments.

After each drive, the whole air samplers were then installed in the analysis rack inside the NOAA trailer in order to be sampled by the GC-MS. The WAS sampling manifold is evacuated via a diaphragm pump, briefly flushed with humidified UHP nitrogen, then evacuated again to reduce the chance of cross-contamination before each individual canister is analyzed. The pressurized canister sample stream is directed through its individual port on the 6-channel sample selector valve to the GC-MS. Periodically, we collect manifold blanks which consist of the nitrogen stream used to flush the WAS manifold in order to ensure that the manifold and the flush gas are free of major contaminants.

Transfer Standard Samples:

We use a custom blended, secondary standard to characterize the instrument response over relevant timescales. This gas standard consists of 57-component ozone precursor hydrocarbon standard (Scott Specialty Gases) diluted to a nominal mixing ratio of 0.40 ± 0.05 ppbv in UHP nitrogen. We also added six different long-lived halocarbons diluted to atmospheric values. We collected at least one transfer sample

per day, often more if conducting instrument tests or diagnosing instrument issues. A total of 62 transfer standard samples were collected during RECAP-CA over the 35-day sample period. These samples are used to normalize the data as described below.

Calibration Standards:

We employed a total of 13 different multi-component gas mixtures to calibrate the GC-MS and PTR-MS instruments. Prior to initial field deployment, we conducted a quick set of calibrations using 3 of these tanks in order to test initial instrument performance and produce field data. After RECAP-CA, we then conducted more detailed calibrations using all 13 tanks in order to calibrate the largest number of individual VOCs over the observed dynamic ranges and instrument settings used during the RECAP-CA experiment. Since the GC-MS is known to have non-linear sensitivities, we calibrate using at least 5 different setpoints typically ranging from 0.050 to 20 ppbv depending on the tank contents. We use a dynamic dilution system to generate the desired calibration gas mixing ratios in a humidified nitrogen stream and sample using the ambient air sample pump and port. Each setpoint is sampled for several hours to ensure the dilution system is at equilibrium and generate statistically-robust calibrations. These comprehensive calibrations were used to produce the final data.

Sample Pre-concentration:

After the sample selector-valve, the sample stream is plumbed to two separate 10-port chromatography valves that determine the flow paths through each of the two channels of the sampling system.

- Channel one is optimized for the collection and separation of C1-C6 hydrocarbons and halocarbons and consists of three separate traps: a NaOH-coated silica (Ascarite II) trap used to reduce both $CO_2$ and $O_3$ in the sample stream, a water trap to reduce liquid water in the sample stream, and a sample trap to pre-concentrate the targeted gases. The Ascarite traps were changed daily. Separate water traps for both channels consist of 0.5 m length of 0.8 mm (1/32") PFA tubing cooled to -35°C. The channel one sample trap consists of 10 cm of $Al_2O_3$ PLOT column material (0.53 mm ID) cooled to -165°C.
- Channel two is optimized for the collection and separation of C5-C11 hydrocarbons, and simple C1-C8 oxygen-, nitrogen, sulfur-, and halogen-containing gases. The channel two sample trap consists of 10 cm of bare silica column material (0.53 mm ID) cooled to -155°C.

The flow for each channel is set to 60 sccm via separate low delta-P mass flow controllers located downstream of all sample traps. The entire sampling line up to the two 10-port sampling valves is flushed with the sample gas for 90 seconds, then both 10-port valves simultaneously change to the load position. Two 240 mL samples, one for each channel, are simultaneously collected over the 4-minute sampling time and repeats every 20 minutes. After sample collection is complete, the 10-port valves change back to the transfer position so that the permanent gases (e.g., nitrogen and oxygen) can be flushed from the traps by the carrier gas so that the samples can be serially injected onto their respective chromatographic columns for analysis. The water traps are heated and flushed with helium carrier gas in preparation for the next sample collection sequence.

Sample Analysis:

The channel one sample is analyzed first by rapidly heating the tap from -165 to -60 °C in 5 seconds and 2 sccm of UHP helium carrier gas pushes the sample to the channel one column ($Al_2O_3$/KCl PLOT column, 30 m, 0.25 mm ID, 4 um film thickness) which is ramped from 35 to 190°C in 190 seconds. The

column effluent is direct to the mass-selective detector (MSD, Agilent 5975C) by way of a four-port valve. When channel one analysis is nearly complete, we rapidly heat the channel two sample trap from -155 to +40 C in 5 seconds and use 2 sccm of UHP helium carrier gas to push the sample to the channel two column (DB-624, 30 m, 0.25 mm ID). The 4-port valve then changes position to direct the column effluent from channel 2 to the detector. The channel 2 column is ramped from 40 to 180°C in 518 seconds. Both columns are back-flushed with 5 sccm of helium carrier gas, heated, and cooled back down in preparation for the next sample collection sequence.

The MSD detector is a quadrupole mass spectrometer (Agilent 5975C) run in SIM/SCAN mode. In order to increase sensitivity and decrease signal-to-noise, we have programed twenty-three ion windows that selectively monitor 3 to 10 m/z values at specific times in the chromatogram in order to target a wide-ranging, but select group of target analytes. The MSD is tuned when a new detector or filament is installed. Detector response decays slowly with time, so we periodically increase the electron multiplier voltage, but do not re-tune. We use the transfer standard samples and long-lived halocarbons to fully characterize and account for changes in the detector response over time.

### *2.3.2 GC-MS INSTRUMENT PERFORMANCE*

During RECAP-CA, the GC-MS had two separate issues that affected the sample trap temperatures and ultimately the instrument sensitivity for certain analytes. One issue was the result of faulty sample trap electronics which initially failed to maintain constant sample trap injection temperatures at the start of the project. This time period is identified by the "unstable injection temperatures" marker in *Figure 6*. This was rectified in the field by turning off the super capacitors and relying on a different, slightly slower heating cycle that was more stable. Changes in these temperature settings were accounted for in the post-field calibrations. Channel one species (C3-C6 hydrocarbons and halocarbons) were the only analytes affected. The end result was a relatively small increase in the noise (decrease in measurement precision) from 10% to 20% for this short period of time. There was no systemic bias in the measurements. The decrease in measurement precision was dwarfed by the natural ambient variability of these species, such that there was no discernible change in VOC/VOC and VOC/CO ratios except for the longest-live halocarbons which showed greater noise.

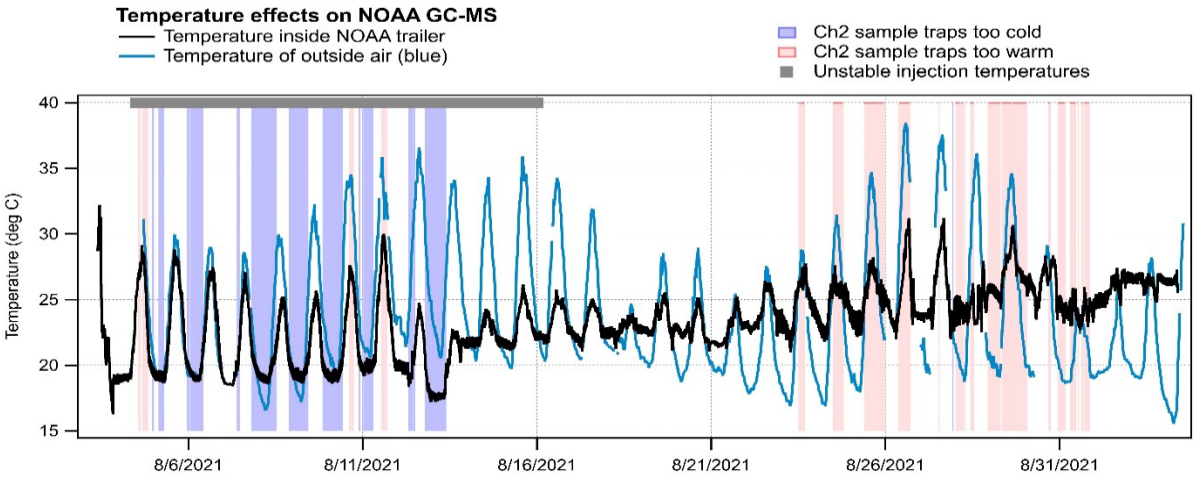


*Figure 6. GC-MS instrument performance timeline*

The second issue related to the temperature inside the NOAA trailer that housed the GC-MS. The trailer could get rather warm during the day and colder at night when the air conditioners could provide enough cooling. Changes in the trailer temperature caused changes in the GC-MS sample trap temperature readings due to a cold-junction on the thermocouples used to monitor and control the trap temperatures. This was evidenced by the appearance of a $CO_2$ peak at the start of the channel 2 chromatogram when the trailer was too cold indicating that the traps were actually colder than their setpoints. This was mitigated by simply increasing the setpoint on the air conditioners overnight. When the trailer was too warm during the daytime, we saw a decrease in the trapping efficiency of the most volatile hydrocarbons and halocarbons on channel 2 but there was no way to mitigate this issue. Since many of the early channel two analytes also elute on channel 1, we simply report channel 1 species instead. For the non-redundant species such as the small oxygenates, we compare our measurements to both the NOAA PTR-MS and NOAA LGR CO measurement to remove any suspect data related to these temperature effects.

Lastly, one of the sample lines connecting the sample trap to the chromatography column on channel two degraded over time such that the chromatography for the C8-C9 aromatics was so significantly degraded that we are unable to report these species and utilize the PTR-MS measurements for this analysis.

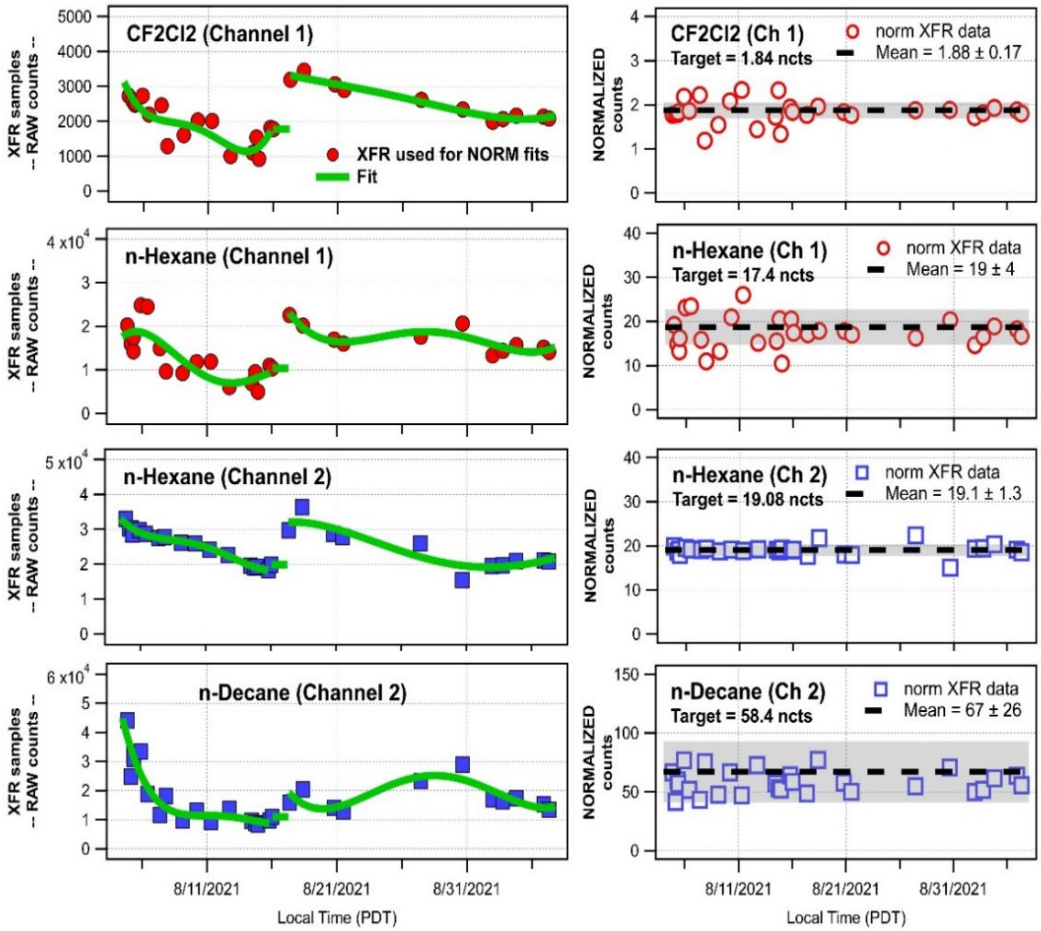


*Figure 7. Example of transfer standard samples (XFR) used to normalize GC-MS data.*

### *2.3.3 GC-MS FINAL DATA*

We use custom software program, TERN [Isaacman-VanWertz et al., 2017], in the Igor Pro (WaveMetrics) platform to reduce all chromatographic peak areas. Raw peak areas are normalized to account for changes in the instrument sensitivity related to the above temperature effects and/or changes in the MSD detector response. A normalization factor is calculated for every analyte in every sample based on the measured and fitted responses of each VOC in the secondary standard (XFR), as shown in *Figure 7*. For analytes that are not in the transfer standard we assign normalization factors based on analytes with similar retention times, chemical functionality, and/or quantification ions. We use the simple equation: NF = Target/Fit, where the target response is specific to each species in the transfer standard and the fit is determined from the instrument response during RECAP-CA. Once the data is normalized, we apply the non-linear calibration factors specific to each analyte we individually calibrate for.

*Table 2. VOCs reported from RECAP-CA*

***Hydrocarbons*** — *Total Uncertainty for Hydrocarbons and Halocarbons = 20%*

| Alkanes | Alkenes | Alkynes | Aromatics | Biogenics | Cycloalkanes |
|---|---|---|---|---|---|
| Ethane | Ethene | Ethyne | Benzene* | Isoprene | Methylcyclopentane |
| Propane | Propene | | Toluene* | a-Pinene | Cyclohexane |
| iso-Butane | 1-Butene | | ~~Ethyl Benzene~~ | b-Pinene | Methylcyclohexane |
| n-Butane | cis-2-Butene | | ~~o-Xylene~~ | | Cyclopentane |
| iso-Pentane | trans-2-Butene | | ~~m- & p-Xylenes~~ | | |
| n-Pentane | ~~2-Methylpropene~~ | | ~~1,2,3-Trimethylbenzene~~ | | |
| n-hexane | 1-Pentene | | ~~1,2,4-Trimethylbenzene~~ | | |
| n-heptane | cis-2-Pentene | | ~~1,3,5-Trimethylbenzene~~ | | |
| n-octane | trans-2-Pentene | | ~~iso-Propylbenzene~~ | | |
| n-nonane | 1,3-butadiene | | ~~n-Propylbenzene~~ | | |
| n-decane | 3-methyl-1-butene | | ~~Styrene~~ | | |
| 2,2-Dimethylpropane | 2-methyl-1-butene | | ~~1-ethyl-2-methylbenzene~~ | | |
| 2,2-Dimethylbutane | 2-methyl-2-butene | | ~~1,3-diethylbenzene~~ | | |
| 2,3-Dimethylbutane | | | ~~1,4-diethylbenzene~~ | | |
| 2-Methylpentane | | | | | |
| 3-Methylpentane | | | Sum C9 Aromatics* | Sum Monoterpenes* | |
| 2,4-Dimethylpentane | | | Sum C8 Aromatics* | | |
| 2,2,4-Trimethylpentane | | | | | |
| 2,3,4-Trimethylpentane | | ~~VOC~~ = | *Not reported by GC-MS due to instrument issues* | | |
| 2-Methylheptane | | * = | *Reported by NOAA PTR-MS* | | |
| 3-Methylheptane | | ** = | *Reported by CARB* | | |
| | | *** = | *Reported by NOAA I-CIMS* | | |

***Oxygen-Containing VOCs*** — *Total Uncertainty for oxygen- and nitrogen-VOC = 30%*

| Alcohols | Aldehydes | Ketones | Other Oxygen |
|---|---|---|---|
| Methanol* | Formaldehyde** | Acetone* | Methyl Acetate |
| Ethanol* | Acetaldehyde* | MEK (2-butanone)* | Ethyl Acetate |
| iso-Propanol* | ~~propanal~~ | MVK (methylvinylketone) | Formic Acid *** |
| | Methacrolein | | Furan* |
| | Sum MVK + MACR* | | Methyl Furans* |
| | | | D5-Siloxane * |

***Nitrogen-Containing VOCs***

| Alkyl Nitrates | Other Nitrogen |
|---|---|
| Methyl nitrate | Acetonitrile* |
| Ethyl Nitrate | Benzenenitrile* |
| iso-Propyl Nitrate | Nitromethane |
| n-Propyl Nitrate | |

***Halogenated-VOCs and Other VOCs***

| | |
|---|---|
| Chloroform | F-11, F-113, F-114 |
| Methylene chloride | |
| 1,2-dichloroethane | p-Chlorotrifluorobenzene (PCTBF)* |
| 1,1-dichloroethene | |
| Trichloroethene | |
| Tetrachloroethene | |

All VOCs reported by the GC-MS are listed in *Table 2*. The total uncertainty of the GC-MS measurements incorporates uncertainties of the calibration gas tank contents, errors in the fits to the calibration curves, and an estimate of the overall precision from the transfer standard samples collected during calibration and during RECAP-CA. Total uncertainty is estimated to be ± 20% for the hydrocarbon and halocarbon analytes and ± 30% for the oxygenated and nitrogen-containing VOCs. Limits of detection are compound dependent, but are typically less than 10 pptv for most hydrocarbons and halocarbons and 50 pptv for the oxygenated and nitrogen-containing VOCs.

### *2.4 PTR-MS*

The NOAA proton transfer reaction time of flight mass spectrometer (PTR-ToF-MS, PTR-MS) provides high-time, and high-mass resolution measurements of aromatics, biogenics, and a wide-range of oxygenated VOCs. The PTR-MS relies on analyte reactions with protonated water ($H_3O^+$) resulting in the ionized analyte ($VOC{\bullet}H^+$) for VOC that have a higher proton affinity than water [Yuan et al., 2016]. For many analytes, the protonated product is the primary signal detected; however, secondary reactions, dehydration, fragmentation, and water clustering can complicate the analysis of some analytes [Coggon et al., 2023a]. Additionally, The PTR-MS is not able to resolve isomers without the use of a custom gas chromatography (GC) front-end which was used intermittently throughout the project to resolve isomeric masses and identify measurement interferences [Coggon et al., 2023a].

During RECAP-CA, PTR-MS instrument backgrounds were determined every 2 h for ground site experiments and every ~30 minutes during drives by passing air through a platinum catalyst heated to 350°C. Data were processed using the Tofware package in Igor Pro by WaveMetrics [Stark et al., 2015]. The PTR-ToF-MS was calibrated using gravimetrically-prepared gas standards for typical VOCs such as acetone, methyl ethyl ketone, toluene, and C8-aromatics. Many compounds not stable in gas standards were calibrated by liquid calibration methods [Coggon et al., 2018b]. All other compounds that are not calibrated for are quantified using sensitivities estimated by ion-molecule collision process [Sekimoto et al., 2017], but are assigned larger uncertainties.

#### *2.4.1 PTR-MS COMPARISONS TO GC-MS*

For this analysis, we have averaged the PTR-MS data over the 4-minute sample collection period of the GC-MS. The results of the correlation plots of the PTR-MS vs. GC-MS are listed in *Table 3*. The measurements agree well and within measurement uncertainties for all but two species, ethanol and acetaldehyde. The reason for the discrepancy is unknown as the same calibration standards were used for the two instruments. It is likely that the GC-MS may be biased low due to the instrument performance issues detailed in *Section 2.3.2* and that the PTR-MS may be biased too high, particularly for ethanol, due to interferences described in Coggon et al. [2023]. In this report, we will include both measurements where appropriate and suggest using these measurements as the likely range of expected values. For the isoprene comparison, the y-intercept was forced through the origin to account for PTR-MS interferences on the isoprene mass at night as detailed in Coggon et al. [2023]. For this analysis, we will rely on isoprene measurements from the GC-MS which was free of interferences.

*Table 3. Comparisons of PTR-MS vs. GC-MS during RECAP-CA*

| | Slope | *Slope Sigma* | Y-int | *Y-int Sigma* | r2 |
|---|---|---|---|---|---|
| Isoprene | 1.04 | *0.01* | 0 | *0* | 0.92 |
| Benzene | 1.05 | *0.01* | -0.020 | *0.003* | 0.85 |
| Toluene | 1.18 | *0.01* | -0.02 | *0.004* | 0.92 |
| Acetone | 1.08 | *0.01* | 0.09 | *0.05* | 0.9 |
| MethylEthylKetone (MEK) | 1.13 | *0.02* | -0.11 | *0.01* | 0.72 |
| Methanol | 1.36 | *0.02* | -0.4 | *0.09* | 0.76 |
| Ethanol | 1.69 | *0.02* | 0.014 | *0.12* | 0.89 |
| Acetaldehyde | 2.47 | *0.04* | 0.03 | *0.05* | 0.72 |

### *2.5 I-CIMS*

The NOAA iodide chemical ionization time-of-flight mass spectrometer (I-CIMS) provided measurements of formic acid (HCOOH) in addition to highly oxygenated and nitrogenated species such as nitrous acid (HONO), acyl peroxynitrates (PAN), and isoprene nitrates [Robinson et al., 2022]. Formic acid was calibrated hourly with a permeation tube device, yielding a limit of detection of 300 pptv and calibration uncertainty of 22% ± 25 pptv. Please refer to Robinson et al. [2022] for more measurement details.

### *2.6 PICARRO GAS ANALYZERS*

There were a variety of Picarro gas analyzers used during RECAP-CA in order to measure CO, $CO_2$, $H_2O$, HCHO, and ammonia ($NH_3$). *Figure 8* shows the timeseries, active measurement periods, correlation plots used for comparisons, and the statistics for the 1-minute composite data described in *Section 2.11*. Similar plots and analysis for $CH_4$ and $CO_2$ are included in the Appendix *Figures A1-A2*, respectively.

- A Picarro G2307 Gas Concentration analyzer operated by CARB provided important measurements of formaldehyde (HCHO), a toxic, photolytic, and highly-reactive VOC. Precision at 2 seconds is 1.2 ppb for HCHO as stated by the manufacturer. Posted data was of 1-minute averages.
- The CARB Picarro SI2103 Gas Concentration analyzer was used to measure ammonia. Precision at 5 minutes is 0.30 ppb as stated by manufacturer. Posted data was of 1-minute averages.
- Three Picarro G2401 analyzers were operated by NOAA, CARB, and Caltech groups. These were used to measure CO, $CO_2$, $CH_4$, and $H_2O$. For the NOAA Picarro, precision at 5 seconds, 5 minutes, and 60 minutes is 15, 1.5, and 1 ppb for CO; 50, 20, and 10 ppb for $CO_2$; and 1, 0.5, and 0.3 ppb for $CH_4$. Maximum drift at standard temperature and pressure (STP) over 24 hours was 10 ppb for CO; 100 ppb for $CO_2$; and 1 ppb for $CH_4$. The instrument was calibrated weekly in the field using tanks that were calibrated before and after the field project using standards obtained from NOAA's Global Monitoring Laboratory. These standards are tied to the WMO standard for greenhouse gases with known uncertainties. The field tanks were connected to the Picarro sample inlet and the calibration flow was sufficient to replace the entire sample flow of the instrument. The total uncertainty for the project is estimated to be ±(16 ppb + 2%) for CO, ±(0.2 ppm + 1%) for $CO_2$; and ±(2 ppb + 1%) for $CH_4$.

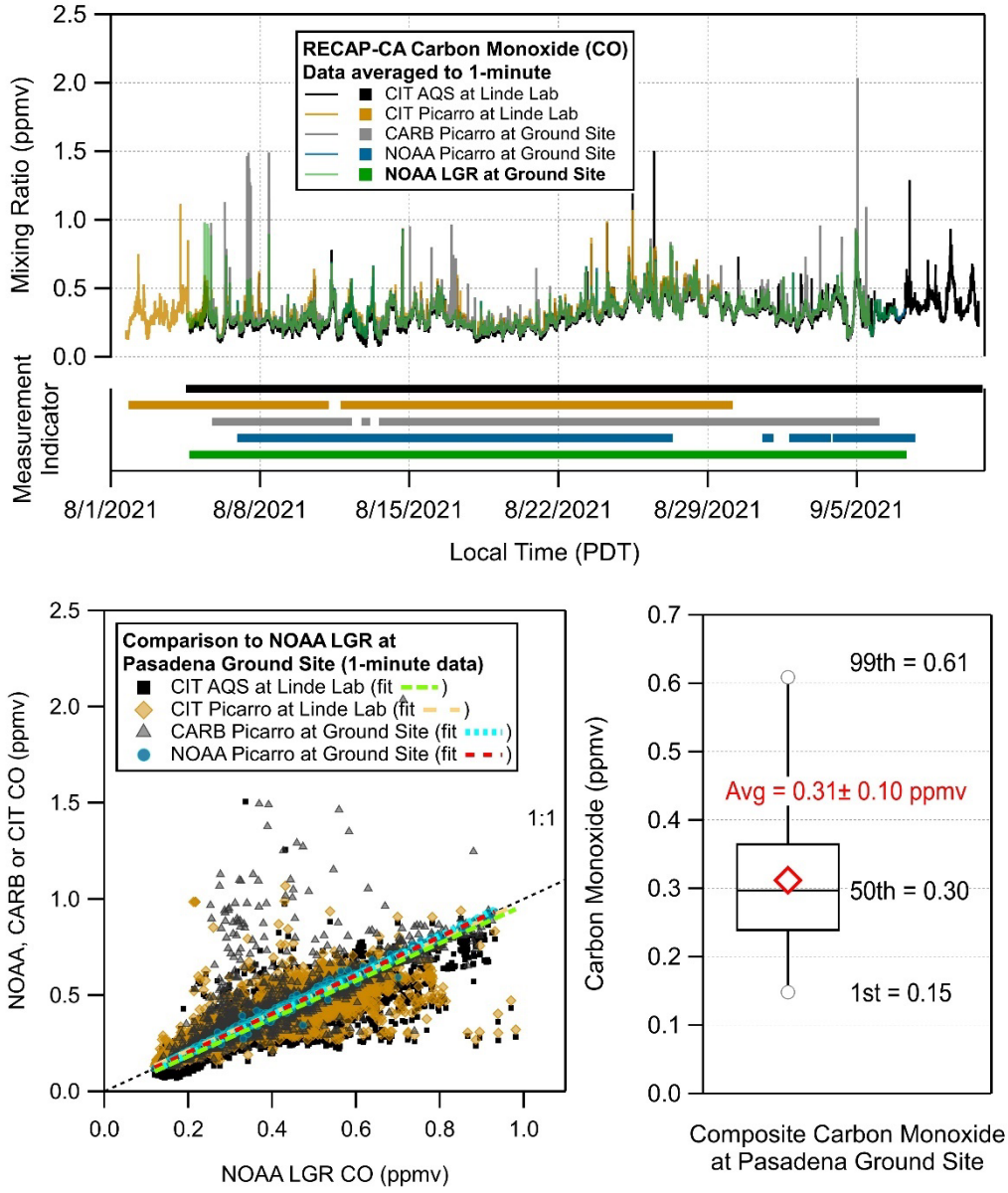


*Figure 8. Comparison of CO measurements during RECAP-CA.*

318

319 *2.7 LGR GAS ANALYZER*

320 The NOAA Los Gatos Research (LGR) spectrometer was used to measure CO, dinitrogen oxide (N2O)
321 and H2O by off-axis integrated cavity output spectroscopy. Ambient air was sampled approximately 10 m
322 above ground level through a 10-m stainless steel tube (3.2 mm OD, 1.6 mm ID) and data were recorded
323 at 1 Hz. Final data were reported as 1-minute averages. The instrument was calibrated in the laboratory
324 to the World Meteorological Organization CO_X2014A scale immediately before and after the
325 field project. The precision of the 1-minute data was 0.2 ppbv, and the estimated uncertainty is 1%. All
326 data are reported as dry air mole fractions.

Comparison of the 1-minute LGR CO to the other measurements at the two ground sites is shown in *Figure 8*. The LGR agrees extremely well with the NOAA Picarro (slope = 1.0017 ± 0.0002, $r^2$ = 0.998) which had an inlet co-located with the LGR. Scatter in the other measurements is likely due to the different sampling heights and locations. The two CO measurements at the Linde Laboratory also agree very well (slope = 1.002 ± 0.0002, $r^2$ = 0.984) with each other. For this analysis, we rely primarily on the NOAA LGR measurements of CO for the determination of all VOC/CO ratios.

### *2.8 NOXCARD, NO-LIF, AND TECO*

$NO_x$ (=NO + $NO_2$) and ozone ($O_3$) were measured by a custom-built, four channel Cavity Ring Down Spectroscopy (CRDS) instrument that had a nominal sensitivity and precision of 20 ppt at one second. The CRDS instrument provides true $NO_2$ from direct absorption at 405 nm. It measures total $NO_x$ through conversion of NO to $NO_2$ in excess $O_3$, and total reactive nitrogen ($NO_y$) through thermal conversion to NO and $NO_2$ in a quartz inlet heated to 650 °C. It measures $O_3$ through conversion to $NO_2$ in excess NO. Calibrations are done in the laboratory via standard additions of $O_3$ that are subsequently converted to $NO_2$ using the same conversion in excess NO used to measure $O_3$ in ambient air. In-field calibrations are done via standard additions from an $NO_2$ cylinder, which is compared to the laboratory calibration standard. Measurements are also compared to other $NO_x$ and $O_3$ instruments, including a custom NO laser induced fluorescence (NO-LIF) instrument with a photolytic converter for $NO_2$ (1 ppt precision at one second and 8-15% uncertainty) and $O_3$ TECO monitors based on UV absorption. The accuracy of final data has 6-9% accuracy for NO, $NO_2$ and $O_3$, and 15% accuracy for $NO_y$.

### *2.9 LIDAR*

The NOAA Stationary Doppler LIDAR (Light Detection and Ranging) On a Trailer (StaDOT) system consists of a scanning 200S Leosphere LIDAR that produces 15-minute wind, aerosol, and vertical velocity variance profiles as well as an estimate of the boundary layer height (BLH) [Bonin et al., 2018]. The operational mode consisted of a repeating 15-minute scan sequence. During the first 5 minutes of each sequence, the system performed azimuthal scans (used to calculate horizontal wind profiles) and the last 10 minutes were used to stare vertically (in order to calculate profiles of vertical velocity variance and aerosol backscatter intensity).

### *2.10 METEROLOGICAL MEASUREMENTS AND MODELS*

Ambient temperature, wind speed, wind direction, and humidity were measured by various instruments installed aboard the NOAA and CARB mobile labs stationed at the Pasadena site. Meteorological data for the Linde Laboratory site was reported by the Total Carbon Column Observing Network site (TCCON, https://tccon-wiki.caltech.edu/).

Back trajectory air parcel paths across the Los Angeles Basin were determined on a quarter hourly basis throughout the measurement period using the locations (latitude & longitude) of the center-of-mass from the main cluster of particles outputted from the Lagrangian FLEXible PARTicle dispersion model driven with meteorological input provided by the Weather Research and Forecasting numerical weather prediction model (FLEXPART-WRF) [Brioude et al., 2013; Verreyken et al., 2019].

The NOAA High-Resolution Rapid Refresh smoke (HRRR-smoke) model output was used to identify measurement periods impacted by low-level smoke from regional wildfires. HRRR-Smoke modeling system integrates the HRRR model, WRF-Chem, and Fire Radiative Power (FRP) data from the Visible

Infrared Imaging Radiometer Suite (VIIRS) sensor on the Suomi satellite to simulate the emissions and transport of smoke from wildfires in real-time in high spatial resolution. The model output is for the CONUS domain (3km horizontal grid resolution) and is initialized daily at 00 and 12UTC using input files for the meteorology from the real-time HRRR experimental runs. The model is then run to produce 36-hour forecasts. We accessed archived forecasts for the "HRRR-NCEP smoke (operational)" model over the Southwest (SW) domain starting at 00 UTC for "near-surface smoke" (https://rapidrefresh.noaa.gov/hrrr/HRRRsmokeold/).

### *2.11 CALCULATION OF COMPOSITE MEASUREMENTS AND DATA AVERAGING*

In order to integrate the continuous measurements with the discrete sampling of the NOAA GC-MS, we have 1) generated composite timeseries for CO, $CO_2$, $CH_4$, NO, $NO_2$, and $O_3$ to fill in any missing data gaps before 2) averaging the high-time-resolution measurements over the 4-minute sample collection time of the GC-MS or the open/close times of the whole air samples. If any data is missing from the primary measurement listed in then we use the secondary measurement identified in *Table 4*. The equations used for the composite timeseries were generated from correlation plots of the primary vs. secondary measurement similar to those in *Figure 8* and *Appendix Figures A1-A5*. For the LIDAR measurements, we use the data that most closely matches the mid-time of the GC-MS and LIDAR samples. For all other chemical or meteorological measurements, we averaged the posted data over the GC-MS and WAS sample collection times. We use the GC-MS/WAS averaged data for all subsequent analyses presented in this report noting that this represents only a small fraction of the data collected by the fast-response instruments.

*Table 4. Calculation of composite timeseries for trace gases.*

| | Instruments | | From Primary vs. Secondary Correlations |
|---|---|---|---|
| **Analyte** | **Primary** | **Secondary** | **Equation Used to fill gaps in Primary Measurement** |
| CO | NOAA LGR | NOAA Picarro | composite = (NOAA Picarro - 0.00195)/1.0017 |
| $CO_2$ | NOAA Picarro | CARB Picarro | composite = (CARB Picarro + 9.95)/1.017 |
| $CH_4$ | NOAA Picarro | CARB Picarro | composite = (CARB Picarro - 0.0040)/0.9966 |
| NO | NOAA NO-LIF | NOAA NOxCaRD | composite = NOxCaRD |
| $NO_2$ | NOAA NOxCaRD | NOAA LIF | composite = NO-LIF |
| $O_3$ | NOAA TECO | NOAA NOxCaRD | composite = NOxCaRD |

### *2.12 FIVE-VCP EMISSIONS INVENTORY*

We utilize the FIVE-VCP emissions inventory developed at NOAA Chemical Sciences Laboratory (https://csl.noaa.gov/groups/csl7/measurements/2021sunvex/emissions/) to compare to our calculated emission ratios. Briefly, mobile source emissions in FIVE are estimated using fuel sales for activity and emission factors normalized to fuel use based on roadway measurements and laboratory studies for off-road engines. VOC speciation profiles are based on measurements of the composition of gasoline and diesel fuel and exhaust [Gentner et al., 2012; Gentner et al., 2013b]. A more complete description of the inventory methods can be found in McDonald et al. [2018b]. Volatile chemical product emissions are estimated by performing a mass balance of the petrochemical industry to estimate chemical product usage and organic solvent content, and emission factors account for the volatilized fraction of VOCs to

the atmosphere. VOC speciation profiles are based on CARB surveys of consumer products [CARB, 2019], architectural coatings [CARB, 2018a], and fragrances [CARB, 2018b]. More details on the VCP emissions inventory methodology can be found in McDonald et al. [2018a] and Coggon et al. [2021b]. All other point and areawide emissions are from the US National Emissions Inventory 2017 [EPA, 2020]. Near real-time activity adjustment factors derived from monthly energy and economic datasets are applied to account for changes in consumer and economic activities during and after the COVID-19 pandemic [He et al., submitted].

### *2.13 DATA AVAILABILITY*

All the calibrations and quality assurance/control protocols for all NOAA instruments at the Pasadena ground site have been finalized. The data for these instruments and those from the other instrument groups are publicly available on the NOAA CSL website in ICARTT and Igor format and will remain available via the NOAA CSL data archive. The data can be provided to CARB in a different format on request.

https://csl.noaa.gov/groups/csl7/measurements/2021sunvex/GroundLV/DataDownload/

https://csl.noaa.gov/groups/csl3/measurements/2021sunvex/dalek01/

Data for the NOAA Mobile Lab data (not funded by CARB) is currently available via a password protected site on the NOAA CSL website. This data will eventually become public, but is available now upon request.

https://csl.noaa.gov/groups/csl7/measurements/mobilelab/MobileLabSUNVEx/DataDownload/

# 3.0 RESULTS AND DISCUSSION

Here we discuss the results of the four main foci of this work in an effort to characterize VOC emissions sources and their subsequent impact on air quality. Our research foci include 1) characterizing temporal variability of speciated VOC emissions downwind of Los Angeles, 2) identifying VOC source signatures impacting the measurement site, 3) determining VOC emission ratios and comparing them to other urban datasets and available VOC emission inventories, 4) investigating the potential $O_3$ and SOA formation from measured VOC emissions as discussed below.

## *3.1 CHARACTERIZING TEMPORAL AND SPATIAL VARIABILITY*

### *3.1.1 OVERVIEW OF METEROLOGICAL OBSERVATIONS*

The weather during RECAP-CA was typical for Southern California summertime. *Figure 9* includes timeseries of the photolysis rate for $NO_2$ ($jNO_2$) as proxy for the amount of sunlight, water concentration (%), air temperature and wind speed for both ground sites, and the boundary layer heights as determined by the NOAA stationary LIDAR. There were only four days with decreased sunlight (8/18, 8/21, 8/31, and

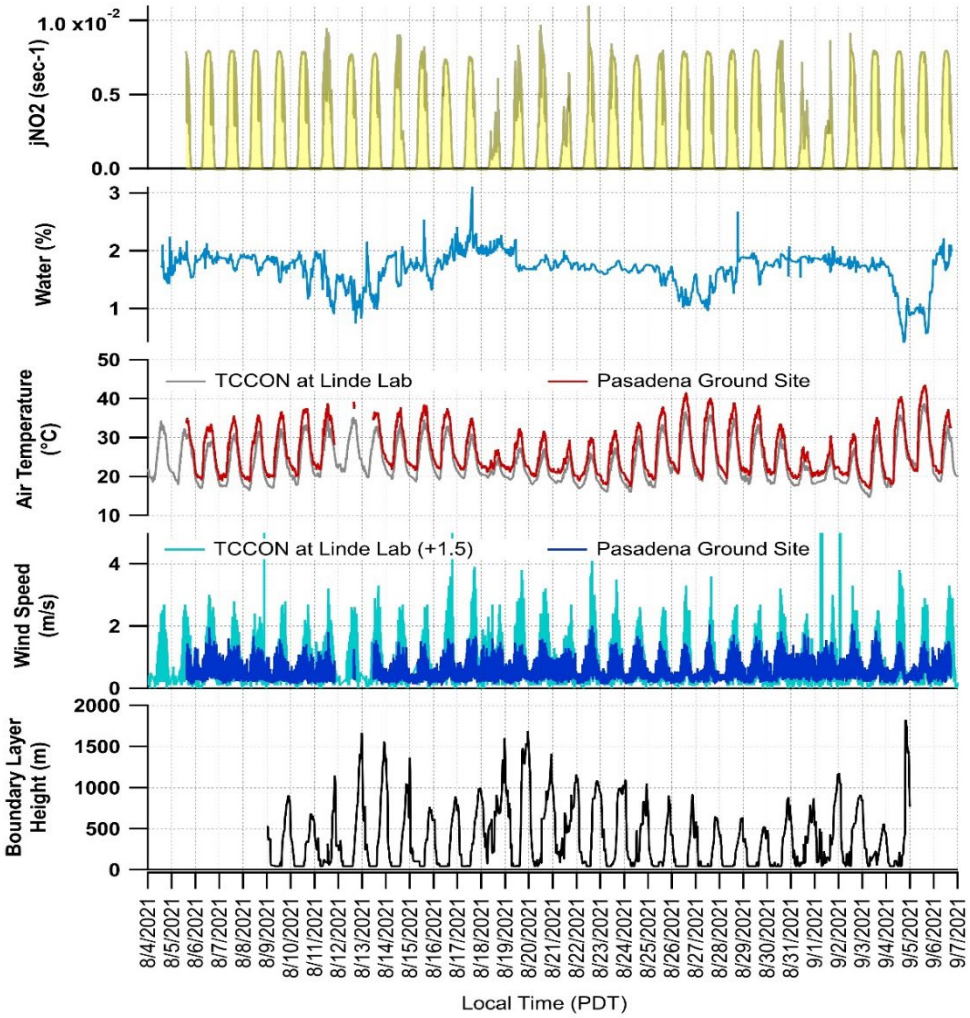


*Figure 9. Meteorological observations during RECAP-CA. Data is 1-minute average values.*

9/1/2021). There were three periods of lower atmospheric water vapor (8/11-8/13, 8/26-27, and 9/4-5/2021). Relative humidity ranged from 10% to 75%, with daily minimums occurring at 15:00 PDT and maximums at 06:00 PDT near sunrise. At the Pasadena ground site, the average temperature was 26 ± 6 °C (min = 16.8 °C on 9/3/2021, max = 43.5 °C on 9/5/2021), which is much warmer than the average temperature observed during CalNex 2010 (18.2 ± 1.5°C). The average wind speed during RECAP-CA was very light at 0.5 ± 0.2 m/s (range = 0.1 to 2.0 m/s). Slightly lower temperatures and higher wind speeds at the Linde Laboratory site are attributed to the increased measurement height at the top of the laboratory. The average boundary layer height was 384 ± 376 m with nighttime values as low as 45 m and daily maximums between 750 and 1300 m. Some morning fog was observed at the site on 9/5/2021, but there were no other notable precipitation events.

The wind at the Pasadena site came predominately from the southwest (SW, 225°N) during the day and the south-southwest (SSW, 202°N) at night (*Figure 10*). During the daytime, the winds direction typically moved from the ESE (100°N) to the WNW (300°N) before swing back to the south. The strongest winds were most often from due west of the site. This wind pattern was very similar to that observed during the CalNex 2010 measurements.

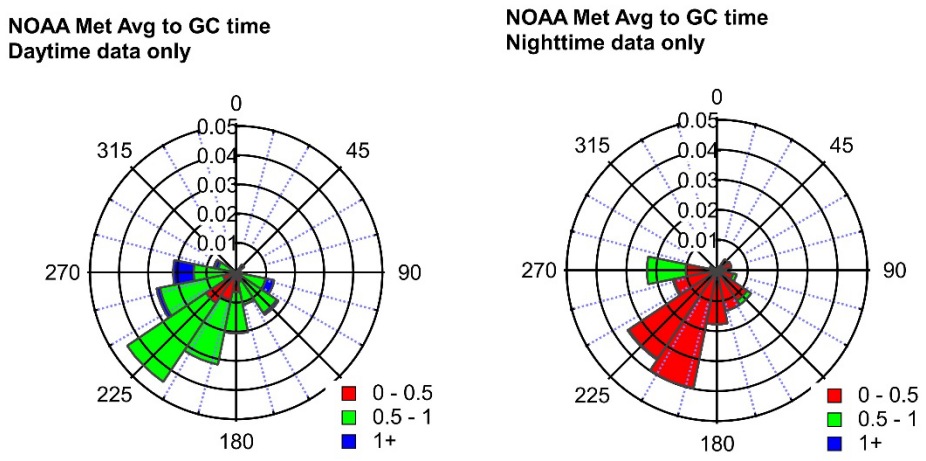


*Figure 10. Wind roses for daytime and nighttime at Pasadena ground site. Data is averaged over GC-MS sample time.*

Ground-level wind direction measurements are not always indicative of where an air mass came from as it is more susceptible to influence from surrounding buildings and/or geographic features. Since the goal of this study is to measure emissions downwind of Los Angeles, we have also conducted back-trajectory analyses for every day of measurements during RECAP-CA as shown in *Figure 11*. We used the FLEXPART model to generate nine-hour (9-hr) back trajectory paths for airmasses arriving at the Pasadena site every hour of every day of measurements. The overall paths of the trajectories match the ground-level wind directions in *Figure 10* and clearly show that air masses arriving at the Pasadena site will pass directly over the major urban areas of the Los Angeles Basin. This makes Pasadena a good receptor site to understand the upwind emission sources and subsequent photochemical processing of VOC sources in the greater Los Angeles metro area.

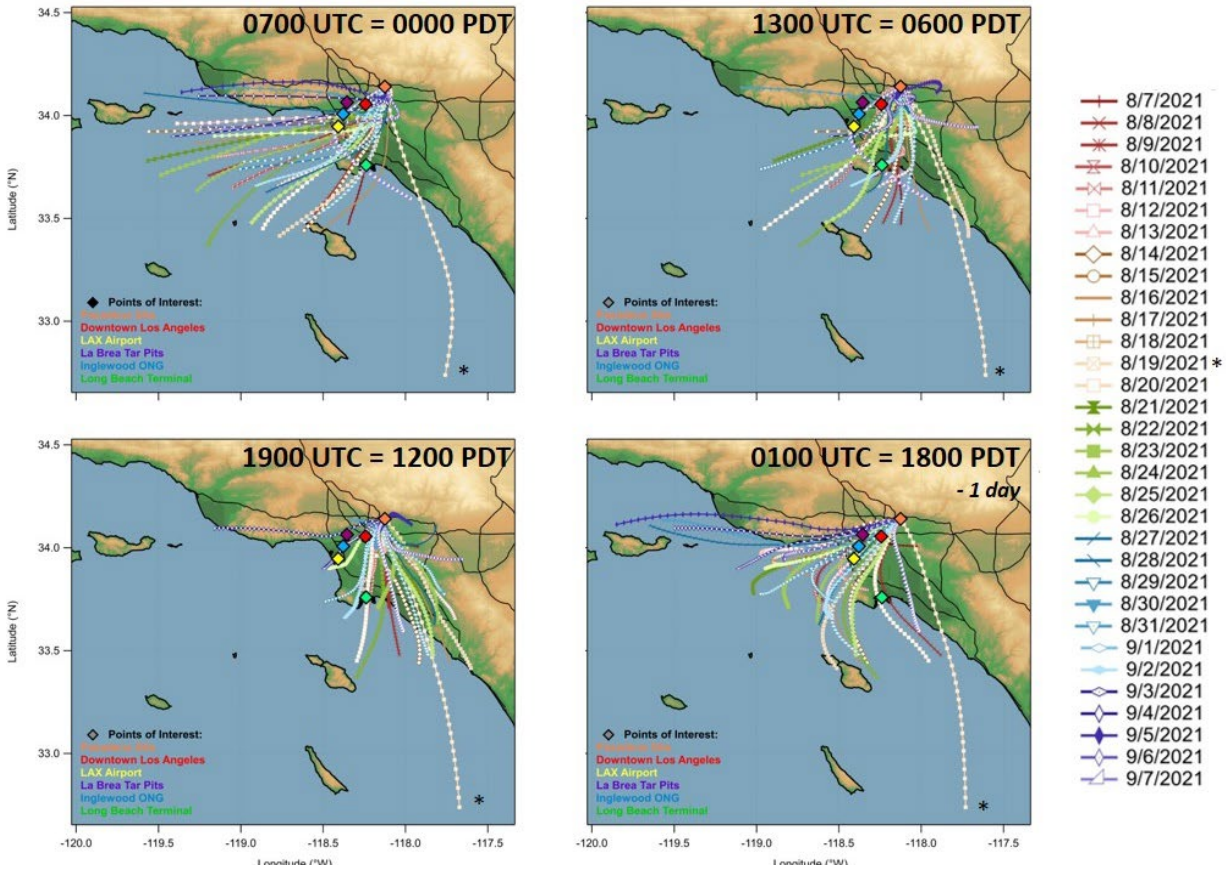


*Figure 11. Nine-hour back trajectory paths of air masses arriving at the Pasadena ground site at the indicated times for each day of measurements. Markers represent 15-minute increments along trajectory paths.*

### *3.1.2 OVERVIEW OF CHEMICAL OBSERVATIONS*

The timeseries of CO, $NO_2$, $O_3$, formaldehyde, and benzenenitrile are shown in *Figure 12*. CO and $NO_2$ are combustion tracers common to tail pipe emissions, domestic burning sources, and wildfires. Ozone is photochemically formed in the atmosphere from reactions involving VOCs. Formaldehyde is an air toxic that has an array of primary emission sources and is a common secondary product of many VOC oxidation reactions. Both benzenenitrile and formaldehyde are directly emitted from wildfires [Yokelson et al., 2009].

The observations can be segmented into approximately four different periods for ease of discussion:

- From 8/5 to approximately 8/16/2021, is classified here as typical urban emissions with active photochemical production of ozone and formaldehyde. The daily minimum values for CO, $NO_2$, and benzenenitrile are relatively constant during this time.
- From 8/17 to 8/21/2021, there is a relatively clean period where we observed decreases in CO and $NO_2$ mixing ratios and decreases in the ozone and formaldehyde daily maximums. This time period corresponds with drops in temperature and sunlight, but no obvious changes to windspeed or boundary layer height as shown in *Figure 9*. The back-trajectory analysis shows that air masses

during this time (e.g., 8/19/2021 trajectory identified by the * in *Figure 11*) came from much further away and spent more time over the open ocean compared to the other days.

- From approximately 8/22 to 9/1/2021, we see a broad increase in the CO and benzenenitrile that proceeds a gradual buildup of $NO_2$, ozone and formaldehyde. We will show in *Section 3.2.4* below, that aged wildfire smoke influenced the observations of the longest-lived combustion tracers. We categorize this time period as a mix of fresh urban emissions on an aged smoke background.

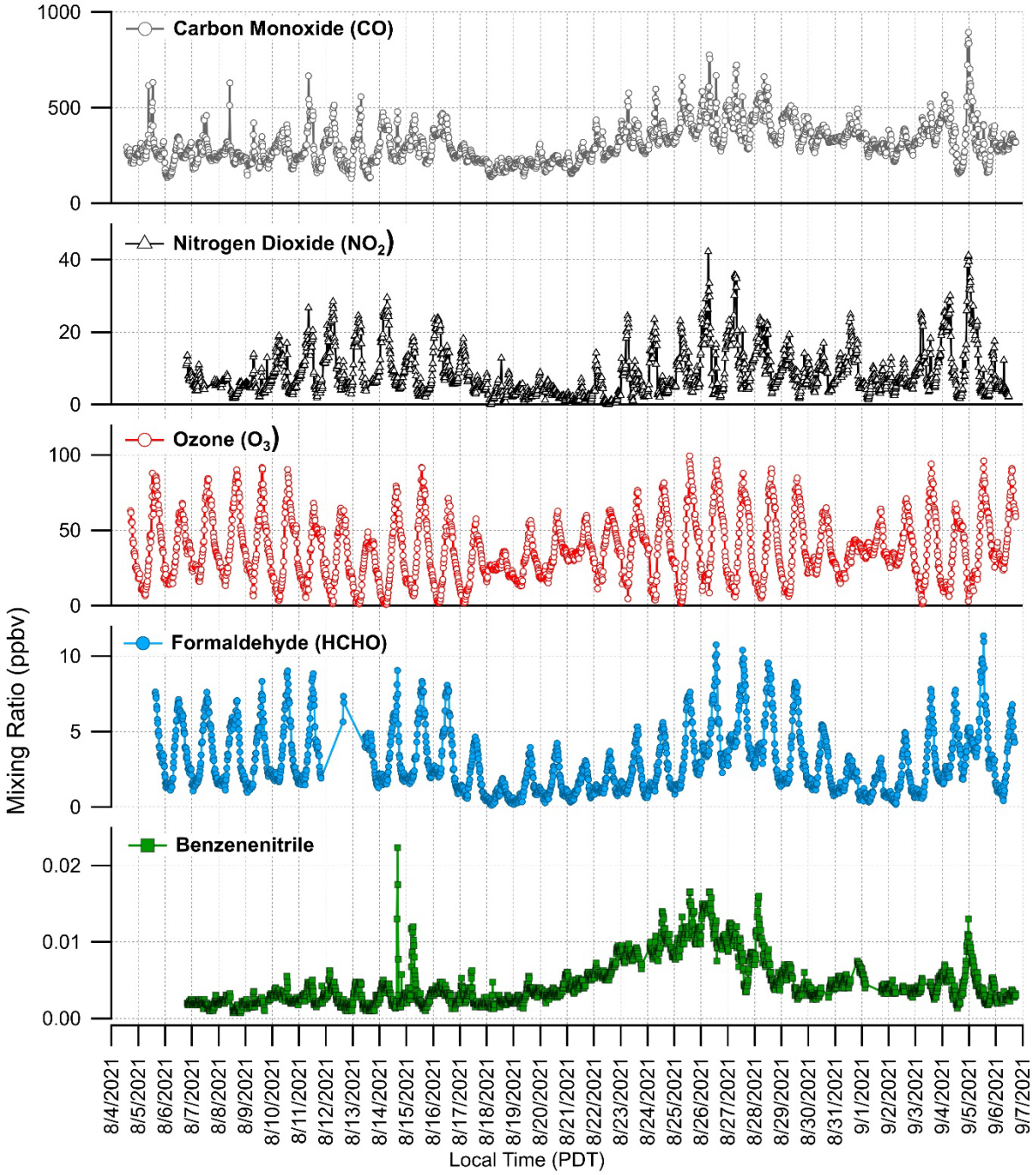


*Figure 12. Timeseries of chemical measurements during RECAP-CA.*

- The observations from 9/2 to 9/7 are characterized by another buildup of primary emissions with active photochemistry and perhaps some aged smoke influence as well – a mix of the three previously defined time periods.

The median observed mixing ratios for all non-methane organic gases measured during RECAP-CA are included in *Figure 13*. The top panel is organized by descending median mixing ratios for each species, which is color-coded by its chemical class. It is evident that the oxygenated VOCs are among the most abundant species followed by the light alkanes, ethane and propane. The bottom panel of *Figure 13* displays the ratio of the median daytime-to-nighttime mixing ratios. This serves to highlight those species such as isoprene which has a short lifetime during the day and emissions that scale with sunlight and temperature and its oxidation products methyl vinyl ketone (MVK), methacrolein (MACR), and isoprene nitrates. Other species with higher daytime mixing ratios will have either a strong photochemical source and/or higher emission rates during the daytime which outweigh any chemical or photolytic losses. *Appendix Table 1* contains the statistics for all gas-phase species measured during RECAP-CA.

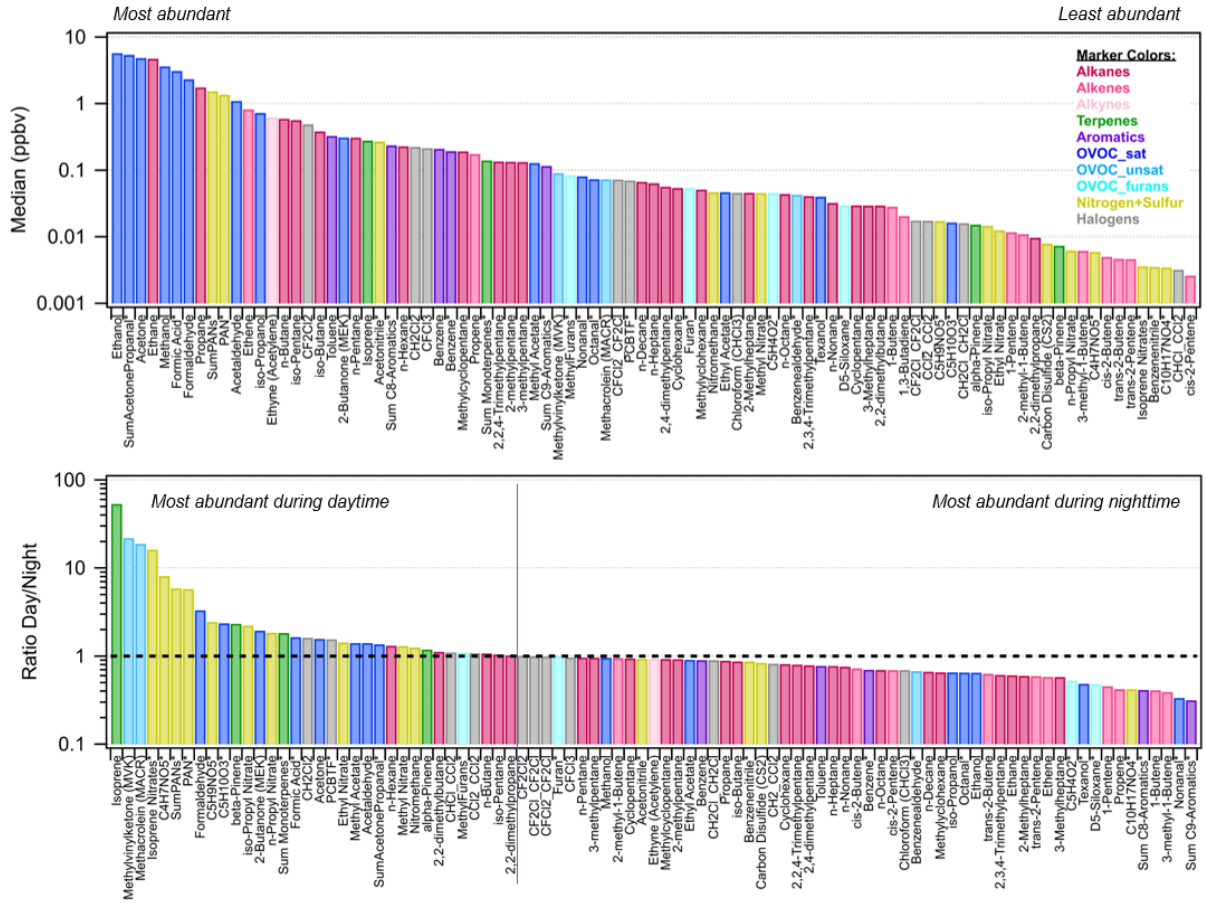


*Figure 13. (Top) Median observed mixing ratios (ppbv) for all VOCs measured during RECAP-CA. (Bottom) Ratio of daytime-to-nighttime median mixing ratios.*

### *3.1.3 DIEL PROFILES*

The relative importance of emissions, chemistry, and boundary layer dynamics is examined here using mean diel profiles of various trace gases and VOCs during the RECAP-CA 2021 and CalNex 2010 projects as shown in *Figure 14*. The diurnal profiles of VOC absolute mixing ratios can be affected by emissions, chemistry (removal or photochemical production), and dilution, with the relative importance of each of these processes changing throughout the day.

- VOCs and trace gases that are directly emitted from anthropogenic sources including on-road emissions, cooking, volatile chemical product usages, etc. tend to have higher nighttime diel mean mixing ratios as these species are emitted into an atmosphere with a shallow boundary layer and weaker wind speeds. Examples shown here include CO, toluene, methanol, ethyne, ethane, and 1,3-butadiene.
- VOCs and trace gases that are predominantly from on-road emission sources (e.g., CO, NO, toluene, ethyne, 1,3-butadiene) have a peak in the diel profile between 06:00 and 07:00 PDT. We associate this with the morning rush hour traffic emissions mixing into a shallow boundary layer. A second small peak appears around 13:00 PDT for some of the longer-lived species such as CO, toluene, and ethyne. This has been attributed to the transport of the photochemically process plume from Los Angeles arriving at the Pasadena site [Borbon et al., 2013]. The back-trajectory analysis indicates these air masses most commonly traversed over the central L.A. Basin (e.g., Long Beach, Huntington Beach, and Anaheim areas).
- Many of the above species tend to dilute in the afternoon, as a consequence of an expanded boundary layer, higher daytime temperatures, and higher wind speeds, which result in increased mixing throughout the boundary layer. Additional losses due to chemistry with either the hydroxyl (OH) radical and/or ozone will also lead to a daytime decrease in the mean diel profile.
- Secondary formation of ozone and certain oxygenated VOCs such as formaldehyde, acetaldehyde, and acetone result in daytime diel maximums as both sunlight, ozone, and hydroxyl radical concentrations formed from ozone are at their diel maximums.
- The mean diel profile for isoprene observed during RECAP-CA and CalNex 2010 is consistent with a natural source that is very local and highly temperature-dependent.

The diel profiles are also useful ways to compare the GC-MS and PTR-MS measurements from RECAP-CA. The instrument performance of the GC-MS was affected by the trailer temperature and certain masses measured by the PTR-MS are impacted by interferences that vary throughout the day [Coggon et al., 2023a]. As shown in *Figure 14*, the diel profiles for isoprene, acetaldehyde, toluene, and methanol are higher at night for the PTR-MS compared to the GC-MS at the Pasadena site. Coggon et al. [2023] has identified an interference on the isoprene mass from emissions of octanal and nonanal from cooking emissions that build up during the nighttime as discussed in *Section 3.2.2*. Additionally, large sources of ethanol can cause interferences on the mass normally assigned to acetaldehyde [Coggon et al., 2023a]. The GC-MS measurement of acetaldehyde appears to be anonymously low during the peak mid-day temperatures resulting in a lower than expected mixing ratio compared to the PTR-MS.

We also note here that there are several interesting differences in the diel profiles compared to CalNex 2010 observations. While CO was comparable between the two datasets, ethyne was much lower and ethane was much higher for RECAP-CA 2021 compared to CalNex 2010. This was also observed by van Rooy et al. [2021] during 2020 measurements on the Caltech campus. Ethane has previously been

attributed to natural gas use and production in the Los Angeles Basin [Peischl et al., 2013]. Lastly, ozone, formaldehyde and isoprene were much greater for RECAP-CA primarily due to higher daytime temperatures and increased sunlight compared to CalNex 2010.

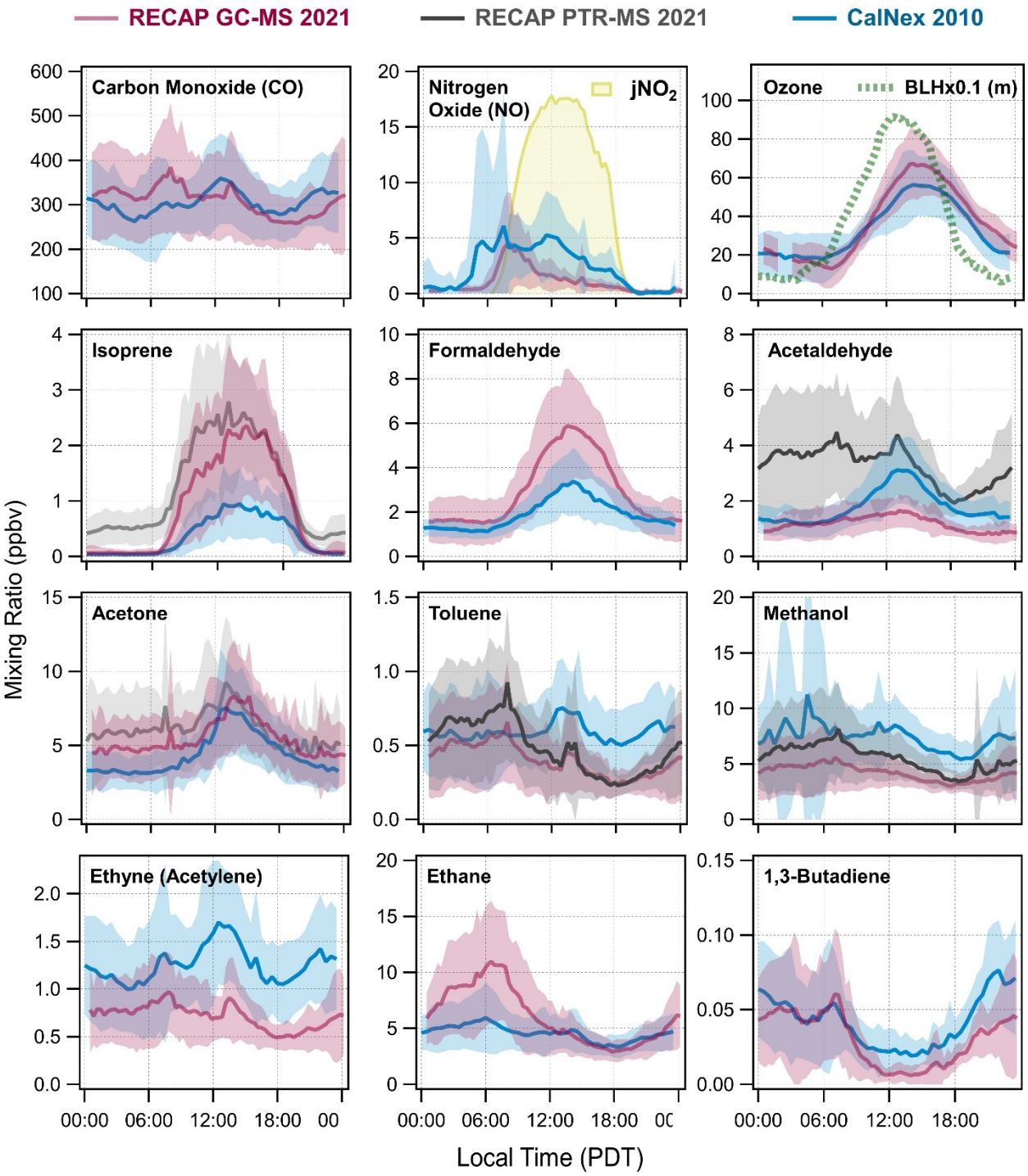


*Figure 14. Diel mean profiles VOC and trace gases observed during RECAP-CA 2021 and CalNex 2010. Diel mean profiles for $jNO_2$ (scale not shown) and boundary layer height (BLH, meters) are also included.*

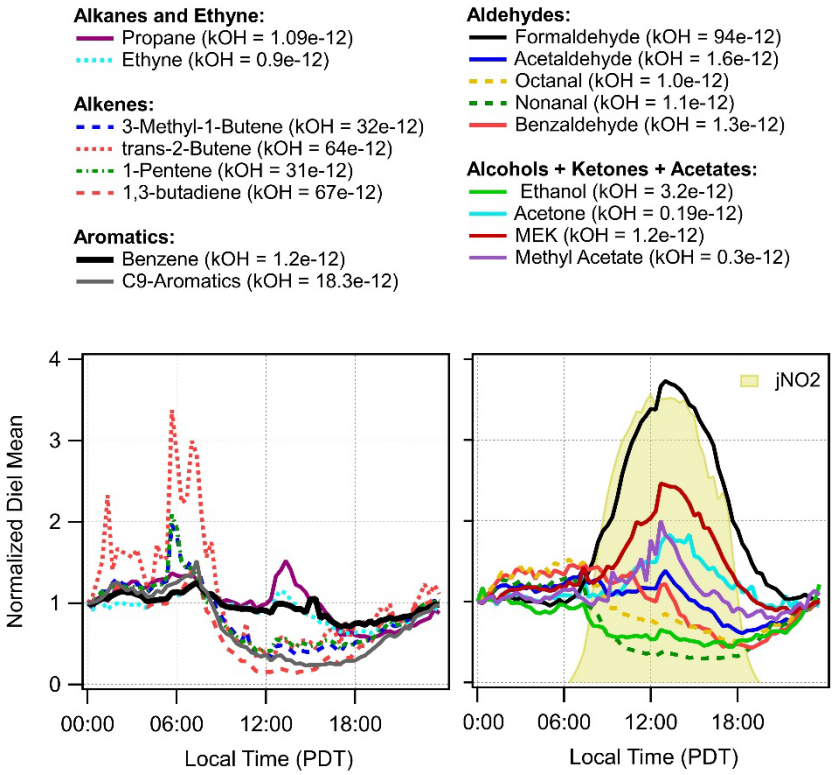


*Figure 15. Normalized diel mean profiles for select VOCs and their reaction rate constants with the hydroxy radical (kOH at 298K, $cm^3$ molecule $^{-1}$ $s^{-1}$). The diel profile for $j_{NO2}$ (scale not shown) is included as a proxy for sunlight.*

In order to better compare the diel profiles for species with varying absolute mixing ratios, we have normalized the respective diel mean profiles to a value of one at midnight local time (00:00 PDT) as originally presented in Borbon et al. [2013] and de Gouw et al. [2017, 2018] (*Figure 15*). For relatively unreactive species that have constant and diverse sources such as ethyne and benzene, the observed mixing ratios have a relatively weak dependence on the time of day. Both of these species are most commonly associated with on-road emission sources that are distributed across the Los Angeles Basin. Propane is also relatively unreactive, but the normalized diel profile shows a distinct midday peak at 13:00 PDT which is associated with the arrival of the Los Angeles Basin plume at the Pasadena ground site. This is indicative of a propane source that is not related to on-road emission sources that is upwind of the Pasadena site.

Normalized diel profiles for the reactive alkenes show a prominent spike centered on 07:00 PDT that we associate with the morning rush hour, and mid-day minimums associated with the increased mixing and photochemical removal. These species correlate well with benzene and ethyne at night, but are depleted relative to these compounds during the day because of their faster removal by the hydroxyl (OH) radical. This is evidenced by daytime minimums in the normalized diel profiles that scale with the reaction rate constants of the VOCs with the hydroxyl radical (kOH, $cm^3$ molecule $^{-1}$ $s^{-1}$).

A strong photochemical source of formaldehyde, acetone, and methyl ethyl ketone (MEK) are evident in the broad daytime increase in the normalized diel profile that closely matches that of $jNO_2$, a proxy for sunlight. Methyl acetate, acetaldehyde, and benzenealdehyde also show mid-day peak coincident with

peak photochemical production but also the arrival of the L.A. Basin plume. The normalized diel profiles of these oxygenated species have more features in common with propane than formaldehyde suggesting that the diel variations are driven more by direct emissions than secondary production. The diel profiles of ethanol, octanal, and nonanal exhibit daytime minimums similar to the reactive alkenes; however, these OVOCs are not particularly reactive with the hydroxyl radical or ozone. This indicates that the diel variations are largely driven by boundary layer dynamics, other daytime sinks, and/or significant nighttime sources that increase the abundance of these species during the evening hours.

### *3.1.4 SPATIAL AND TEMPORAL VARIABILITY*

The NOAA Mobile Laboratory conducted ten drives during RECAP-CA. These were done at the beginning (8/3 to 8/6/2021) and the end (9/1 to 9/3/2021) of the measurement intensive so as to minimize measurement disruptions at the primary Pasadena ground site. The map in *Figure 16* consists of all of the individual drive tracks colored and sized by the observed CO measurements (NOAA Picarro, 1-Hz measurements). Larger CO enhancements are observed near downtown Los Angeles, on the north-south running highways and throughout the northwestern quadrant. This map helps to illustrate the abundance of combustion sources upwind of the Pasadena site and shows the accumulation of pollutants on the eastern edges of the South Coast Air Basin due to the local meteorology and topography.

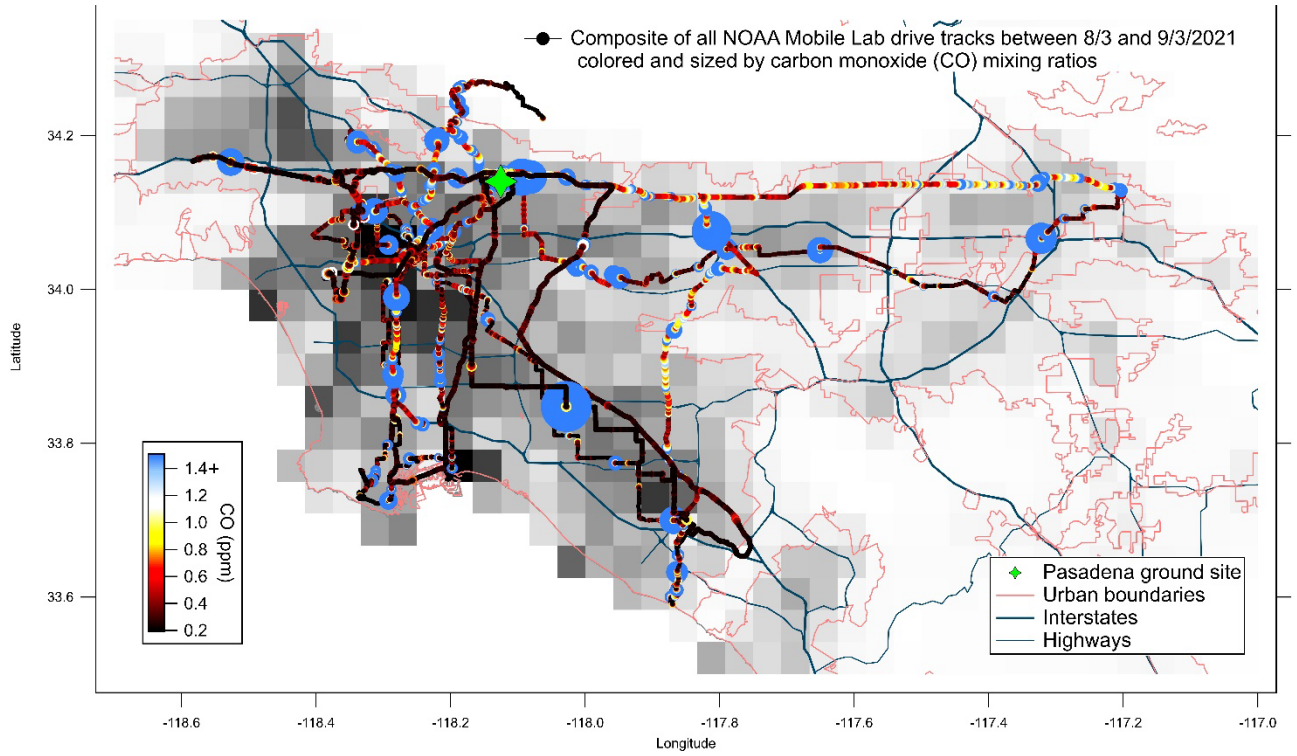


*Figure 16. NOAA Mobile Laboratory drive tracks colored and sized by carbon monoxide (CO). Population density, urban boundaries, and roadways are also included.*

There was a total of 187 NOAA whole air samples collected along the drives which help illustrate the spatial distribution of select VOCs across the basin as shown in *Figure 17*. Both benzene and ethyne have similar spatial patterns with higher mixing ratios observed near downtown Los Angeles. Lower mixing ratios for all species were observed along the western coastline. Propane is elevated throughout the interior basin and show a gradient of increasing mixing ratios towards the northeastern quadrant which is consistent with the work of Warneke et al. [2012]. Isoprene was most prevalent on the far northern edges of the basin and closest to the San Bernardino National Forest.

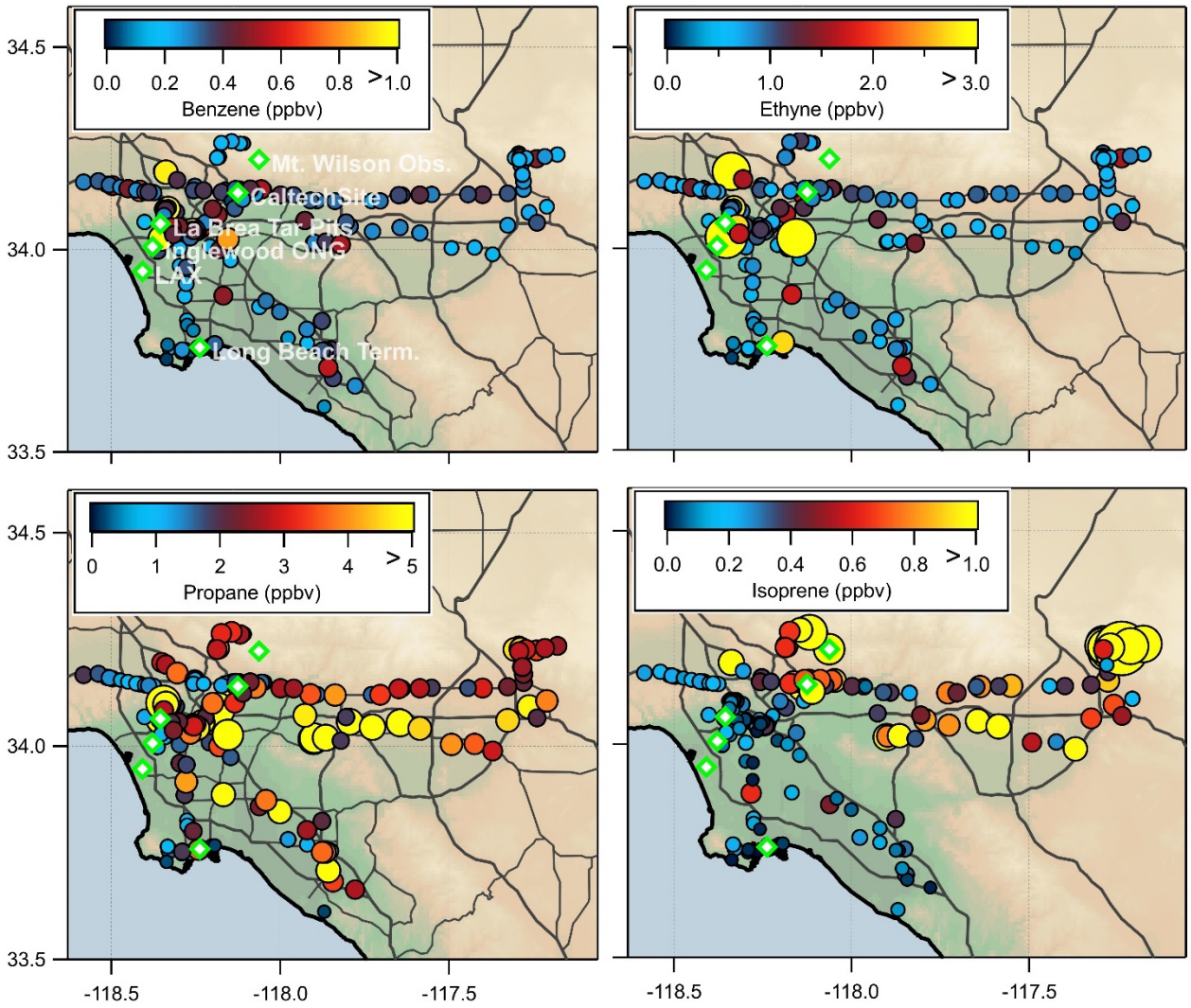


*Figure 17. Map of NOAA whole air samples collected along drive track in the South Coast Air Basin.*

### *3.2 VOC SOURCE SIGNATURES*

A comprehensive analysis of the VOC measurements that are used to identify the source signatures of various emission sources including volatile chemical products, cooking emissions, biogenic sources, and wildfire emissions. We present the results from RECAP-CA in comparison to recent field work in major US metropolitan areas has characterized the distribution of urban VOCs to assess the chemical fingerprint of understudied emission sources, such as VCPs and cooking.

#### *3.2.1 VOLATILE CHEMICAL PRODUCTS*

McDonald et al. [2018a] identified volatile chemical products as the largest petrochemical source of urban organic emissions in Los Angeles using observations from CalNex 2010. Following that work, we have utilized advancements in our scientific instrumentation, laboratory studies, and field studies in Boulder, CO and New York City, to identify and characterize unique tracers for various VCP emission sectors [Coggon et al., 2021b; Coggon et al., 2018b; Gkatzelis et al., 2021a; Gkatzelis et al., 2021d; Stockwell et al., 2021]. Here we compare the mixing ratios observed during RECAP-CA of the following tracers included in *Figure 18*:

D5-siloxane (Decamethylcyclopentasiloxane) is a tracer for personal care products as it is prevalent in shampoos, lotions, deodorants, and antiperspirants [Wang et al., 2009] and has been found to correlate well with population density [Gkatzelis et al., 2021d]. It is estimated that over 90% of D5-siloxane is emitted to the atmosphere through evaporative emissions after applying personal care products that contain D5-siloxane [Mackay et al., 2015]. The mean D5-siloxane mixing ratio observed in Pasadena was 0.040 ppbv. This is in line with concentrations observed in Boulder, CO (~ 0.010 ppb); Toronto, Canada (~0.050 ppb); and in New York City, NY (up to 0.100 ppb) [Coggon et al., 2018b; Stockwell et al., 2021]. The diel mean profile shows a gradual increase overnight with a diel mean maximum occurring at 07:00 local time coincident with the morning rush hour before decreasing throughout the afternoon. This is consistent with that observed in Toronto and Boulder. Coggon et al. [2018b] calculated D5-siloxane emission rates which peak between 06:00 and 07:00 local time and decay exponentially throughout the day. This can be attributed to increased product usage in the morning hours as people prepare for their daily activities and subsequent evaporation of D5-siloxane throughout the day.

PCBTF (para-chlorobenzotrifluoride) is a tracer for solvent-based coatings. PCBTF is classified as an "exempted" VOC by CARB, as PCBTF is not expected to contribute to ozone formation due to its low volatility. We observed a mean concentration of 0.08 ppbv PCBTF in Pasadena, which is comparable to that observed in New York City [Stockwell et al., 2021]. There was a spike in PCBTF (> 12 ppbv) on 8/25/2021 at 07:20 PDT from a local source showing that large, transient emissions of PCBTF could be prevalent in the Los Angeles Basin. The diel mean profile is markedly different that of the other tracers and benzene, a mobile source tracer, which we have scaled to match PCTBF for comparison. PCBTF's diel mean maximum is coincident with the LA plume arriving at the Pasadena site. This suggests that the PCBTF primary emission rate is greater during the daytime hours than the evening, perhaps due to faster evaporation and/or increased product usage during workday hours. The emission rate of PCBTF is significant enough to counteract the effects of increased boundary layer mixing and dilution in the afternoon.

Texanol (2,2,4-trimethyl-1,3-pentanediol monoisobutyrate, TPM) is a tracer for water-based coatings. Texanol is typically the most abundant VOC used in water-based architectural coatings and has no other commercial use other than in coatings [Goliff et al., 2012]. Goliff et al. [2012] first measured Texanol in southern California in 2009 with mean mixing ratios up to 0.020 ppbv in summertime mornings and 0.010

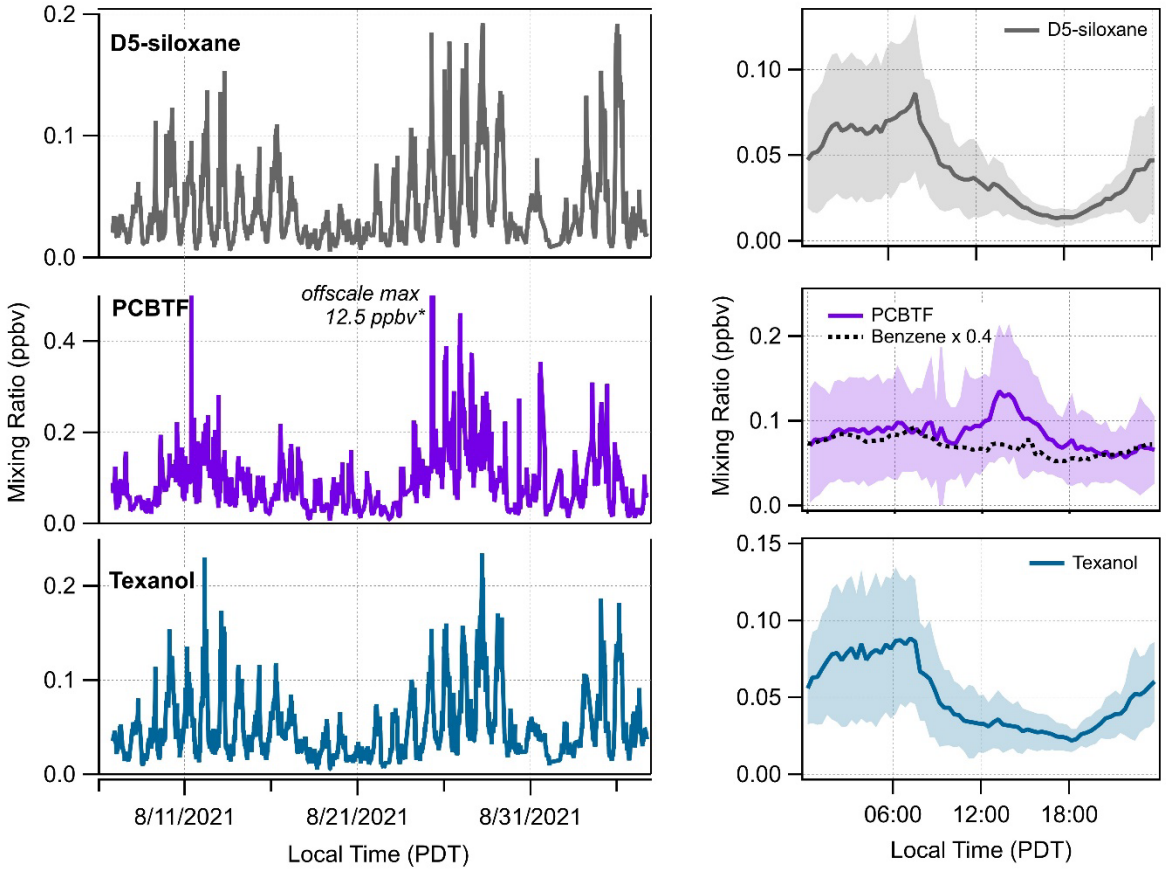


*Figure 18. Timeseries and diel mean profiles of D5-siloxane, PCBTF, and Texanol. Diel mean of benzene has been scaled to match PCBTF for ease of comparison.*

ppbv in the afternoons. They found that emissions were largest in summer when painting/coating/construction activities are typically the highest. During RECAP-CA we observed mixing ratios up to 0.23 ppbv, with a campaign-average of 0.05 ppbv. Mean morning concentrations were on the order of 0.08 ppbv, 4-fold higher compared to Goliff et al. [2012], and afternoon mean mixing ratios of 0.30 ppbv, which was still larger but more comparable to that observed in 2009. The diel profile of PCBTF is very similar to that of D5-siloxane where we attribute daytime minimums to increased mixing and dilution.

Ethanol, methanol, and acetone have a wide variety of urban sources including on-road mobile sources, cooking, and solvent usage. They are also common ingredients of many products such as personal care, cleaning, and coatings products. These species were amoung the most abundant VOCs measured during RECAP-CA. VOC emissions measured during CalNex 2010 and the New York Investigation of Consumer Emissions (NY-ICE) in New York City in 2018 were similarly dominated by methanol, ethanol, and acetone and were associated primarily with solvent usage [Gkatzelis et al., 2021a; McDonald et al., 2018a]. Acetone emissions in Los Angeles increased from 1990 to 2010 even though other hydrocarbons in gasoline exhaust markedly decreased [Warneke et al. 2012] indicating an increase in solvent-based emissions relative to on-road sources. The normalized diurnal profile analysis also suggests that acetone has an additional daytime source associated with photochemical production.

n-Hexane and dichloromethane are two species that had a large, localized source in close proximity to the RECAP-CA ground site. The mixing ratios of these two species were highly variable over very short timescales and had higher daytime mixing ratios than nighttime even though they are not expected to be photochemically produced in the atmosphere. We attribute the emissions of these two species to solvent usage on the Caltech campus, possibly from organic chemistry laboratories.

### *3.2.2 COOKING EMISSIONS*

During RECAP-CA, Coggon et al. [2023b] utilized the PTR-MS and GC-PTR-MS measurements aboard the NOAA Mobile Laboratory to characterize cooking emissions directly downwind of various restaurants in Los Angeles and in ambient air while parked at the Pasadena ground site. We briefly summarize the most relevant results here and refer the reader to the manuscript for more detail.

Cooking is a source of oxygenated VOCs that is rich in aldehydes and fatty acids [Klein et al., 2016a]. Studies that have speciated VOCs from a variety of Western cooking styles (e.g., charbroiling, grilling, frying) and ingredients (e.g., oils, meats, and vegetables) show that aliphatic $C_1$-$C_{11}$ aldehydes account for a large fraction of measured VOCs [e.g., Bastos et al., 2010; Klein et al., 2016b; Peng et al., 2017; Schauer et al., 1999a]. For example, Klein et al. [2016b] showed that aldehydes represent > 60% of the VOC mass emitted from frying or charbroiling meats and vegetables. The high abundance of aliphatic aldehydes from cooking suggests that they may be useful markers to constrain cooking VOC emissions in urban areas.

A time series of PTR-MS measurements from the NOAA Mobile Laboratory that was parked downwind of restaurants in Los Angeles, CA where large enhancements in VOCs were frequently observed is shown in *Figure 19*. Aliphatic aldehydes octanal and nonanal were among the major species observed in PTR-ToF-MS spectra. Traces for D5-siloxane (personal care product tracer) and benzene (motor vehicle emissions tracer) are included for context. The highlighted boxes show periods where the mobile laboratory was parked to sample restaurant emissions. All other data reflect sampling periods when the mobile laboratory was driven through densely populated areas of Los Angeles.

Aldehyde mixing ratios downwind of restaurants often exceeded 1 ppb, though differences were observed based on wind speeds and mobile laboratory proximity to restaurant exhausts. Generally, these mixing ratios were elevated relative to the surrounding densely populated regions. Octanal and nonanal mixing ratios were not significantly enhanced in tailpipe emissions, which is consistent with previous studies showing that on-road emission factors of these from US vehicles are low [Gentner et al., 2013a]. Nonanal and octanal were not strongly correlated with mixing ratios of D5-siloxane, though there were

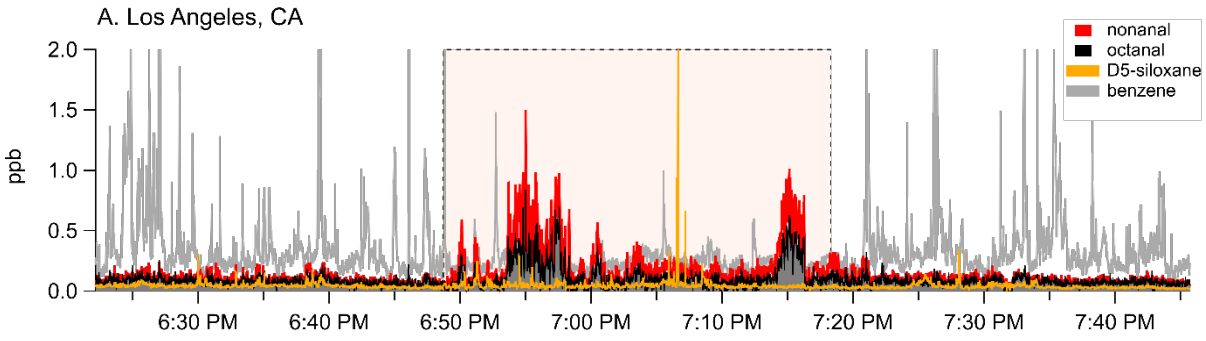


*Figure 19. Time series of NOAA Mobile Laboratory measurements of nonanal, octanal, D5-siloxane, and benzene in Los Angeles, CA. Figure adapted from Coggon et al. [2023b].*

periods when aldehyde and D5-siloxane enhancements were coincident. This may result from the co-location of food and people or a possible human emission source. Octanal and nonanal are known to be produced from skin ozonolysis [Liu et al., 2021; Wang et al., 2022] and carbonyls are potential ingredients in fragranced consumer products, though emissions inventories and measurements of fragrance formulations do not indicate that nonanal and octanal are significant components of VCPs [Hurley et al., 2021; McDonald et al., 2018a; Yeoman et al., 2020].

Ground site observations in Las Vegas and Los Angeles show temporal trends in aldehyde mixing ratios and demonstrate the importance of primary emission sources on regional scales. *Figure 20* shows the time series of octanal and nonanal at the ground sites in Las Vegas and Pasadena. The two species are well-correlated ($R^2$ > 0.86) and most abundant in the evening, which is due to a combination of meteorology (i.e., lower nocturnal boundary layer) and higher emissions. These patterns are in contrast to those of common OH oxidation products, such methyl vinyl ketone + methacrolein, which are mostly enhanced during the daytime when ozone and other secondary species are produced. These diurnal patterns suggest that secondary production is not a significant contributor to the temporal patterns of octanal and nonanal.

Nighttime mixing ratios of octanal and nonanal are correlated to other gases with primary sources, such as CO with $R^2$ = 0.68 (slope 3.8x10$^{-3}$ g g$^{-1}$) and 0.58 (slope 2.2x10$^{-3}$ g g$^{-1}$), respectively. This correlation is likely driven by meteorology and spatial/temporal overlap in emissions sources. Similar correlations have been observed for personal care product markers, such as D5-siloxane, which correlates to fossil fuel markers in cities due to the mixing of sources over coincident spatial and temporal scales [Coggon et al., 2018a; Gkatzelis et al., 2021a; Gkatzelis et al., 2021c]. This correlation of long-chain aldehydes to CO can be leveraged to estimate an emission rate for octanal and nonanal by multiplying the observed emission ratio with CO emission estimates. Similar approaches have been used to estimate emissions for other markers, including D5-sioxane and monoterpenes from VCPs [Coggon et al., 2021a; Coggon et al., 2018a;

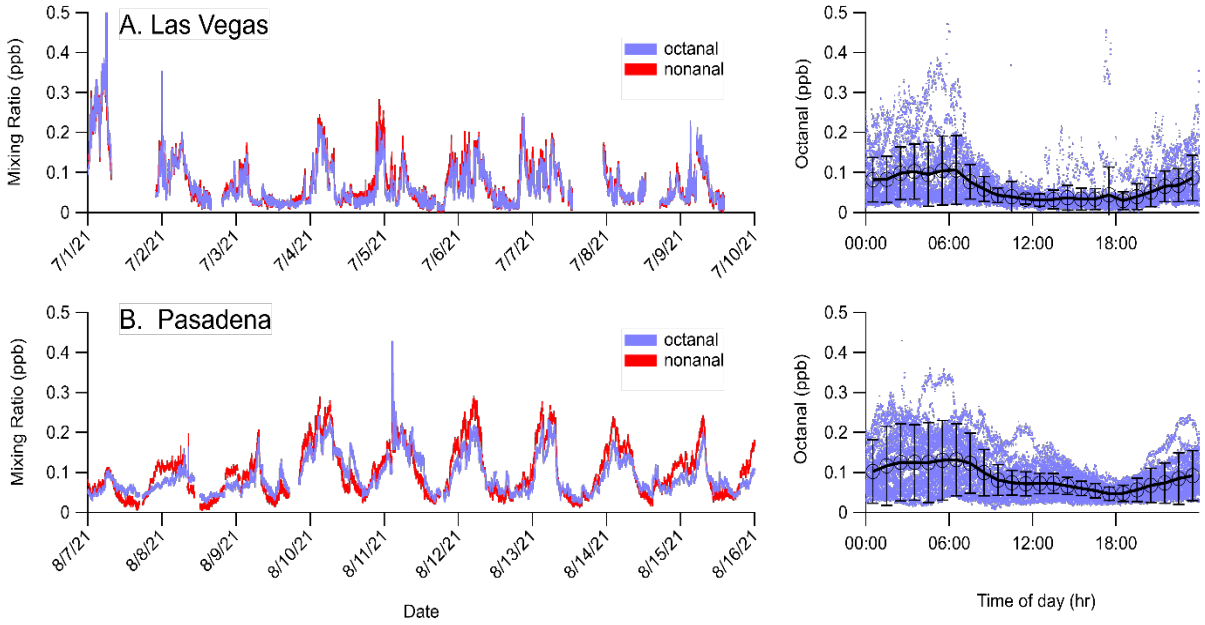


*Figure 20. Time series and diurnal pattern of octanal and nonanal in Las Vegas, NV and Pasadena, CA. Figure from Coggon et al. [2023b].*

Gkatzelis et al., 2021a; Gkatzelis et al., 2021c] and also evaluate emissions inventories against observations in Los Angeles [McDonald et al., 2018a]. CO emissions are reasonably represented by fuel-based emissions inventories and previous assessments of CO fluxes calculated from bottom-up inventories, such as FIVE-VCP, show good agreement with CO fluxes derived by aircraft mass balance methods [Coggon et al., 2021a]. Coggon et al. [2023b] validated the FIVE-VCP inventory in the Los Angeles Basin against aircraft and ground site observations during RECAP-CA. In the Southern California Air Basin, CO emissions were estimated to be $1.5x10^3$ t $d^{-1}$, or 88 g $person^{-1}$ $d^{-1}$ assuming a population of 17 million people. Multiplying these emission rates by the aldehyde emission ratios, we estimate that octanal and nonanal are emitted at a rate of 5.6 t $d^{-1}$ (or 0.33 g $person^{-1}$ $d^{-1}$) and 3.2 t $d^{-1}$ (0.19 g $person^{-1}$ $d^{-1}$), respectively [Coggon et al., 2023b].

### *3.2.3 BIOGENIC EMISSIONS*

Isoprene:

Biogenic emissions of isoprene and monoterpenes represent a significant source of reduced carbon to the troposphere affecting photochemistry from local to global scales [Guenther et al., 2006]. Isoprene is the dominant biogenic VOC emitted by urban foliage and is a major contributor to urban OH reactivity and ozone production [Calfapietra et al., 2013], so accurate identification and quantification of isoprene is important. We refer here to the work presented in Coggon et al. [2023] who identified the potential for substantial interferences on the isoprene signal (m/z 69, $C5H8^+$) from C8-C9 aldehydes emitted from cooking. As shown in *Figure 21*, the m/z 69 signal measured by the PTR-MS which is traditionally identified as isoprene had a positive bias compared to the GC-MS. This was especially prevalent during the nighttime when isoprene emissions are at their diel minimums but octanal and nonanal are still elevated. Coggon et al. [2023] details how to best correct for this interference and shows how the agreement between the GC-MS and PTR-MS improves for the RECAP-CA dataset ($r^2$ = 0.89 and Slope = 0.96).

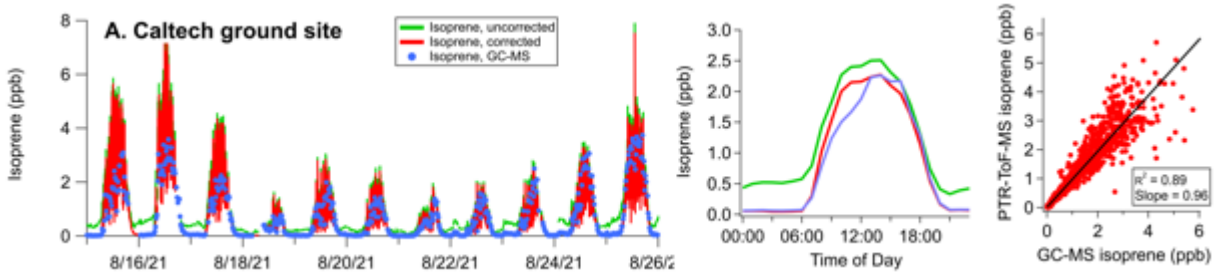


*Figure 21. Isoprene interference correction on the reported timeseries and diel pattern of isoprene at the Pasadena ground site. Figure adapted from Coggon et al. [2023].*

Monoterpenes:

In urban environments, monoterpenes consist of naturally emitted species from urban vegetation, such as alpha- and beta-pinene, along with isomers predominantly emitted from anthropogenic sources, such as limonene resulting from fragranced consumer products and degreasing agents [Coggon et al., 2021b; Gkatzelis et al., 2021b; Hurley et al., 2021]. In very densely populated regions, anthropogenic monoterpenes can outweigh emissions from natural sources [Coggon et al., 2021b]. Anthropogenic monoterpenes can be distinguished from natural emissions by evaluating the composition of the monoterpenes and their temporal variabilities, which we examine here.

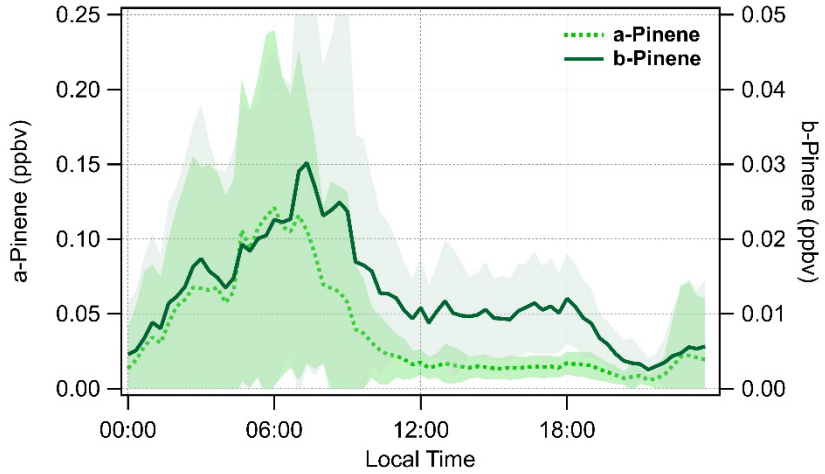


*Figure 22. Diel mean profiles of a-Pinene and b-Pinene during RECAP-CA.*

The diel mean profiles of alpha-pinene and beta-pinene are shown in *Figure 22*. These were the two dominant monoterpene isomers observed by the GC-MS at the Pasadena site. We monitored for other isomers including d-limonene, 3-carene, camphene, alpha-terpinene but these species were routinely at or below the limit of detection of the GC-MS so they were not quantified. The PTR-MS measures the sum of all the monoterpene isomers. The diel profile of the PTR-MS Sum Monoterpenes (not shown) is in excellent agreement with that of a-Pinene measured by the GC-MS; however, the PTR-MS reports a total monoterpene signal that is a factor 3 higher than the sum of a- and b-pinene isomers measured by the GC-MS. While we expect the total monoterpene signal to be greater than only two isomers, we do not expect that the two dominant isomers measured by the GC-MS to only account for 30% of the total monoterpene signal suggesting that the PTR-MS measurements are likely biased high. The mass attributed to monoterpenes on the PTR-MS might include fragments of monoterpenoids and monoterpene alcohols.

The diel means for a- and b-pinene both steadily increase during the evening hours as emissions continue to build in a shallow boundary layer. While both species are reactive with ozone and $NO_3$, which are the dominant nighttime oxidants [de Gouw et al., 2017], a-pinene is the more reactive of the pair. Interestingly, the diel profiles of the pinenes start to diverge starting at 07:00 PDT when the sunrises and temperatures begin to rise. The ratio of [b-pinene]/[a-pinene] remains elevated throughout the daytime hours indicating a much stronger daytime source for b-pinene relative to a-pinene. The daytime atmospheric lifetimes of the pinenes are approximately equal as the higher reactivity of a-pinene with ozone is offset by the higher reactivity of b-pinene with the hydroxyl radical. The stronger b-pinene daytime source appears to be mostly natural as the correlation between the pinenes remains strong ($r^2$ = 0.70). Any anthropogenic sources of monoterpenes were obfuscated by the large natural emission source at the Pasadena site.

Biogenic Oxidation Products:

Oxidation of isoprene results in the production of oxygenated VOCs including formaldehyde (HCHO), methacrolein (MACR), methyl vinyl ketone (MVK) and nitrogen-containing species such as isoprene nitrates (ISOPN) [Mayhew et al., 2022; Stroud et al., 2001]. These reaction products are also highly reactive and can further contribute to photochemical ozone and particulate formation. Here we examine the direct reaction products of isoprene oxidation observed during RECAP-CA as shown in *Figure 23*.

MVK, MACR, formaldehyde and isoprene nitrates have strong correlations with isoprene ($0.69 < r^2 < 0.83$). The larger variability of formaldehyde mixing ratios at low isoprene values indicate the presence of additional formaldehyde sources, which is expected for urban environments. The daily daytime mean values for isoprene = 1.94 ± 1.23 ppbv (± 1 stand. Dev.), MVK = 0.47 ± 0.35 ppbv, MACR = 0.42 ± 0.22 ppbv, and sum of isoprene nitrates as measured by the NOAA I-CIMS = 0.018 ± 0.013 ppbv. The ratio of [MVK]/[MACR] observed during the daytime was 1.13 and 0.88 at night. A higher daytime ratio is consistent with the higher production of MVK relative to MACR from isoprene oxidation (Isoprene + OH → 0.32 MVK + 0.23 MACR, [Carter et al., 1996]) and the faster removal of MACR by the OH radical. The observed daytime ratio of 1.13 is within 25% of that expected from direct isoprene oxidation indicating that the primary source of MVK and MACR in Pasadena is oxidation of isoprene rather than anthropogenic sources.

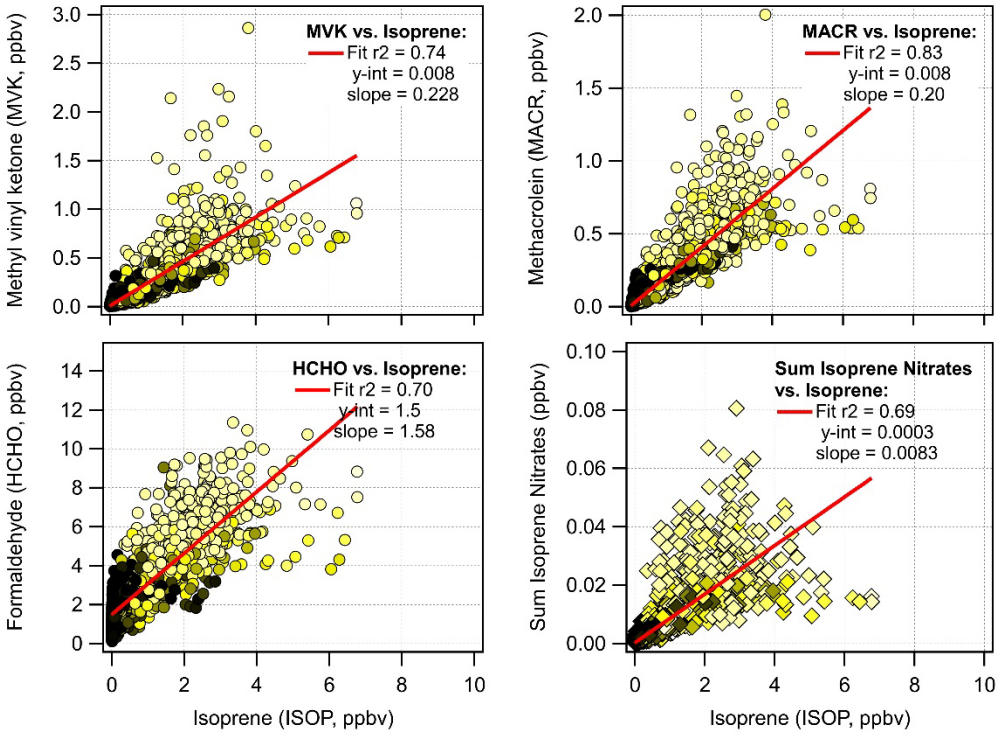


*Figure 23. Correlations of MVK, MACR, formaldehyde, and isoprene nitrates vs isoprene.*

### *3.2.4 WILDFIRE INFLUENCES*

Wildfires are large sources of CO, $CO_2$, NOx, toxic and reactive VOCs, and particulate matter – all of which degrade air quality and impact health. Wildfire emissions share many of the same chemical compounds as other anthropogenic combustion sources in urban areas (e.g., tailpipe emissions, cooking, residential wood burning, natural gas use, etc.), which could complicate source attribution of VOCs if/when wildfire and urban emissions mix. Here we identify benzonitrile as a distinct tracer of wildfire influenced air during the RECAP-CA measurements and suggests that only the longest-lived combustion tracers were influenced by aged smoke observed at the measurement site.

In recent years, there has been a substantial increase in the number of acres burned by wildfires over the last decade (*Figure 24*, data from www.fire.ca.gov). Four of the largest fires of 2021 occurred during the RECAP-CA measurement period. While these fires were located in Northern California far removed from Pasadena, there was a distinct particulate haze common to wildfire smoke that hung over the Los Angeles Basin during much of the measurement period. This haze is evident in the photo we took from the Mount Wilson Observatory while measuring with the NOAA Mobile Laboratory (*Figure 24*).


*Figure 24. Acres of land burned in California by year overlaid on photo from Mt. Wilson Observatory on 8/11/2021 [Photo credit: J. Gilman].*

Acetonitrile is a commonly used biomass burning combustion tracer [Coggon et al., 2016; Gilman et al., 2015]. Emissions of nitrogen-containing VOCs, such as acetonitrile, depend on the fuel nitrogen content which is higher for fuels burned in wildfires (i.e., natural vegetation that still contains a green/leafy component) compared to domestic wood burning (i.e., heartwood with a low nitrogen content) or other combustion sources [Coggon et al., 2016]. Additionally, Coggon et al. [2016] showed that solvent usage of acetonitrile, which is more prevalent in urban areas, complicates the use of acetonitrile as a biomass burning combustion marker. This is consistent with what we observed during RECAP-CA.

In Figure 25, we compare the acetonitrile versus CO correlations observed during RECAP-CA to those measured during the Fire Influence on Regional to Global Environments and Air Quality Experiment in 2019 (FIREX-AQ) [Gkatzelis et al., 2023]. There is a very weak correlation between acetonitrile and CO during RECAP-CA data, but the observed mixing ratios are within the ranges observed during FIREX-AQ 2019. The slope of acetonitrile versus benzene ( slope = 29 ± 2 ppbv/ppbv) is a factor of 2 greater than that observed from wildfire emissions [Gilman et al., 2015]. Transient spikes in acetonitrile that are not associated with CO or benzenenitrile are likely from use of acetonitrile as a solvent.

Benzenenitrile observed during RECAP-CA was at very low concentrations (mean background = 0.002 ppbv) and had small sample-to-sample variability for the majority of RECAP-CA as shown in the time series in *Figure 12*. This indicates that there is no large anthropogenic/urban emission source of benzenenitrile in close proximity of the Pasadena site. As shown in *Figure 12*, the background levels of benzenenitrile broadly increased from 2 pptv up to 10 pptv between 8/22 to 9/1/2021, with the apex occurring on 8/26/2023. In *Figure 26*, we compare HRRR-smoke forecasts for days when benzenenitrile was at its background minimum (8/19/2021, left panel) and at its apex (8/26/2021, right panel) indicating that there

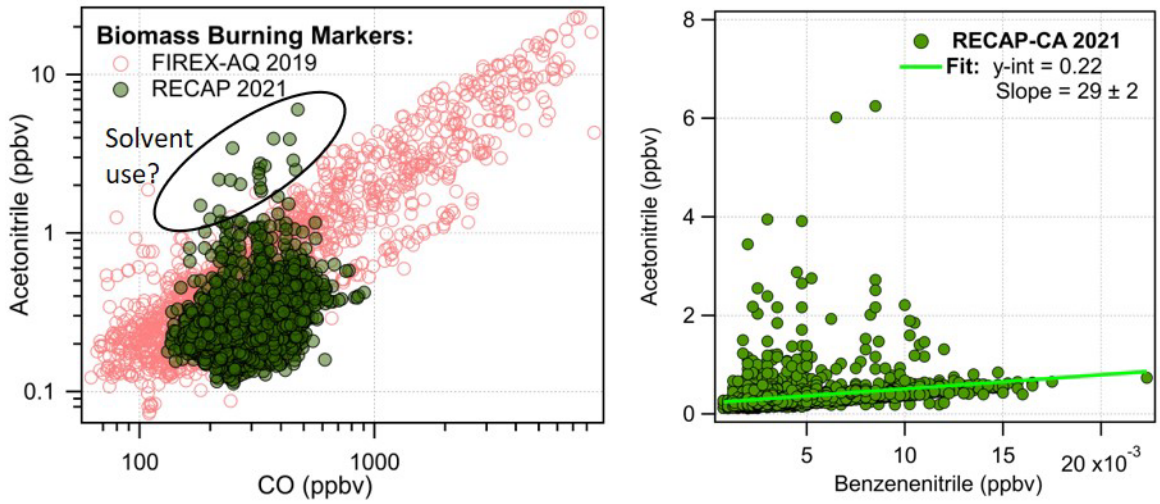


Figure 25. Correlations of acetonitrile with CO and benzenenitrile.

was wildfire influenced air impacting the measurement site coincident with the broad increases in benzenenitrile background values.

Using benzenenitrile as our indicator for wildfire emissions, we looked for similar baseline features and/or correlations with all other VOCs and trace gases measured at the Pasadena site. There was a distinct change in the background values of CO, which increased from 0.143 to 0.212 ppmv CO, that we attribute to the wildfire emissions as discussed in *Section 3.3.1*. There were only minor influences on the background levels of benzene and ethyne that may be attributed in part to wildfire emissions. Overall, we assess that any wildfire influenced air impacting the Pasadena site was well aged and was not a significant source of reactive VOCs such as alkenes, aromatics, or furans.

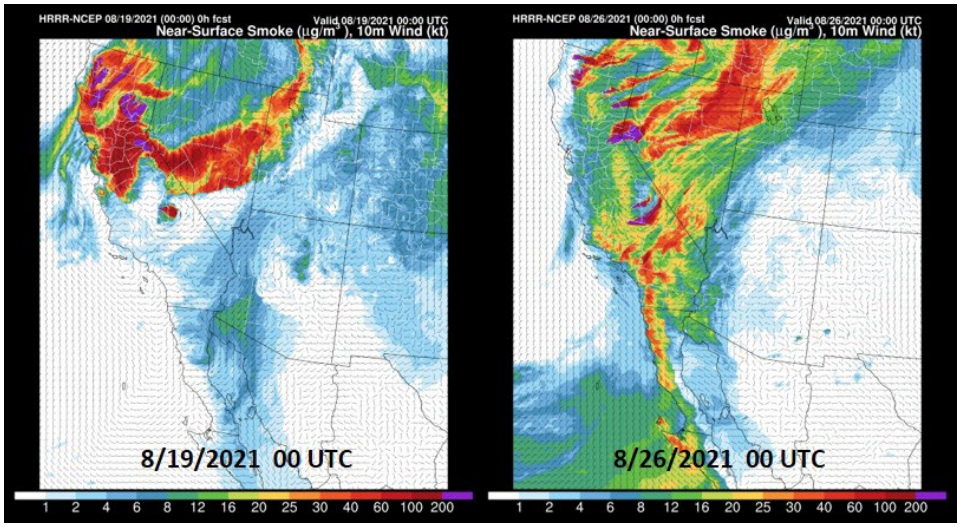


*Figure 26. HRRR-Smoke 0-hour forecast for near-surface smoke at 00 UTC (1700 PDT – 1 day) for the dates shown. Warmer colors represent higher particle counts attributed to smoke. Wind barbs indicate wind speed (knots) and direction at 10 m.*

### *3.2.5 NATURAL GAS SOURCES*

One feature of the RECAP-CA dataset was the unexpectedly high concentration of ethane, particularly at night, when compared to other light alkanes and those observed during CalNex 2010 (refer to *Figure 14*). As shown in *Figure 27*, ethane was tightly correlated with methane (Slope = 36.81 ppbv ethane/ppmv $CH_4$, $r^2$ = 0.95) during RECAP-CA suggesting a common fossil source. Peischl et al. [2013] quantified the sources of methane and ethane in the Los Angeles Basin and showed that the largest common source of these two species is from pipeline dry natural gas. The ethane/methane enhancement ratio observed during RECAP-CA is a factor of 1.8 greater than that observed during CalNex 2010 and a factor of 2 higher than that expected from pipeline-quality dry natural gas and traffic emissions [Peischl et al., 2013]. However, Wunch et al. [2016] reports that since 2010, the emissions of methane have been steady while ethane emissions have nearly doubled from 2007-2016. The observed increase in ethane is to be expected if natural gas emissions continue to be one of the largest sources of methane to the Los Angeles Basin. The same tight correlation and slope was observed during three different flights over the Los Angeles Basin as part of the Atmospheric Emissions and Reactions Observed from Megacities to Marine Areas (AEROMMA) campaign in August 2023 (*Figure 27*). We note that AEROMMA dataset is preliminary field-quality data.

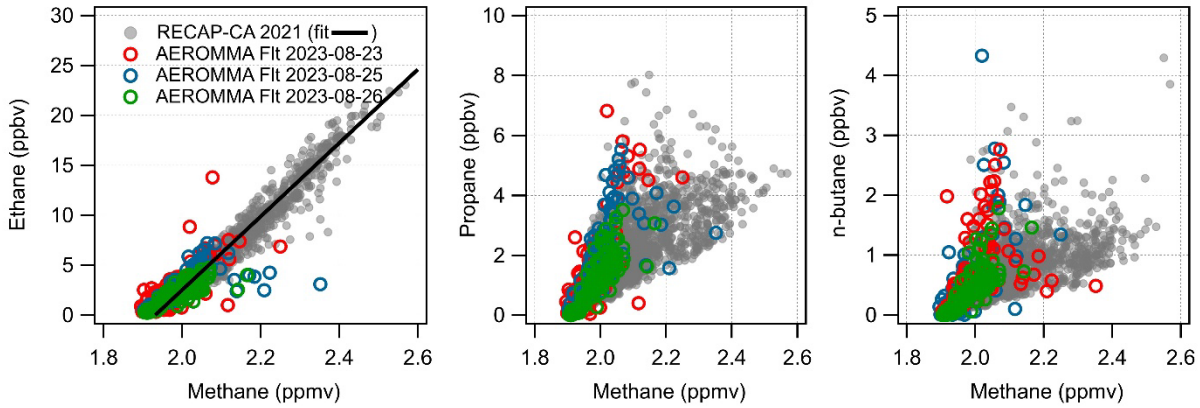


*Figure 27. Correlations of ethane, propane, and n-butane with methane for RECAP-CA ground based and AEROMMA 2023 airborne measurements.*

We observed a wider range of propane/methane and n-butane/methane ratios at the RECAP-CA ground site and during the AEROMMA flights. Both propane and n-butane were determined to be largely emitted from local natural gas production in the Los Angeles Basin [Peischl et al., 2013]. All three gases are commonly used fuels for heating and/or cooking, while n-butane is also used as a propellent in aerosolized products (i.e., from VCP usage).

The spatial distribution of ethane (natural gas tracer) and benzene (mobile source tracer) are compared for the AEROMMA samples collected aboard the NASA DC-8 research aircraft as it conducted low-altitude flights across the basin as shown in *Figure 28*. Both analytes show a strong east/west gradient commonly observed from onshore wind flow and the accumulation of pollutants along the base of the San Gabriel and San Bernardino Mountains. Both ethane and benzene have the largest enhancements over central Los Angeles Basin, but ethane also has a larger enhancement relative to benzene over the Port of Long Beach area.

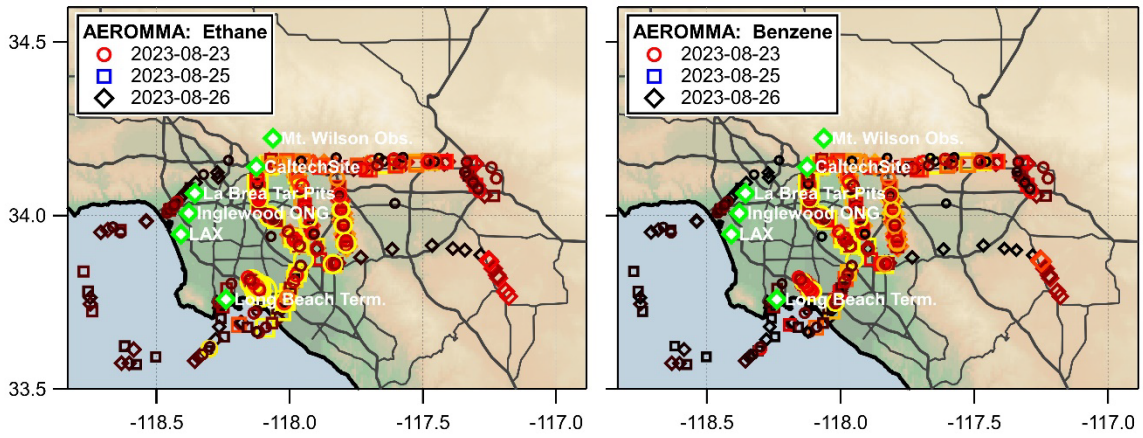


*Figure 28. Map of NOAA iWAS samples from AEROMMA 2023 flights over the Los Angeles Basin colored and sized by ethane and benzene mixing ratios.*

856

857 ### *3.3 EMISSION RATIOS*

858 VOCs can be strongly affected by chemical transformation processes, so that the observed
859 enhancement ratios can be significantly different from actual emission ratios, particularly for the most
860 reactive VOCs. Here we determine emission ratios relative to carbon monoxide (CO) and ethyne
861 (acetylene, $C_2H_2$) by employing methods detailed in de Gouw et al. [2017 and 2018]. We can account for
862 the effects of chemical removal and/or formation of various VOCs by 1) using nighttime data only, when
863 chemical losses or production from OH chemistry are minimized but reactions with $NO_3$ and $O_3$ should be
864 considered, or 2) by extrapolating to a photochemical age of zero using VOC ratios that are selectively
865 sensitive to a particular oxidant. We note that the emission ratios determined by these techniques
866 represent the total urban emissions. Individual source categories cannot be easily distinguished by this
867 method. A table with all emission ratios is included in Appendix Table 2.

868 We then compare the emission ratios determined from the RECAP-CA 2021 dataset to those from
869 CalNex 2010 [Borbon et al., 2013; de Gouw et al., 2018; de Gouw et al., 2017] and the Los Angeles Air
870 Quality Study (LAAQS) which took place from April to July 2020 on the Caltech campus during the COVID-
871 19 pandemic [Van Rooy et al., 2021]. During LAAQS 2021 study, traffic counts ranged from 55% to 80%
872 of their pre-COVID levels as many people switched to working remotely. Urban VOC/CO emission ratios
873 can be used to validate and/or improve emissions inventories. Here we compare the RECAP-CA emission
874 ratios to NOAA's Fuel-based Inventory of Vehicle Emissions with Volatile Chemical Products (FIVE-VCP) as
875 described in 2.12.

876 #### *3.3.1 CORRECTING FOR VARIABLE CO BACKGROUND DURING RECAP-CA*

877 Here we document the variability in the "background" carbon monoxide (CO) mixing ratios observed
878 during RECAP-CA and how we corrected the CO mixing ratios to account for the enhanced background
879 due to wildfire emissions examined in *Section 3.2.4*. *Figure 29* shows a timeseries of 1-minute averaged
880 data and daily mean values between 1700-1859 PDT for a) CO and benzenenitrile, a long-lived biomass

burning tracer, and b) $CO_2$. A transition period occurs between approximately 8/21/2021 and 9/3/2021 where there is an enhancement in the CO background, which leads to a bifurcation in nearly all correlation plots when comparing trace gas measurements with CO. As an example, the bottom panel in *Figure 29* shows a clear increase in the daily mean $CO/CO_2$ ratio during the time of enhanced CO background shown by the blue box.

In order to simplify the analysis for all CO correlations and VOC/CO emission ratio calculations, we have corrected CO for this enhanced background by subtracting 0.084 ppmv CO for all data between 8/21/2021 19:30 and 9/3/2021 19:29 PDT. While the enhanced CO background occurred gradually (i.e., not a step function), we choose this time window based on the observed changes in the $CO/CO_2$ and

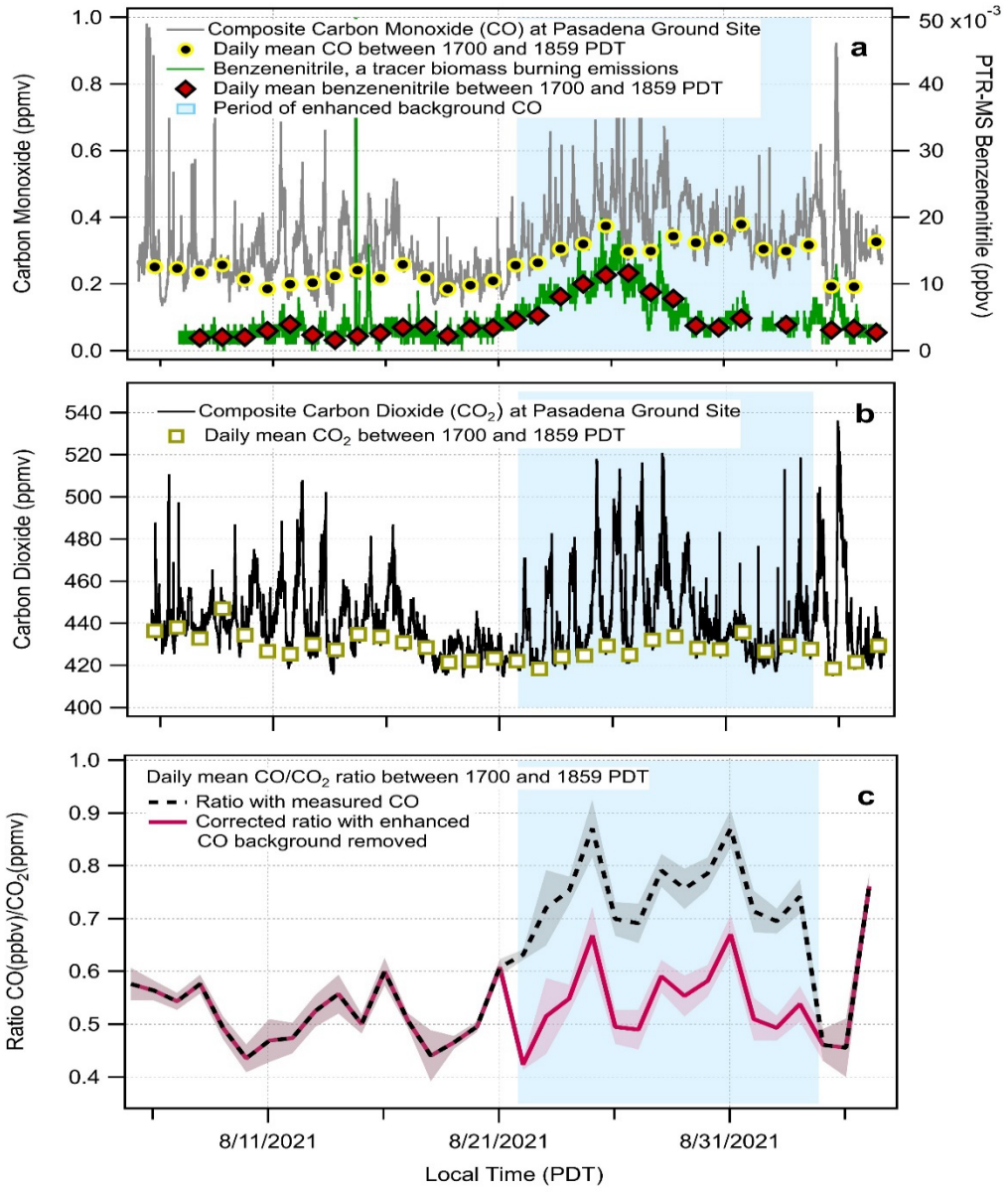


*Figure 29. Time series of CO, $CO_2$, benzenenitrile, and ratio of $CO/CO_2$ used to identify time period of enhanced CO background from wildfire emissions.*

VOC/CO ratios and split the data at the day-to-night transition time. *Figure 30* displays the cumulative probability distributions of the observed CO and $CO_2$ mixing ratios for 1-minute averaged data at the Pasadena site. While the cumulative probability curves for $CO_2$ are comparable for the two data subsets ("normal" and "enhanced" CO backgrounds), there is a marked difference in the CO probability curves. When comparing the 0.1$^{th}$-percentile, CO = 0.212 ppmv for the "enhanced CO background" time period while CO for all other data is 0.128 ppbv which more closely matches the expected seasonal CO background value. The difference between the 0.1$^{th}$-percentile values is 0.084 ppmv CO, which was the value used to correct the CO background to better match the "seasonal background" value. The result of this correction is shown in *Figure 29c* where the $CO/CO_2$ ratios is now more consistent across the entire measurement period. The corrected composite CO mixing ratio data will be used for all analysis utilizing CO correlations.

For all ΔVOC/ΔCO calculations, we use an overall $CO_{bnkd}$ value of 0.143 ppmv which corresponds to the 1$^{st}$ percentile shown in *Figure 30* and from the analysis of CO/VOC ratios. The $CO_{bknd}$ estimated for this work is 24-60% greater that reported by de Gouw [2017] $CO_{bknd}$ = 0.115± 10 ppmv and Van Rooy [2021] $CO_{bknd}$ = 0.090 ± 15% ppmv for measurements made at Caltech in 2010 and 2020, respectively.

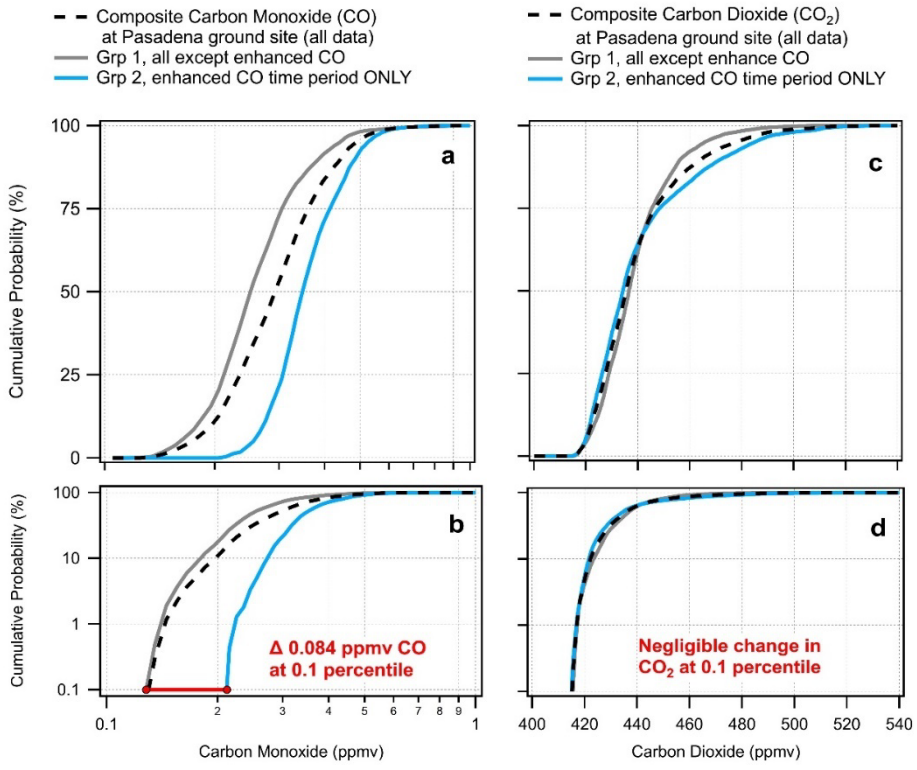


*Figure 30. Cumulative probability curves used to quantify CO and $CO_2$ backgrounds.*

### *3.3.2 NIGHTTIME EMISSION RATIOS TO ETHYNE AND CO*

Nighttime enhancement ratios are commonly used as proxies for emission ratios because photochemical processing is minimal at night for the majority of compounds except those that react efficiently with ozone and/or the nitrate radical ($NO_3$). Nighttime enhancement ratios are simple to calculate and are useful to compare observations across datasets as the ratios will minimize the effects of air mass mixing and dilution. CO and ethyne are commonly used denominators because they are routinely measured and combustion sources are a large source of VOCs in urban areas.

For this analysis, we calculated the slopes of the correlation plots of all gas-phase species measured during RECAP-CA versus both CO and ethyne for nighttime data (22:00-05:00 PDT) and daytime (10:00-18:00 PDT) only data. Each VOC and trace gas were first averaged over the GC-MS sample collection time and was lightly filtered by masking any samples with VOC/CO ratios greater than 2x the standard deviation of the mean. This was done to minimize the effects of any transient, extremely localized sources of a particular analyte would bias the slope.

Correlation plots of ethyne, propene, and 1,3-butadiene versus CO are shown in *Figure 31*. Ethyne and CO correlate well and have similar daytime and nighttime enhancement ratios (Night ER = 3.7 ppbv ethyne/ppmv CO, r = 0.89). The daytime ratios are much lower for propene and 1,3-butadiene owing to their faster daytime reactions with the hydroxyl radical ($k_{OH+ethyne}$ = 0.8 x$10^{-12}$, $k_{OH+propene}$ = 26x$10^{-12}$, $k_{OH+1,3-butadiene}$ = 67x$10^{-12}$ $cm^3$ $molec^{-1}$ $s^{-1}$ at 298K). Using nighttime data only minimizes the effect of OH chemistry, but emissions ratios determined by this method may be underestimated for species that are highly reactive with ozone ($k_{O3+VOC}$ > $10^{-16}$ $cm^3$ $molec^{-1}$ $s^{-1}$at 298K) and/or the nitrate radical ($k_{NO3+VOC}$ > $10^{-13}$ $cm^3$ $molec^{-1}$ $s^{-1}$at 298K) which may still be prevalent at night. We note that nearly all species had stronger correlations with CO at night compared to ethyne and that, overall, correlations were weaker than those observed during CalNex 2010. This may be indicative of non-combustion sources becoming more prevalent in the Los Angeles Basin over the last decade.

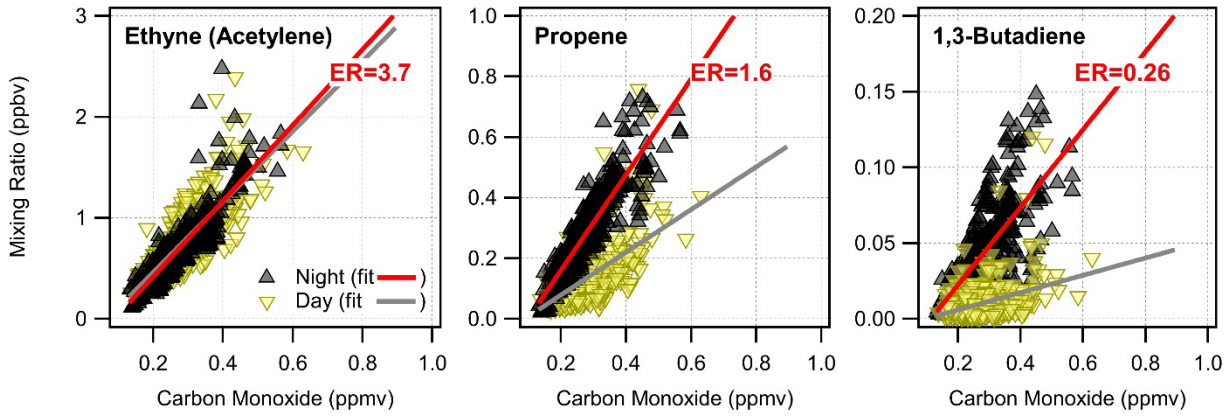


*Figure 31. Comparison of VOC/CO ratios for nighttime and daytime only.*

The VOC/CO and VOC/ethyne nighttime emission ratios for RECP-CA are compared to CalNex 2010 and LAAQS 2020 in *Figure 32*. Overall, the VOC/CO nighttime emission ratios for RECAP-CA agree within a factor of two compared to both CalNex 2010 and LAAQS 2020. When comparing the VOC/ethyne ratios, RECAP-CA was a factor of 2 higher than CalNex 2010. This is mainly driven by larger VOC/ethyne ratios for many oxygenated VOCs, which could be indicative of a shift in the relation between hydrocarbon combustion sources and oxygenated VOC emissions over time. Overall, RECAP-CA observed lower VOC/ethyne ratios for many of the hydrocarbons except for the C7+ alkanes. This could be due to a

difference in sampling locations or due to higher evaporative losses of these species during the warmer RECAP-CA experiment. Ethane is the one species that is an outlier in all comparisons. As discussed in *Section 3.2.5*, ethane was much higher at night during RECAP-CA than that observed during CalNex. Van Rooy et al. [2021] reported a nighttime ethane/CO emission ratio of 58.34 ppb/ppmv CO that is almost a factor of two higher than that from RECAP-CA (ER = 30.3 ppb/ppmv CO), both of which are substantially higher than CalNex 2010 (ER = 18.4 ppbv ethane/ppmv CO) [Borbon et al., 2013].

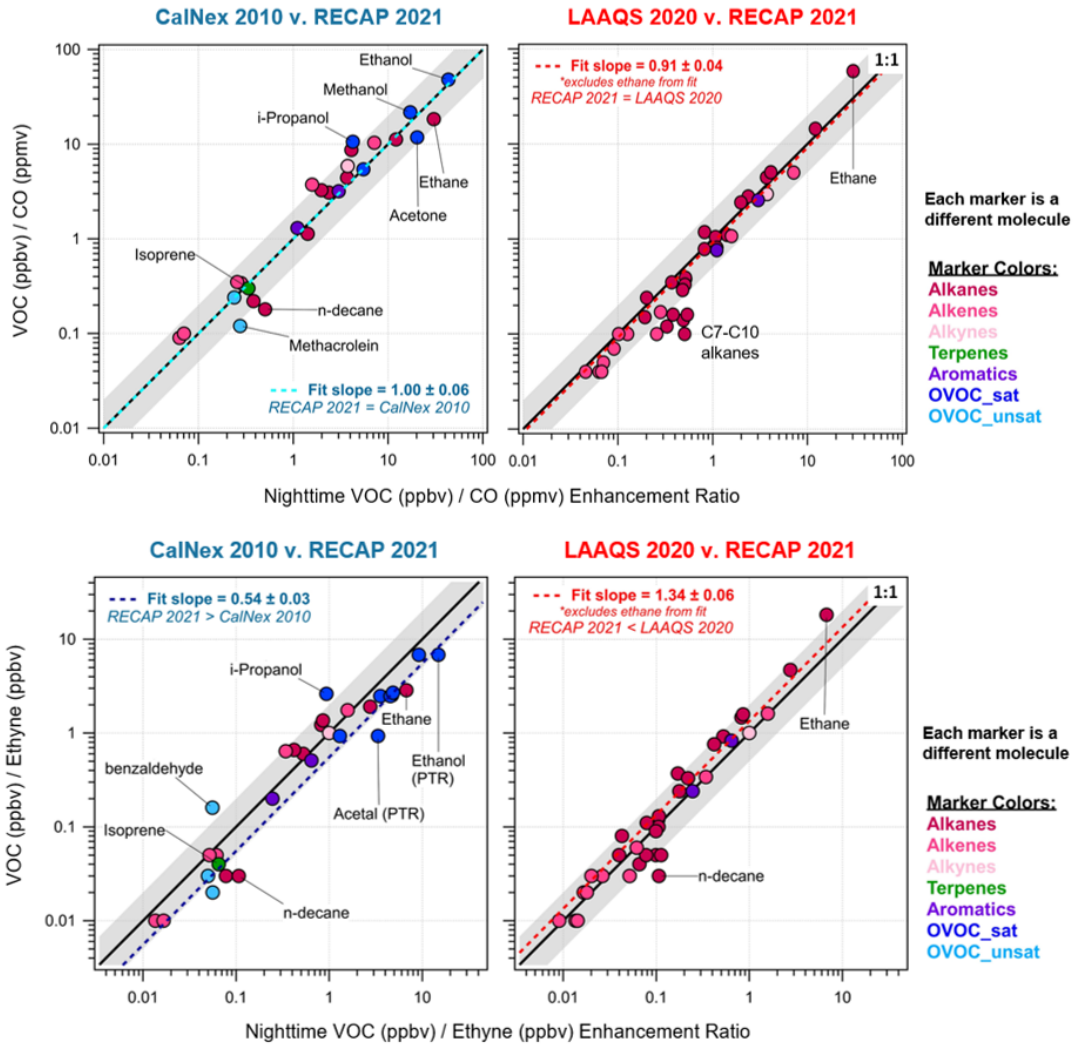


*Figure 32. Comparison of RECAP-CA 2021 VOC/CO and VOC/ethyne emission ratios determined using nighttime data are compared to previous measurements in Pasadena, CA as part of CalNex 2010 [Borbon et al, 2013] and LAAQS 2020 [Van Rooy et al., 2021]. Each marker represents a different VOC. The markers are color coded by the compound class. The solid black line is the 1:1 and the grey shaded region represents the 2:1 and 1:2 bands.*

### *3.3.3 PHOTOCHEMICAL AGE METHOD FOR EMISSION RATIOS*

Here we determine emission ratios using the photochemical age method using the kinetic-based equations detailed in de Gouw et al. [2017, 2017]. The photochemical age method utilizes observed hydrocarbon ratios to estimate the degree of photochemical processing that an air mass has experienced. The correlation of the observed VOC/CO ratios are then extrapolated to zero photochemical age, which is defined as the emission ratio. Various hydrocarbon ratios can be utilized to examine the effects of oxidation via OH radical or ozone, referred to here as the "OH-exposure" and "$O_3$-exposure". There are several steps involved in the calculation of emission ratios using this method including determination of background CO ($CO_{bknd}$) used to correct CO ($\Delta CO = CO_{obs} - CO_{bknd}$), calculation of the OH- and $O_3$-exposures, and fits to the kinetic equations used to determine the $\Delta VOC/\Delta CO$ emission ratios. We discussed how we arrived at a $CO_{bknd}$ = 0.143 ppbv ± 15% Section 3.3.1.

Evidence for the need to correct the observed nighttime $VOC/\Delta CO$ ratios to account for reactions with nighttime oxidants is highlighted in *Figure 33*. Here we plot the median daytime to nighttime mixing ratios of all hydrocarbons and halocarbons (excluding biogenics) versus their reaction rate coefficient with the hydroxyl radical ($k_{OH}$). With a few exceptions, the decrease in the daytime mixing ratios can be explained by a single exponential fit. The outliers dichloromethane ($C_2Cl_2$), ethane, and n-hexane were shown to have significant emission sources from non-mobile sources (ethane = natural gas usage, dichloromethane and n-hexane = local solvent usage). The remaining outliers are all alkenes which are reactive with ozone. The higher than expected daytime/nighttime ratio can be explained by removal via nocturnal ozone oxidation which will cause the ratio to increase above that expected from daytime OH-oxidation alone.

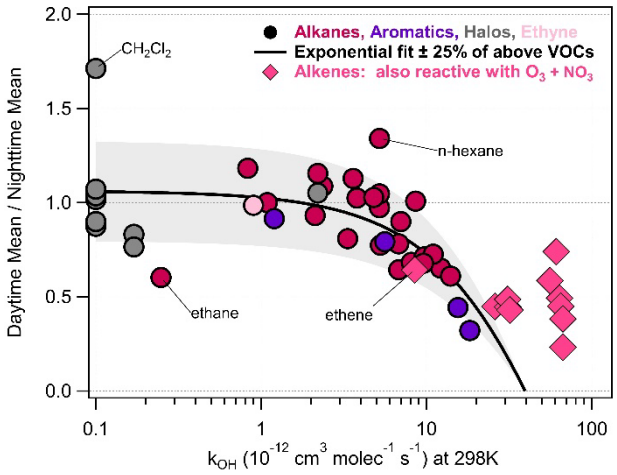


*Figure 33. Ratio between daytime and nighttime median mixing ratios versus the reaction rate for different hydrocarbon species measured during RECAP-CA. An exponential fit*

Determination of OH-Exposure:

The time-integrated exposure of VOCs to OH, here referred to as OH-exposure or $[OH]\Delta t$, can be calculated using hydrocarbon pairs that are emitted from similar sources but have substantially different reaction rates with the hydroxyl radical. Traditional pairs include benzene with either toluene or 1,2,4-trimethylbenzene. For RECAP-CA, we utilized the sum of the C8 and C9 aromatics from the PTR-MS because we were unable to quantify the individual isomers via GC-MS. We determined emission ratios of

[Benzene]/[C8-Aromatics] = 0.457 ppbv/ppbv and [Benzene]/[C9-Aromatics] = 0.853 ppbv/ppbv using the y-intercept of the correlation plots and analysis of the timeseries of the ratios such as that shown for the diel mean profile of [Benzene]/[C8-Aromatics] ratio in *Figure 34*. Because we are using the sum of several isomers we had to estimate $k_{OH+C8\text{-}Aro}$ = 15.5 x $10^{-12}$ and $k_{OH+C9\text{-}Aro}$ = 23.6 x $10^{-12}$ $cm^3$ $molec^{-1}$ $s^{-1}$ at 298K based on the distribution of C8- and C9-aromatics observed during CalNex 2010 and LAAQS 2020. A comparison of the calculated OH-exposure using two different hydrocarbon pairs is shown in *Figure 34*. We use the average of the calculated OH-exposures for all subsequent calculations. The maximum of the diel mean OH-exposure = 7.5 x $10^{10}$ molecules $cm^{-3}$ s. We estimate the uncertainty for the OH-exposure calculations at ± 30%. This is in good agreement with LAAQS 2020 [Van Rooy et al., 2021], but is higher than that determined for CalNex 2010 = 3.2 x $10^{10}$ molecules $cm^{-3}$ s [de Gouw et al., 2017]. The greater OH exposure for RECAP-CA relative to CalNex is likely due to the higher temperatures, increased sunlight, and ozone observed during RECAP-CA. Van Rooy et al. [2021] also notes that NOx levels during LAAQS 2020 were approximately 50% lower compared to 2010 which would result in a smaller sink related to $NO_2$+OH reactions leading to an increased OH lifetime with respect to $NO_2$.

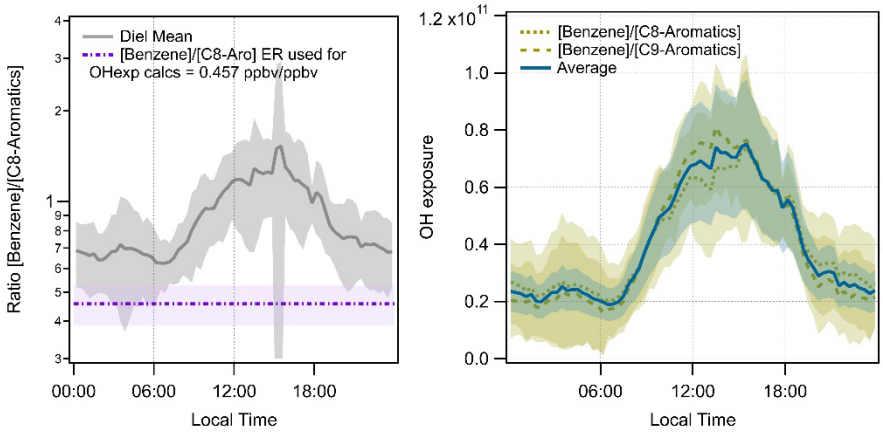


*Figure 35. Diel mean of [Benzene]/[C8-aromatics] ratio and comparison of OH exposure calculated using various hydrocarbon pairs.*

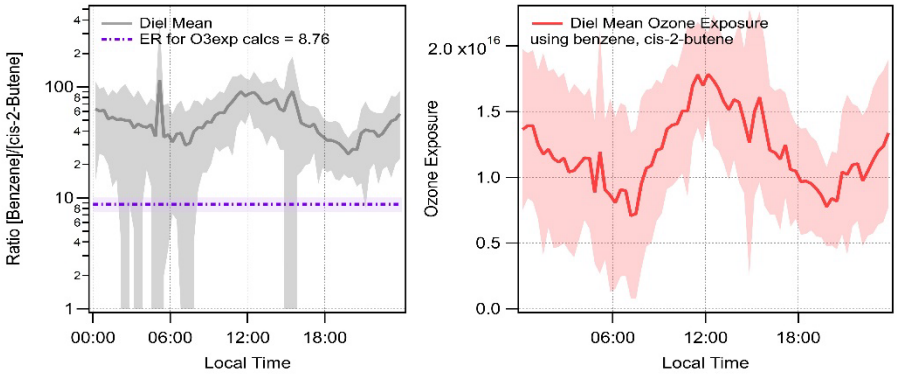


*Figure 34. Comparisons of the diel mean profiles for O3-exposure calculated using various hydrocarbon pairs (left) and comparison of the diel mean profiles for OH- and $O_3$-exposures used for this analysis (right).*

Determination of $O_3$-exposure:

The time-integrated exposure of VOCs to ozone, referred to here as $O_3$-exposure or $[O_3]\Delta t$, is calculated in a similar manner as the OH-exposure but here we utilize hydrocarbon pairs that have similar sources but differing reaction rates with ozone. The results for the $O_3$-exposure calculations are shown in *Figure 35*. The maximum of the diel mean $O_3$-exposure = 1.7 x $10^{16}$ molecules $cm^{-3}$ s. We estimate the uncertainty for the $O_3$-exposure calculations at ± 30%. The diel mean maximum for $O_3$-exposure during RECAP-CA is nearly identical compared to CalNex 2010 even though ozone concentrations were higher during RECAP-CA [de Gouw et al., 2017]. Reactions of the hydrocarbon pairs used to determine $O_3$-exposure will also react with hydroxyl radical as there is no hydrocarbon that reacts exclusively with ozone and not OH. For this reason, we will only use nighttime data when extrapolating VOC/ΔCO ratios to zero $O_3$-exposure.

Multivariate Functions Used to Derive Emission Ratios:

We refer the reader to the kinetic-based equations detailed in de Gouw et al. [2017, 2018] as we will present a simplified discussion here. We used three different multivariate functions to fit the observed variability in select VOCs as a function of ΔCO, $k_{CO+OH}$ = 0.05x$10^{-12}$ $cm^3$ $molec^{-1}$ $s^{-1}$ at 298K, and either OH- or $O_3$-exposures in order to mathematically solve for VOC background mixing ratios ($VOC_{bknd}$), emission ratios (ΔVOC/ΔCO), and chemical reactivities of the analytes.

- **Method 1**: This fit function is used to derive emission ratios of all hydrocarbons and select oxygenated VOCs that are expected to have only primary emission sources (negligible secondary formation) and are reactive with the hydroxyl radical. This is referred to as the OH-exposure corrected emission ratios. Background values were manually set to zero for highly reactive species ($k_{OH}$ > 5 x $10^{-12}$).
- **Method 2**: This fit function is similar to method one except we utilize the $O_3$-exposure metric to fit the observed nighttime mixing ratios of reactive alkenes with ozone. This is referred to as the $O_3$-exposure corrected emission ratios. All $VOC_{bknd}$ were set to zero.
- **Method 3**: This fit function includes an additional term that relates to the potential for secondary formation from unknown precursors. The observed variability in select oxygenated VOCs is then fit using the OH-exposure metric and solved for the emission ratios (ERs) related to primary emissions of the oxygenate-VOC ($ER_{ovoc}$) and the primary emissions of the hydrocarbon precursors ($ER_{Precursors}$) and their reactivities with the hydroxyl radical. For oxygenated VOCs that have strong primary emission sources, the derived emission ratios will be similar to that determined by Method 1. We present both results in Appendix Table 2 for select species.

Comparison of the Multivariate Function Results:

In *Figure 36* we compare the mixing ratios determined from the multivariate regression analysis to the measurements for each method used in order to assess how well the multivariate function was able to predict ambient mixing ratios for the given inputs and constraints. There was good to excellent agreement between the modeled and measured results for a majority of the analytes. There was a higher degree of variability for species such as ethane (fit v. meas. $r^2$ = 0.52), which has a large emission source that does not correlate strongly with CO and it is not particularly reactive so it will have a weaker dependence on the OH-exposure.

Compared to the nighttime VOC/CO emission ratios for the reactive alkenes (Section 3.3.2), the OH-exposure corrected emission ratios were 13-57% and the $O_3$-exposure corrected emission ratios were 17-

90% higher. Clearly it is important to account for chemical removal of highly reactive alkenes in order to accurately determine their emission ratios.

Acetaldehyde was readily resolved by Method 3 into its three principal components: background ($VOC_{bknd}$ = 0.45 ± 0.02 ppbv, 33% of total resolved mixing ratio), primary emissions ($ER_{acetal}$ = 2.10 ppbv ppmv $CO^{-1}$, 11% of resolved mixing ratio) and secondary production (55% of resolved mixing ratio). The only other OVOCs that had a non-negligible contribution from secondary production were MEK, formic acid, and methyl acetate. We could not get the equation to solve properly for formaldehyde, methyl vinyl ketone, and methacrolein. These fits would not converge properly and would return a negative emission ratio no matter the number of free or constrained variables. We think this is due the domination of secondary production sources causing the model to overcompensate and push the primary emission ratio calculation into the negative. The variability for all other oxygenated VOCs was attributed solely to primary emissions with a small contribution from $VOC_{bknd}$.

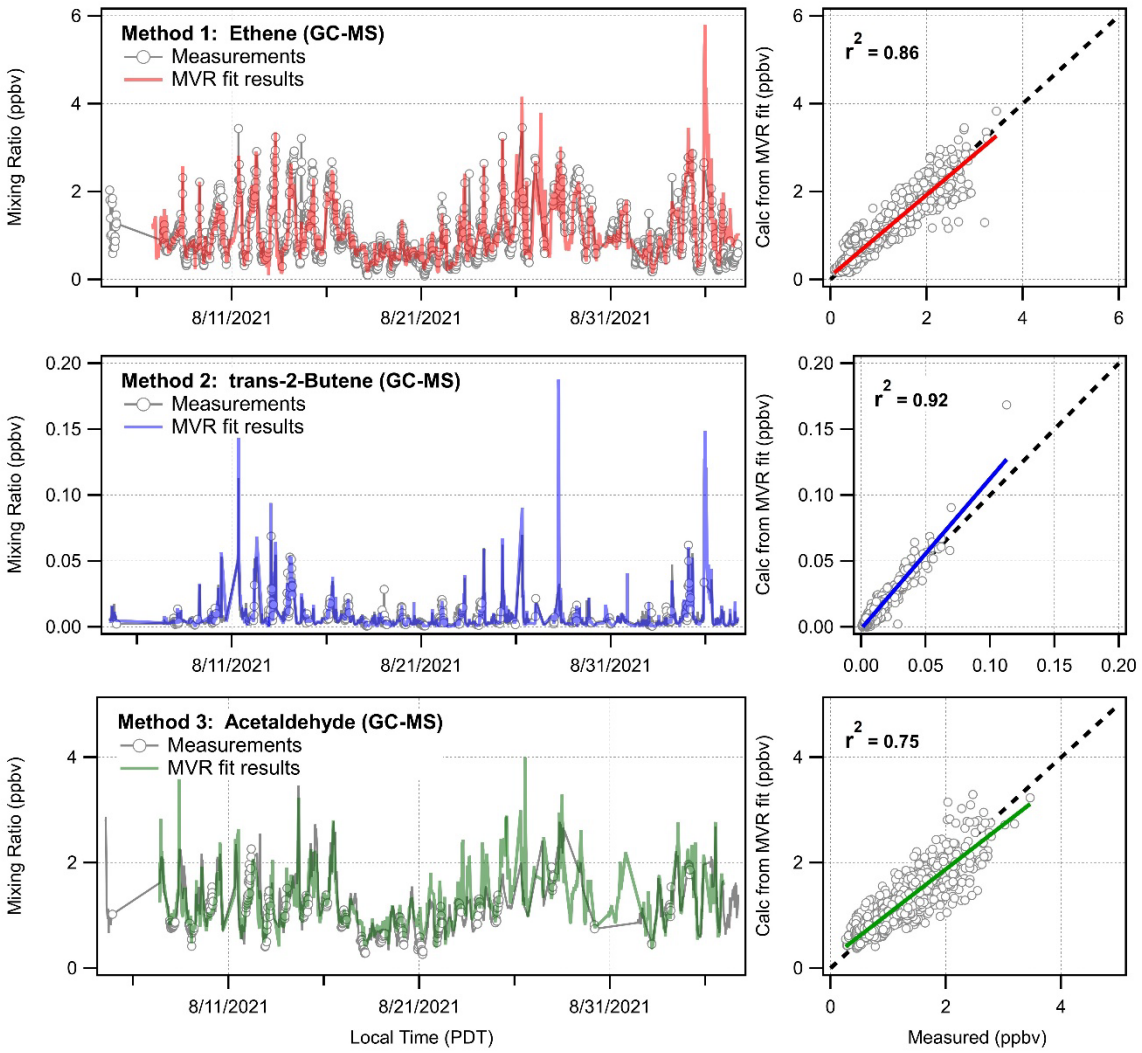


*Figure 36. Comparison of measurements and fit results from the three multivariate methods used to determine emission ratios for ethene, trans-2-butene, and acetaldehyde.*

Comparison of RECAP-CA Emission Ratios to CalNex 2010 and LAAQS 2020:

The emission ratios derived using similar photochemical age correction methods are shown in *Figure 37* for CalNex 2010 [de Gouw et al., 2018; de Gouw et al., 2017] and LAAQS 2020 [Van Rooy et al., 2021] datasets collected in Pasadena, CA. The RECAP-CA emission ratios agree within a factor of two for nearly all species reported. CalNex 2010 emission ratios were slightly higher compared to RECAP-CA, particularly for iso-propanol. Ethane and nitromethane emission ratios were greater for RECAP-CA. We think that nitromethane may have been anomalously low for the CalNex 2010 dataset due to a bad calibration factor. RECAP-CA emission ratios agree well compared to LAAQS 2020. As noted previously, ethane emissions are much higher for both LAAQS 2020 and RECAP-CA 2021.

Ethyne/CO emission was greatest for CalNex 2010 ($ER_{ethyne}$ = 6.4 ppbv/ppmv CO), followed by RECAP-CA 2021 ($ER_{ethyne}$ = 3.5 ppbv/ppmv CO), and finally LAAQS 2020 ($ER_{ethyne}$ = 2.91 ppbv/ppmv CO) had the lowest. It's possible that the wildfire influence is responsible for the slightly higher ethyne/CO emission ratio derived here, as we corrected the CO background for wildfire influence but did not do so for ethyne, but the strong correlation of ethyne with CO (r = 0.89, see *Figure 31 and Appendix Table 2*) indicates this is unlikely. Van Rooy et al. [2021] noted that the LAAQS 2020 VOC/ethyne emission ratios compared well with CalNex 2010, but the VOC/CO emission ratios have decreased by approximately 60% of their 2010 values. They posit that mobile sources are still the dominant source of the combustion-derived VOCs, but there has been a relative shift in these combustion sources from being dominated by on-road sources towards off-road sources that have a lower ethyne/CO emission ratio. The RECAP-CA observations support this general shift, but perhaps it was exacerbated for the LAAQS 2020 dataset due to the COVID-19 pandemic and a decrease in traffic counts.

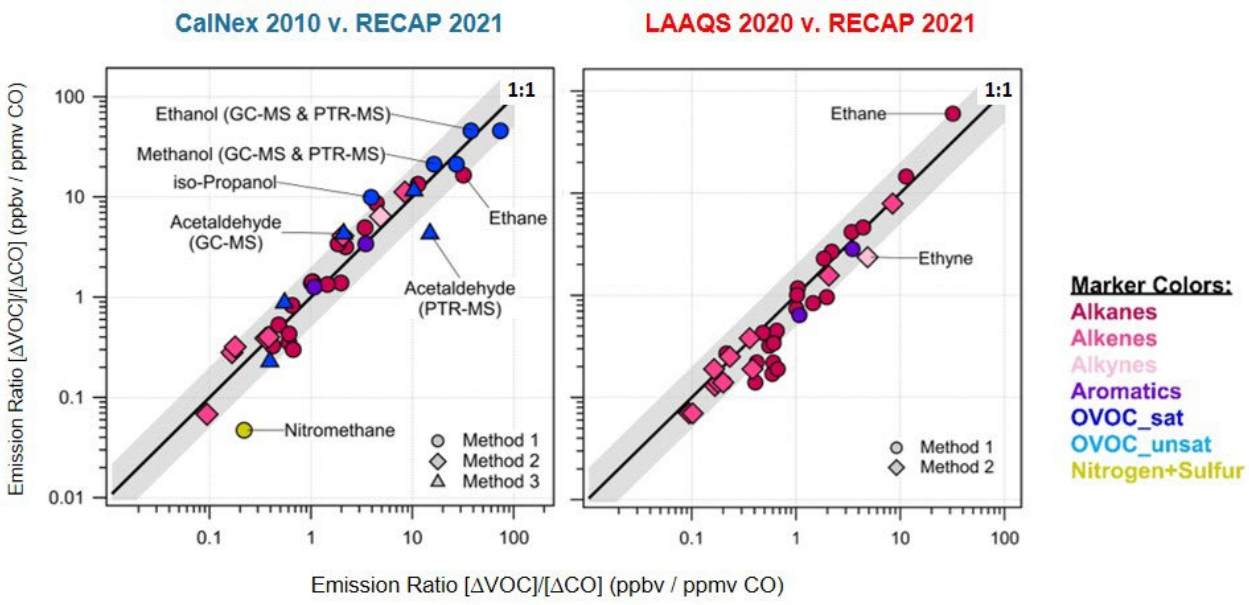


*Figure 37. Comparison of photochemically corrected emission ratios from CalNex 2010 [de Gouw et al., 2017, 2018] and LAAQS 2020 [Van Rooy et al., 2021]. The black line represents the 1:1 line and shading denotes the 2:1 and 1:2 lines.*

Comparison of RECAP-CA emission ratios to the FIVE-VCP emissions inventory:

The FIVE-VCP Emissions Inventory was developed at NOAA Chemical Sciences Laboratory in order to benchmark and evaluate uncertainties in key emission sectors, and is not intended to replaced regulatory models. We show the comparison of the FIVE-VCP Emission Inventory compared to the RECAP-CA derived emission ratios. Overall, there is very good agreement. Ethanol has the highest emission ratio of all species compared and agrees well with the inventory. MEK (10x) is the largest outlier at FIVE-VCP = 10x RECAP-CA followed by acetone (3.5x) , PCBTF (3x), and D5-siloxane (1.8x). For the alkene emission ratios, cis-2-butene and ethyne are a factor of five and two greater for RECAP-CA compared to the inventory.

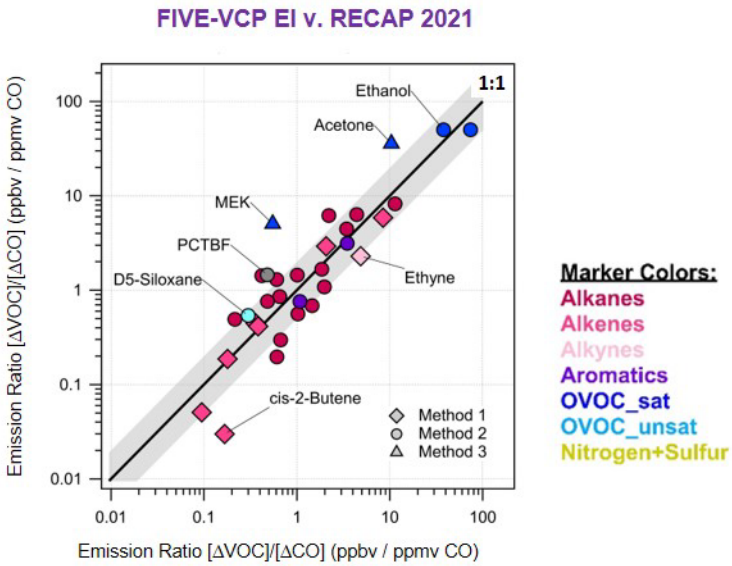


*Figure 38. Comparion of FIVE-VCP Emission Inventory to RECAP-CA emission ratios.*

### *3.4 POTENTIAL OZONE AND AEROSOL FORMATION*

Ozone and secondary organic aerosol are detrimental to human health and decrease visibility. When a VOC reacts in the atmosphere with an oxidant such as the hydroxyl radical in the presence of sunlight and nitrogen oxides ($NO_x$), it starts a chain of reactions that can lead to the formation of ozone and/or particulate matter. To further complicate matters, the production of ozone and particulate matter is non-linear and depends on a myriad of factors including sunlight, temperature, NOx concentrations, etc. These conditions can change throughout the day and across seasons. For these reasons, accurate representation of ozone formation and/or aerosol formation pathways require advanced chemical, meteorological, and/or statistical models. The RECAP-CA dataset presented here will serve as valuable input to these models and will be used to validate them [Zhu et al., 2023].

Here we present some simple, but still useful, metrics to assess the potential to form ozone and particulate matter using our gas-phase observations of ozone and particulate precursors. Statistical models such as Positive Matrix Factorization (PMF) are needed to properly apportion VOC emissions by source sector [Gkatzelis et al., 2021d], which is an active area of research post RECAP-CA. Here we present the discussion based on chemical classes which can be useful when comparing to emission inventories and lumped-species chemical models. In *Figure 39*, we present the relative contributions of VOC chemical classes and trace gases, as determined by their median mixing ratios, to the sum of volumetric and carbon

mixing ratios, mass, ozone formation potential (OFP), reactivity with the hydroxyl radical (OH-reactivity), and potential organic aerosol formation. All metrics used in these calculations are included in Appendix Table 1.

VOC Mixing Ratios and Mass:

The sum of median VOC mixing ratios observed during RECAP-CA was 38 ppbv VOC and 93 ppbC VOC. The median observed NOx mixing ratio was 7.24 ppb NOx. This results in a RECAP-CA median VOC/NOx ratios of 5.2 ppbv VOC per ppbv $NO_x$ and 12.8 ppbC VOC per ppbv $NO_x$. Wu et al. [*Submitted*] conducted ozone sensitivity experiments at the Pasadena ground site concurrent with the measurements presented here. They calculated ozone isopleths under varying NOx and VOC conditions and determined that Pasadena is in the "VOC-limited"/"$NO_x$-saturated" regime [Wu et al., *Submitted*]. In this relatively high-NOx environment, decreasing NOx emissions will lead to increased ozone formation.

The sum of VOC mass was 83 µg $m^3$. All three of these parameters were dominated by oxygenated VOCs followed by alkanes. Ethanol and acetone alone accounted for 27% of the median VOC mass measured during RECAP-CA (ethanol = 13%, acetone = 14%).

Ozone Precursors:

The relative contribution of the measured VOCs and trace gases to potential ozone formation is examined here using two metrics: OH-reactivity and ozone formation potential (OFP). Because most atmospheric reactions involving VOCs begin with a reaction of VOC with hydroxyl radicals (VOC + OH → products), OH-reactivity can be a useful metric for comparing the initial rate of reactions of various VOCs and trace gases in the atmosphere. However, the ultimate impact of a VOC on ozone formation is not limited to the initial reaction but also on all subsequent reactions. OH reactivity (units of $s^{-1}$) is determined by multiplying the observed median analyte concentration (molecule $cm^{-3}$) by its OH reaction rate coefficient ($k_{OH+VOC}$, $cm^3$ $molec^{-1}$ $s^{-1}$). The total OH reactivity for RECAP-CA of all measured analytes = 6.4 $s^{-1}$ with VOCs contributing 58%. The reaction of $OH+NO_2 \rightarrow HNO_3$ represents a OH-sink terminating the ozone production cycle and accounted for 22% of the median OH-reactivity.

Isoprene was the single largest contributor to the VOC-OH reactivity followed by formaldehyde, ethanol, and acetaldehyde. Natural emissions of isoprene and its oxidation products methyl vinyl ketone (MVK) and methacrolein (MACR) accounted for 16% of the VOC-OH reactivity. The overall contribution of biogenic isoprene to potential ozone formation is expected to be even greater as other isoprene oxidation products including formaldehyde and isoprene nitrates will also contribute to ozone formation.

Ozone formation potential (OFP) is a parameter that has been widely used to evaluate the maximum potential contribution to photochemical ozone production from specific VOCs under optimum reaction conditions [Carter, 1994; Carter, 2010; Gu et al., 2021]. OFPs for all carbon-containing gases were calculated based on individual VOC emissions weighted by its corresponding maximum incremental reactivity (MIR) reported by Carter [2010]. For the VOCs, formaldehyde has the largest OFP followed closely by ethanol. Other important VOC contributors to OFP include propene, isoprene, and sum of C8-aromatics. Ethanol is one of the dominant contributors to both the OH-reactivity and OFP and this is due entirely to its abundance in the Los Angeles Basin as it is not a particularly reactive analyte.

Aerosol Precursors:

Secondary organic aerosol formation (SOA) is even harder to predict than ozone production. Similar to ozone, the reactivities of the precursors are important metrics, but also their solubility and vapor pressures which will determine if an analyte partitions to the aerosol phase. The amount of aerosol

produced from a given precursor is the aerosol yield. The amount of potential aerosol formation was calculated based on individual VOC emissions weighted by its corresponding aerosol yield. We utilized aerosol yields calculated using the methods presented in McDonald et al. [2018a], Model A. For comparison, we include the secondary organic aerosol potential (SOAP) using the methods and yields detailed in Gu et al. [2021], Model B. Both studies were aimed at characterizing aerosol formation in the Los Angeles Basin.

Both models point to aromatics as the dominant aerosol precursors measured during RECAP-CA. Model B includes a slightly larger contribution from the C8-C10 alkanes and includes a yield for acetone, which is not included in Model B. We note that the RECAP-CA dataset does not include measurements of analytes in the semi-volatile or intermediate-volatility ranges so we are likely missing a significant source of SOA precursors.

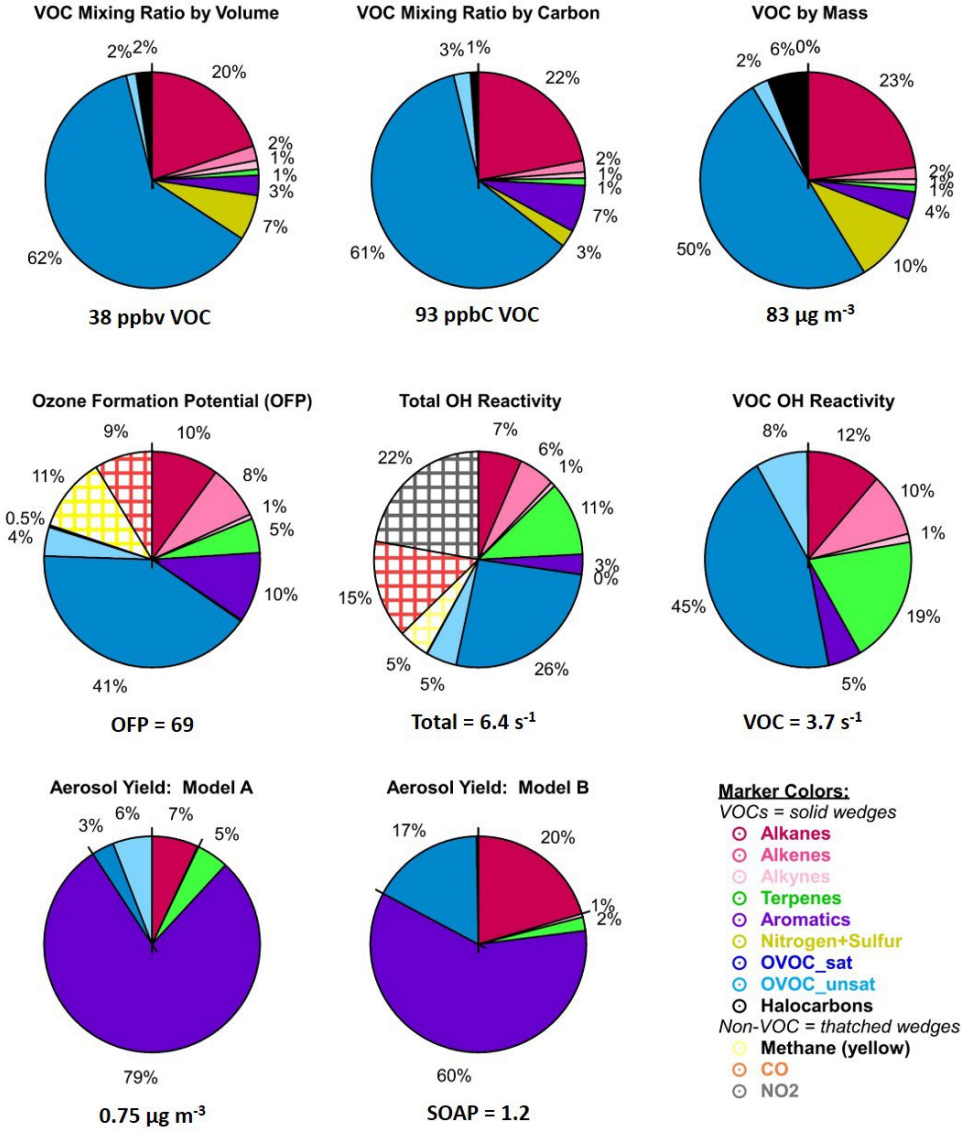


*Figure 39. Relative contributions to VOC mixing ratios, VOC mass, ozone formation potential, OH reactivity, and aerosol production based on median VOC and trace gas mixing ratios observed during RECAP-CA.*

# 4.0 SUMMARY AND CONCLUSIONS

Here we present detailed chemical measurements of a full suite of VOCs and trace gases in summer 2021 as part of the Re-evaluating the Chemistry of Air Pollutants in California (RECAP-CA) campaign in an effort to characterize the chemical, temporal and spatial variability of VOC emissions and chemistry across the basin. The objectives of this study were to evaluate all major VOC sources, including volatile chemical products (VCPs), cooking, natural gas usage, biogenic emissions and secondary products in order to fully characterize emission sources and atmospheric chemistry affecting photochemical ozone formation.

We conducted five weeks of measurements using an array of advanced instrumentation deployed at the Pasadena ground site in August and September 2021. These measurements included critical trace gases and provided extensive chemical detail of volatile organic compound emissions and chemistry. The NOAA gas chromatography-mass spectrometry (GC-MS) instrument collected over 1800 samples providing unparalleled chemical speciation of a full suite of VOCs. These measurements were augmented by five weeks of near-continuous measurements of organic and inorganic gases including important tracers for combustion sources, VCP usage, biogenic oxidation products, reactive nitrogen, and climate-relevant gases. We also deployed the NOAA Mobile Laboratory to conduct ten different surveys across the Los Angeles basin in order to investigate the spatial variability of VOC emission sources and to target emission-rich areas for a variety of source sectors (e.g., oil and natural gas production, downwind or restaurants, etc.).

During RECAP-CA, we had excellent sampling conditions allowing us to characterize the emissions and chemistry downwind of the Los Angeles metropolitan area. Seasonally warm temperatures and plenty of sunlight led to very active photochemistry as evidenced by the strong photochemical formation of ozone, which had a diel mean maximum of 65 ppb ozone with a campaign maximum exceeding 100 ppbv ozone. There were two exceptional events: one was characterized by relatively clean background air and one that was influenced of aged wildfire smoke.

Analysis of diel profiles of over one hundred (100) different analytes were used to assess the relative importance of boundary layer dynamics, transport, primary emission source strength, and both the photochemical degradation of reactive precursors and the subsequent formation of secondary products. Overall, oxygenated VOCs were highly abundant and were associated with a wide array of primary and secondary sources. Ethanol and methanol continue to be the most abundant VOCs measured in Pasadena in both 2010 and 2021, and in other urban areas we have studied including New York City, NY, indicating the prevalence of substantial primary emission sources of these species in urban environments. They are not particularly reactive in the atmosphere and thus exempt from current regulatory actions, but they were significant contributors to the VOC reactivity (one metric used to assess the propensity to form ozone) due to their excessive concentrations.

Other oxygenated VOCs that had strong daytime emissions/sources (coincident with the hours of peak photochemical formation of ozone and organic aerosol) included the secondary formation of formaldehyde, an air toxic, and biogenic oxidation products which serve to highlight the important role that natural isoprene emissions and other reactive precursors will have on air quality in the Los Angeles Basin. Other species of note with increased daytime emission rates was para-chlorobenzotrifluride (PCBTF), a useful VCP tracer for solvent-based coatings. Higher daytime emission rates of PCBTF is conceptually consistent with increased anthropogenic activities (e.g., construction activities) combined with greater evaporation rates due to warmer daytime temperatures.

Observed mixing ratios of Texanol, a VCP marker for water-based coatings, were 1.5 to 4 times higher than the first-ever reported measurements in Southern California in 2009 [Goliff et al. 2012]. Our observations of D5-siloxane, a tracer for personal care product usage, were consistent with those observed in other North American cities and the diel profile was indicative of higher emission rates during the morning rush-hour with subsequent decline throughout the day as the analyte evaporates and is diluted throughout the boundary layer. Octanal and nonanal were identified as useful tracers for cooking emissions and their correlations with carbon monoxide (CO, a combustion tracer) were leveraged to calculate emission rates in the Los Angeles Basin of 5.6 and 3.2 tons per day for octanal and nonanal, respectively, thus providing critical new information on a previously understudied emission source [Coggon et al., 2023b].

We observed a doubling of the ethane/CO emission ratio compared to CalNex 2010, which is consistent with increased ethane emissions from natural gas usage in the Los Angeles Basin [Wunch et al., 2016]. Mobile lab measurements during RECAP-CA and subsequent airborne measurements in 2023 show that ethane and propane are prevalent throughout the basin with prominent ethane sources occurring near the Port of Long Beach.

The RECAP-CA measurements were used to derive VOC/CO and VOC/ethyne emission ratios for 70 different chemical species. Overall, the RECAP-CA VOC/CO emission ratios were lower compared to 2010 values and were largely consistent with those from 2020 [ de Gouw et al., 2017, 2018; Van Rooy et al., 2021]. Notable exceptions include ethane (discussed above), ethyne, and the C7+ alkanes. Ethyne/CO emission ratios were less than 2010, but greater than 2020 values [de Gouw et al., 2017, 2018; Van Rooy et al., 2021]. Van Rooy et al. [2021] posited that a shift from on-road to off-road combustion sources could explain a shift towards lower ethyne/CO emission ratios. The influence of aged wildfire smoke impacting the RECAP-CA measurement site could also be responsible for an increase in the observed ethyne/CO emission ratio. Emission ratios for C7+ alkanes were higher compared to both previous datasets. The reason for this is unknown but could be in part related to higher ambient temperatures during RECAP-CA implicating an evaporative emission source.

The RECAP-CA median VOC/NOx ratios were 5.2 ppbv VOC per ppbv $NO_x$ and 12.8 ppbC VOC per ppbv $NO_x$. Wu et al. [*Submitted*] conducted ozone sensitivity experiments at the Pasadena ground site concurrent with the measurements presented here. They calculated ozone isopleths under varying NOx and VOC conditions and determined that Pasadena is in the "VOC-limited"/"$NO_x$-saturated" regime [Wu et al., *Submitted*]. In this relatively high-NOx environment, decreasing NOx emissions will lead to increased ozone formation. Isoprene and its oxidation products were the dominant contributors to potential ozone formation. Other important species included a strong photochemical source of formaldehyde and large primary emissions of ethanol and methanol. Potential aerosol formation is dominated by aromatics, primarily associated with on-road emission sources. We note that we did not measure VOCs of semi- and intermediate- volatilities, which are expected to be efficient aerosol precursors.

This expansive new dataset will serve as the new foundation to assess emission inventories and chemical models used to understand and predict secondary ozone and aerosol formation in the Los Angeles Basin. Improved understanding of modern emission sources of VOCs and trace gases are critical for California to meet is air quality and climate goals. The results from this project will help inform the development of effective regulatory policies for future State Implementation Plans (SIP) and $O_3$ and PM reduction strategies.

# 5.0 REFERENCES


Bastos, L. C., & Pereira, P. A. (2010). Influence of heating time and metal ions on the amount of free fatty acids and formation rates of selected carbonyl compounds during the thermal oxidation of canola oil. *J Agric Food Chem, 58*(24), 12777-12783. doi:10.1021/jf1028575

Bonin, T. A., Carroll, B. J., Hardesty, R. M., Brewer, W. A., Hajny, K., Salmon, O. E., & Shepson, P. B. (2018). Doppler Lidar Observations of the Mixing Height in Indianapolis Using an Automated Composite Fuzzy Logic Approach. *Journal of Atmospheric and Oceanic Technology, 35*(3), 473-490. doi:https://doi.org/10.1175/JTECH-D-17-0159.1

Borbon, A., Gilman, J. B., Kuster, W. C., Grand, N., Chevaillier, S., Colomb, A., . . . de Gouw, J. A. (2013). Emission ratios of anthropogenic volatile organic compounds in northern mid-latitude megacities: Observations versus emission inventories in Los Angeles and Paris. *Journal of Geophysical Research-Atmospheres, 118*(4), 2041-2057. doi:10.1002/jgrd.50059

Brioude, J., Arnold, D., Stohl, A., Cassiani, M., Morton, D., Seibert, P., . . . Wotawa, G. (2013). The Lagrangian particle dispersion model FLEXPART-WRF version 3.1. *Geosci. Model Dev., 6*(6), 1889-1904. doi:10.5194/gmd-6-1889-2013

Calfapietra, C., Fares, S., Manes, F., Morani, A., Sgrigna, G., & Loreto, F. (2013). Role of Biogenic Volatile Organic Compounds (BVOC) emitted by urban trees on ozone concentration in cities: A review. *Environmental Pollution, 183*, 71-80. doi:https://doi.org/10.1016/j.envpol.2013.03.012

CARB. (2018a). *2014 Architectural Coatings Survey*. Retrieved from Sacramento, CA:

CARB. (2018b). *2016 Fragrance Formulator Survey (Draft)*. Retrieved from Sacramento, CA:

CARB. (2019). *2015 Consumer & Commercial Products Survey*. Retrieved from Sacramento, CA:

Carter, W. P. L. (1994). Development of ozone reactivity scales for volatile organic-compounds. *Journal of the Air & Waste Management Association, 44*(7), 881-899. Retrieved from <Go to ISI>://A1994NX44800006

Carter, W. P. L. (2010). Updated Maximum Incremental Reactivity Scale and Hydrocarbon Bin Reactivities for Regulatory Applications. In: California Air Resources Board.

Carter, W. P. L., & Atkinson, R. (1996). Development and evaluation of a detailed mechanism for the atmospheric reactions of isoprene and NOx. *International Journal of Chemical Kinetics, 28*(7), 497-530. doi:https://doi.org/10.1002/(SICI)1097-4601(1996)28:7<497::AID-KIN4>3.0.CO;2-Q

Coggon, M. M., Gkatzelis, G. I., McDonald, B. C., Gilman, J. B., Schwantes, R. H., Abuhassan, N., . . . Warneke, C. (2021a). Volatile chemical product emissions enhance ozone and modulate urban chemistry. *Proceedings of the National Academy of Sciences, 118*(32), e2026653118. doi:doi:10.1073/pnas.2026653118

Coggon, M. M., Gkatzelis, G. I., McDonald, B. C., Gilman, J. B., Schwantes, R. H., Abuhassan, N., . . . Warneke, C. (2021b). Volatile chemical product emissions enhance ozone and modulate urban chemistry. *Proceedings of the National Academy of Sciences of the United States of America, 118*(32). doi:10.1073/pnas.2026653118

Coggon, M. M., McDonald, B. C., Vlasenko, A., Veres, P. R., Bernard, F., Koss, A. R., . . . de Gouw, J. A. (2018a). Diurnal Variability and Emission Pattern of Decamethylcyclopentasiloxane (D5) from the Application of Personal Care Products in Two North American Cities. *Environ. Sci. Technol., 52*(10), 5610-5618. doi:10.1021/acs.est.8b00506

Coggon, M. M., McDonald, B. C., Vlasenko, A., Veres, P. R., Bernard, F., Koss, A. R., . . . de Gouw, J. A. (2018b). Diurnal Variability and Emission Pattern of Decamethylcyclopentasiloxane (D-5) from the Application of Personal Care Products in Two North American Cities. *Environmental Science & Technology, 52*(10), 5610-5618. doi:10.1021/acs.est.8b00506

Coggon, M. M., Stockwell, C. E., Claflin, M. S., Pfannerstill, E. Y., Lu, X., Gilman, J. B., . . . Warneke, C. (2023a). Identifying and correcting interferences to PTR-ToF-MS measurements of isoprene and other urban volatile organic compounds. *EGUsphere, 2023*, 1-41. doi:10.5194/egusphere-2023-1497

Coggon, M. M., Stockwell, C. E., Xu, L., Peischl, J., Gilman, J. B., Lamplugh, A., . . . Warneke, C. (2023b). Contribution of Cooking Emissions to the Urban Volatile Organic Compounds in Las Vegas, NV. *EGUsphere, 2023*, 1-28. doi:10.5194/egusphere-2023-2749

Coggon, M. M., Veres, P. R., Yuan, B., Koss, A., Warneke, C., Gilman, J. B., . . . de Gouw, J. A. (2016). Emissions of nitrogen-containing organic compounds from the burning of herbaceous and arboraceous biomass: Fuel composition dependence and the variability of commonly used nitrile tracers. *Geophysical Research Letters, 43*(18), 9903-9912. doi:10.1002/2016gl070562

de Gouw, J. A., Gilman, J. B., Kim, S. W., Alvarez, S. L., Dusanter, S., Graus, M., . . . Young, C. J. (2018). Chemistry of Volatile Organic Compounds in the Los Angeles Basin: Formation of Oxygenated Compounds and Determination of Emission Ratios. *Journal of Geophysical Research-Atmospheres, 123*(4), 2298-2319. doi:10.1002/2017jd027976

de Gouw, J. A., Gilman, J. B., Kim, S. W., Lerner, B. M., Isaacman-VanWertz, G., McDonald, B. C., . . . Stutz, J. (2017). Chemistry of Volatile Organic Compounds in the Los Angeles basin: Nighttime Removal of Alkenes and Determination of Emission Ratios. *Journal of Geophysical Research-Atmospheres, 122*(21), 11843-11861. doi:10.1002/2017jd027459

EPA. (2020). *National Emissions Inventory (NEI) 2017, version 1*. Retrieved from Research Triangle Park, N.C.:

Gentner, D. R., Isaacman, G., Worton, D. R., Chan, A. W., Dallmann, T. R., Davis, L., . . . Goldstein, A. H. (2012). Elucidating secondary organic aerosol from diesel and gasoline vehicles through detailed characterization of organic carbon emissions. *Proc Natl Acad Sci USA, 109*(45), 18318-18323. doi:10.1073/pnas.1212272109

Gentner, D. R., Worton, D. R., Isaacman, G., Davis, L. C., Dallmann, T. R., Wood, E. C., . . . Harley, R. A. (2013a). Chemical composition of gas-phase organic carbon emissions from motor vehicles and implications for ozone production. *Environ. Sci. Technol., 47*(20), 11837-11848. doi:10.1021/es401470e

Gentner, D. R., Worton, D. R., Isaacman, G., Davis, L. C., Dallmann, T. R., Wood, E. C., . . . Harley, R. A. (2013b). Chemical composition of gas-phase organic carbon emissions from motor vehicles and implications for ozone production. *Environmental Science & Technology, 47*(20), 11837-11848. doi:10.1021/Es401470e

Gilman, J. B., Lerner, B. M., Kuster, W. C., Goldan, P. D., Warneke, C., Veres, P. R., . . . Yokelson, R. J. (2015). Biomass burning emissions and potential air quality impacts of volatile organic compounds and other trace gases from fuels common in the US. *Atmos. Chem. Phys., 15*(24), 13915-13938. doi:10.5194/acp-15-13915-2015

Gkatzelis, G. I., Coggon, M. M., McDonald, B. C., Peischl, J., Aikin, K. C., Gilman, J. B., . . . Warneke, C. (2021a). Identifying Volatile Chemical Product Tracer Compounds in U.S. Cities. *Environmental Science & Technology, 55*(1), 188-199. doi:10.1021/acs.est.0c05467

Gkatzelis, G. I., Coggon, M. M., McDonald, B. C., Peischl, J., Aikin, K. C., Gilman, J. B., . . . Warneke, C. (2021b). Identifying Volatile Chemical Product Tracer Compounds in US Cities. *Environmental Science & Technology, 55*(1), 188-199. doi:10.1021/acs.est.0c05467

Gkatzelis, G. I., Coggon, M. M., McDonald, B. C., Peischl, J., Gilman, J. B., Aikin, K. C., . . . Warneke, C. (2021c). Observations Confirm that Volatile Chemical Products Are a Major Source of Petrochemical Emissions in U.S. Cities. *Environmental Science & Technology, 55*(8), 4332-4343. doi:10.1021/acs.est.0c05471

Gkatzelis, G. I., Coggon, M. M., McDonald, B. C., Peischl, J., Gilman, J. B., Aikin, K. C., . . . Warneke, C. (2021d). Observations Confirm that Volatile Chemical Products Are a Major Source of Petrochemical Emissions in US Cities. *Environmental Science & Technology, 55*(8), 4332-4343. doi:10.1021/acs.est.0c05471

Gkatzelis, G. I., Coggon, M. M., Stockwell, C. E., Hornbrook, R. S., Allen, H., Apel, E. C., . . . Warneke, C. (2023). Parameterizations of US wildfire and prescribed fire emission ratios and emission factors based on FIREX-AQ aircraft measurements. *EGUsphere, 2023*, 1-31. doi:10.5194/egusphere-2023-1439

Goliff, W. S., Fitz, D. R., Cocker, K., Bumiller, K., Bufalino, C., & Switzer, D. (2012). Ambient measurements of 2,2,4-trimethyl, 1,3-pentanediol monoisobutyrate in Southern California. *Journal of the Air & Waste Management Association, 62*(6), 680-685. doi:10.1080/10962247.2012.666223

Gu, S., Guenther, A., & Faiola, C. (2021). Effects of anthropogenic and biogenic volatile organic compounds on Los Angeles air quality. *Environmental Science & Technology, 55*(18), 12191-12201.

Guenther, A., Karl, T., Harley, P., Wiedinmyer, C., Palmer, P. I., & Geron, C. (2006). Estimates of global terrestrial isoprene emissions using MEGAN (Model of Emissions of Gases and Aerosols from Nature). *Atmospheric Chemistry and Physics, 6*, 3181-3210. Retrieved from <Go to ISI>://WOS:000239463800001

Hayes, P. L., Carlton, A. G., Baker, K. R., Ahmadov, R., Washenfelder, R. A., Alvarez, S., . . . Jimenez, J. L. (2015). Modeling the formation and aging of secondary organic aerosols in Los Angeles during CalNex 2010. *Atmospheric Chemistry and Physics, 15*(10), 5773-5801. doi:10.5194/acp-15-5773-2015

He, J., Harkins, C., O'Dell, K., Li, M., Francoeur, C., Anenberg, S. C., . . . McDonald, B. C. (submitted). COVID-19 Perturbation on US Air Quality and Human Health Impact Assessment. *Proc Natl Acad Sci Nexus*.

Hurley, J. F., Smiley, E., & Isaacman-VanWertz, G. (2021). Modeled Emission of Hydroxyl and Ozone Reactivity from Evaporation of Fragrance Mixtures. *Environmental Science & Technology, 55*(23), 15672-15679. doi:10.1021/acs.est.1c04004

Isaacman-VanWertz, G., Sueper, D. T., Aikin, K. C., Lerner, B. M., Gilman, J. B., de Gouw, J. A., . . . Goldstein, A. H. (2017). Automated single-ion peak fitting as an efficient approach for analyzing complex chromatographic data. *Journal of Chromatography A, 1529*(Supplement C), 81-92. doi:https://doi.org/10.1016/j.chroma.2017.11.005

Klein, F., Farren, N. J., Bozzetti, C., Daellenbach, K. R., Kilic, D., Kumar, N. K., . . . El Haddad, I. (2016a). Indoor terpene emissions from cooking with herbs and pepper and their secondary organic aerosol production potential. *Sci. Rep., 6*, 36623. doi:10.1038/srep36623

Klein, F., Platt, S. M., Farren, N. J., Detournay, A., Bruns, E. A., Bozzetti, C., . . . El Haddad, I. (2016b). Characterization of Gas-Phase Organics Using Proton Transfer Reaction Time-of-Flight Mass Spectrometry: Cooking Emissions. *Environmental Science & Technology, 50*(3), 1243-1250. doi:10.1021/acs.est.5b04618

Lerner, B. M., Gilman, J. B., Aikin, K. C., Atlas, E. L., Goldan, P. D., Graus, M., . . . de Gouw, J. A. (2017). An improved, automated whole air sampler and gas chromatography mass spectrometry analysis system for volatile organic compounds in the atmosphere. *Atmospheric Measurement Techniques, 10*(1), 291-313. doi:10.5194/amt-10-291-2017

Liu, Y., Misztal, P. K., Arata, C., Weschler, C. J., Nazaroff, W. W., & Goldstein, A. H. (2021). Observing ozone chemistry in an occupied residence. *Proceedings of the National Academy of Sciences, 118*(6), e2018140118. doi:doi:10.1073/pnas.2018140118

Mackay, D., Cowan-Ellsberry, C. E., Powell, D. E., Woodburn, K. B., Xu, S., Kozerski, G. E., & Kim, J. (2015). Decamethylcyclopentasiloxane (D5) environmental sources, fate, transport, and routes of

exposure. *Environmental Toxicology and Chemistry, 34*(12), 2689-2702. doi:https://doi.org/10.1002/etc.2941

Mayhew, A. W., Lee, B. H., Thornton, J. A., Bannan, T. J., Brean, J., Hopkins, J. R., . . . Hamilton, J. F. (2022). Evaluation of isoprene nitrate chemistry in detailed chemical mechanisms. *Atmos. Chem. Phys., 22*(22), 14783-14798. doi:10.5194/acp-22-14783-2022

McDonald, B. C., de Gouw, J. A., Gilman, J. B., Jathar, S. H., Akherati, A., Cappa, C. D., . . . Trainer, M. (2018a). Volatile chemical products emerging as largest petrochemical source of urban organic emissions. *Science, 359*(6377), 760-764. doi:10.1126/science.aaq0524

McDonald, B. C., McKeen, S. A., Cui, Y. Y., Ahmadov, R., Kim, S. W., Frost, G. J., . . . Trainer, M. (2018b). Modeling ozone in the Eastern U.S. using a fuel-based mobile source emissions inventory. *Environmental Science & Technology, 52*, 7360-7370. doi:10.1021/acs.est.8b00778

Peischl, J., Ryerson, T. B., Brioude, J., Aikin, K. C., Andrews, A. E., Atlas, E., . . . Parrish, D. D. (2013). Quantifying sources of methane using light alkanes in the Los Angeles basin, California. *Journal of Geophysical Research-Atmospheres, 118*(10), 4974-4990. doi:10.1002/jgrd.50413

Peng, C. Y., Lan, C. H., Lin, P. C., & Kuo, Y. C. (2017). Effects of cooking method, cooking oil, and food type on aldehyde emissions in cooking oil fumes. *J Hazard Mater, 324*(Pt B), 160-167. doi:10.1016/j.jhazmat.2016.10.045

Peng, Y., Mouat, A. P., Hu, Y., Li, M., McDonald, B. C., & Kaiser, J. (2022). Source appointment of volatile organic compounds and evaluation of anthropogenic monoterpene emission estimates in Atlanta, Georgia. *Atmospheric Environment, 288*, 119324. doi:https://doi.org/10.1016/j.atmosenv.2022.119324

Robinson, M. A., Neuman, J. A., Huey, L. G., Roberts, J. M., Brown, S. S., & Veres, P. R. (2022). Temperature-dependent sensitivity of iodide chemical ionization mass spectrometers. *Atmos. Meas. Tech., 15*(14), 4295-4305. doi:10.5194/amt-15-4295-2022

Ryerson, T. B., Andrews, A. E., Angevine, W. M., Bates, T. S., Brock, C. A., Cairns, B., . . . Wofsy, S. C. (2013). The 2010 California Research at the Nexus of Air Quality and Climate Change (CalNex) field study. *Journal of Geophysical Research-Atmospheres, 118*(11), 5830-5866. doi:10.1002/jgrd.50331

Schauer, J. J., Kleeman, M. J., Cass, G. R., & Simoneit, B. R. T. (1999a). Measurement of Emissions from Air Pollution Sources. 1. C1 through C29 Organic Compounds from Meat Charbroiling. *Environmental Science & Technology, 33*(10), 1566-1577. doi:10.1021/es980076j

Schauer, J. J., Kleeman, M. J., Cass, G. R., & Simoneit, B. R. T. (1999b). Measurement of emissions from air pollution sources. 1. C-1 through C-29 organic compounds from meat charbroiling. *Environmental Science & Technology, 33*(10), 1566-1577. doi:10.1021/es980076j

Sekimoto, K., Li, S.-M., Yuan, B., Koss, A., Coggon, M., Warneke, C., & de Gouw, J. (2017). Calculation of the sensitivity of proton-transfer-reaction mass spectrometry (PTR-MS) for organic trace gases using molecular properties. *International Journal of Mass Spectrometry, 421*, 71-94. doi:https://doi.org/10.1016/j.ijms.2017.04.006

Slowik, J. G., Vlasenko, A., McGuire, M., Evans, G. J., & Abbatt, J. P. D. (2010). Simultaneous factor analysis of organic particle and gas mass spectra: AMS and PTR-MS measurements at an urban site. *Atmospheric Chemistry and Physics, 10*(4), 1969-1988. Retrieved from <Go to ISI>://000274851500031

Stark, H., Yatavelli, R. L. N., Thompson, S. L., Kimmel, J. R., Cubison, M. J., Chhabra, P. S., . . . Jimenez, J. L. (2015). Methods to extract molecular and bulk chemical information from series of complex mass spectra with limited mass resolution. *International Journal of Mass Spectrometry, 389*, 26-38. doi:https://doi.org/10.1016/j.ijms.2015.08.011

Stockwell, C. E., Coggon, M. M., Gkatzelis, G. I., Ortega, J., McDonald, B. C., Peischl, J., . . . Warneke, C. (2021). Volatile organic compound emissions from solvent- and water-borne coatings –

compositional differences and tracer compound identifications. *Atmos. Chem. Phys., 21*(8), 6005-6022. doi:10.5194/acp-21-6005-2021

Stroud, C. A., Roberts, J. M., Goldan, P. D., Kuster, W. C., Murphy, P. C., Williams, E. J., . . . Young, V. L. (2001). Isoprene and its oxidation products, methacrolein and methylvinyl ketone, at an urban forested site during the 1999 Southern Oxidants Study. *Journal of Geophysical Research-Atmospheres, 106*(D8), 8035-8046. Retrieved from <Go to ISI>://000168437500018

Van Rooy, P., Tasnia, A., Barletta, B., Buenconsejo, R., Crounse, J. D., Kenseth, C. M., . . . Barsanti, K. C. (2021). Observations of Volatile Organic Compounds in the Los Angeles Basin during COVID-19. *ACS Earth and Space Chemistry, 5*(11), 3045-3055. doi:10.1021/acsearthspacechem.1c00248

Verreyken, B., Brioude, J., & Evan, S. (2019). Development of turbulent scheme in the FLEXPART-AROME v1.2.1 Lagrangian particle dispersion model. *Geosci. Model Dev., 12*(10), 4245-4259. doi:10.5194/gmd-12-4245-2019

Wang, N., Ernle, L., Bekö, G., Wargocki, P., & Williams, J. (2022). Emission Rates of Volatile Organic Compounds from Humans. *Environmental Science & Technology, 56*(8), 4838-4848. doi:10.1021/acs.est.1c08764

Wang, R., Moody, R. P., Koniecki, D., & Zhu, J. (2009). Low molecular weight cyclic volatile methylsiloxanes in cosmetic products sold in Canada: Implication for dermal exposure. *Environment International, 35*(6), 900-904. doi:https://doi.org/10.1016/j.envint.2009.03.009

Warneke, C., de Gouw, J. A., Holloway, J. S., Peischl, J., Ryerson, T. B., Atlas, E., . . . Parrish, D. D. (2012). Multiyear trends in volatile organic compounds in Los Angeles, California: Five decades of decreasing emissions. *Journal of Geophysical Research-Atmospheres, 117*. doi:D00v17

10.1029/2012jd017899

Wu, S., Alaimo, C. P., Zhao, Y., Green, P. G., Young, T. M., Liu, S., . . . Kleeman, M. J. (*Submitted*). O3 sensitivity to NOx and VOC during RECAP-CA: implication for emissions control strategies. *Environmental Science & Technology*.

Wunch, D., Toon, G. C., Hedelius, J. K., Vizenor, N., Roehl, C. M., Saad, K. M., . . . Wennberg, P. O. (2016). Quantifying the loss of processed natural gas within California's South Coast Air Basin using long-term measurements of ethane and methane. *Atmos. Chem. Phys., 16*(22), 14091-14105. doi:10.5194/acp-16-14091-2016

Yeoman, A. M., Shaw, M., Carslaw, N., Murrells, T., Passant, N., & Lewis, A. C. (2020). Simplified speciation and atmospheric volatile organic compound emission rates from non-aerosol personal care products. *Indoor Air, 30*(3), 459-472. doi:https://doi.org/10.1111/ina.12652

Yokelson, R. J., Crounse, J. D., DeCarlo, P. F., Karl, T., Urbanski, S., Atlas, E., . . . Shetter, R. (2009). Emissions from biomass burning in the Yucatan. *Atmospheric Chemistry and Physics, 9*(15), 5785-5812. Retrieved from <Go to ISI>://WOS:000268876600023

Yuan, B., Koss, A., Warneke, C., Gilman, J. B., Lerner, B. M., Stark, H., & de Gouw, J. A. (2016). A high-resolution time-of-flight chemical ionization mass spectrometer utilizing hydronium ions (H3O+ ToF-CIMS) for measurements of volatile organic compounds in the atmosphere. *Atmos. Meas. Tech., 9*(6), 2735-2752. doi:10.5194/amt-9-2735-2016

Zhu, Q., Schwantes, R. H., Coggon, M., Harkins, C., Schnell, J., He, J., . . . McDonald, B. C. (2023). A better representation of VOC chemistry in WRF-Chem and its impact on ozone over Los Angeles. *EGUsphere, 2023*, 1-31. doi:10.5194/egusphere-2023-2742

# 6.0 GLOSSARY OF TERMS, ABBREVIATIONS, AND SYMBOLS

| | |
|---|---|
| AEROMMA | Atmospheric Emissions and Reactions Observed from Megacities to Marine Areas |
| CalNex | California Nexus of Air Quality and Climate |
| CSL | Chemical Sciences Laboratory at NOAA |
| CO | Carbon Monoxide |
| $CO_2$ | Carbon Dioxide |
| FIREX-AQ | Fire Influence on Regional to Global Environments and Air Quality |
| GC-MS | Gas Chromatography – Mass Spectrometry |
| I.D. | Inner Diameter |
| LAAQS | Los Angeles Air Quality Study 2020 |
| NOAA | National Oceanic and Atmospheric Administration |
| NOx | Nitrogen Oxides (NOx = NO + $NO_2$) |
| O.D. | Outer Diameter |
| PFA | Perfluoroalkoxy polymer |
| PSIA | Pounds Per Square Inch Absolute Pressure |
| PSIG | Pounds Per Square Inch Gauge Pressure |
| PTR-ToF-MS/PTR-MS | Proton Transfer Reaction – Time of Flight – Mass Spectrometry |
| RECAP-CA | Re-Evaluating the Chemistry of Air Pollutants in California |
| SCCM | Standard cubic centimeters |
| SLPM | Standard Liter Per Minute |
| SUNVEx | Southwest Urban NOx and VOC Experiment |
| VCP | Volatile chemical product |
| VOC | Volatile Organic Compound |
| WAS | Whole Air Sample |

1502

1503

1504

1505

1506

# 8.0 Appendix

## LIST OF FIGURES



## LIST OF TABLES



## REFERENCES

**MIR values:**
Carter, W. P. L. (2010). Updated Maximum Incremental Reactivity Scale and Hydrocarbon Bin Reactivities for Regulatory Applications. In: California Air Resources Board.
**kOH, kO3, and kNO3 values**
https://kinetics.nist.gov/kinetics/
**LogC* and SOA Yield values:**
McDonald, B. C., de Gouw, J. A., Gilman, J. B., Jathar, S. H., Akherati, A., Cappa, C. D., . . . Trainer, M. (2018). Volatile chemical products emerging as largest petrochemical source of urban organic emissions. *Science, 359*(6377), 760-764. doi:10.1126/science.aaq0524
**SOAP values:**
Gu, S., Guenther, A., & Faiola, C. (2021). Effects of anthropogenic and biogenic volatile organic compounds on Los Angeles air quality. *Environmental Science & Technology, 55*(18), 12191-12201.
**Methods 1 and 2:**
de Gouw, J. A., Gilman, J. B., Kim, S. W., Lerner, B. M., Isaacman-VanWertz, G., McDonald, B. C., . . . Stutz, J. (2017). Chemistry of Volatile Organic Compounds in the Los Angeles basin: Nighttime Removal of Alkenes and Determination of Emission Ratios. *Journal of Geophysical Research-Atmospheres, 122*(21), 11843-11861. doi:10.1002/2017jd027459
**Method 3:**
de Gouw, J. A., Gilman, J. B., Kim, S. W., Alvarez, S. L., Dusanter, S., Graus, M., . . . Young, C. J. (2018). Chemistry of Volatile Organic Compounds in the Los Angeles Basin: Formation of Oxygenated Compounds and Determination of Emission Ratios. *Journal of Geophysical Research-Atmospheres, 123*(4), 2298-2319. doi:10.1002/2017jd027976

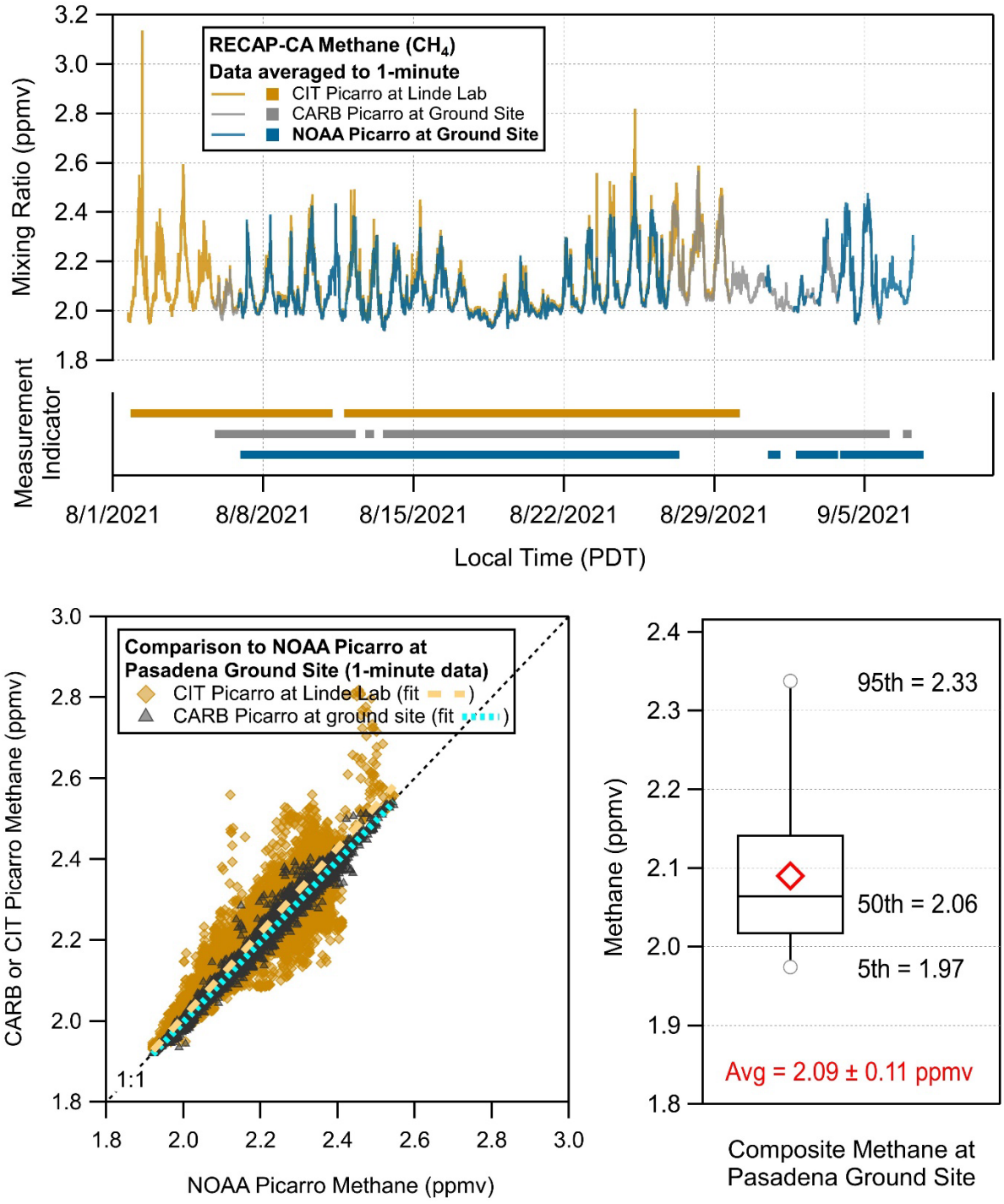


Figure A1. Observations and comparison of methane ($CH_4$) measurements during RECAP-CA.

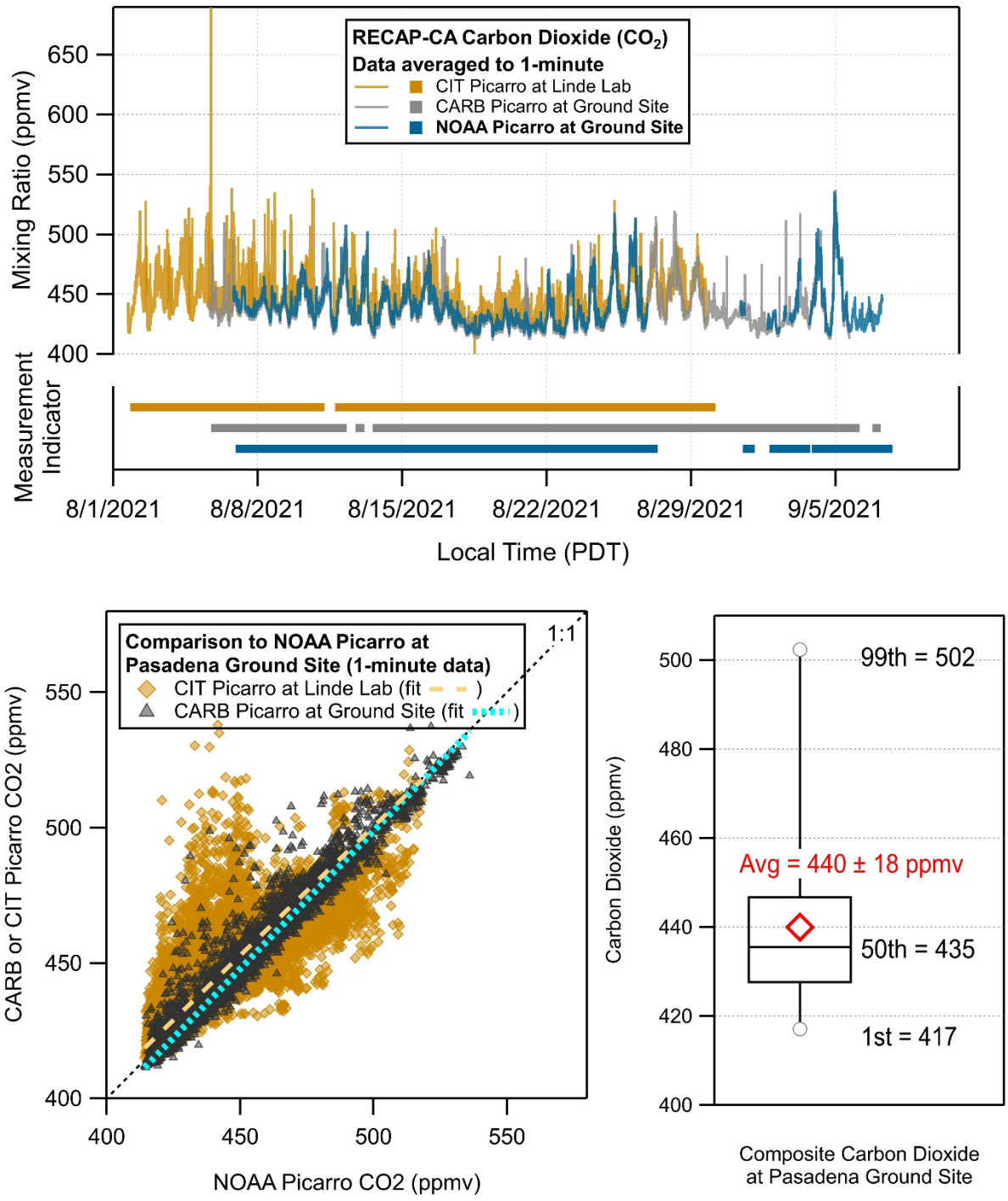


Figure A2. Observations and comparison of carbon dioxide ($CO_2$) measurements during RECAP-CA.

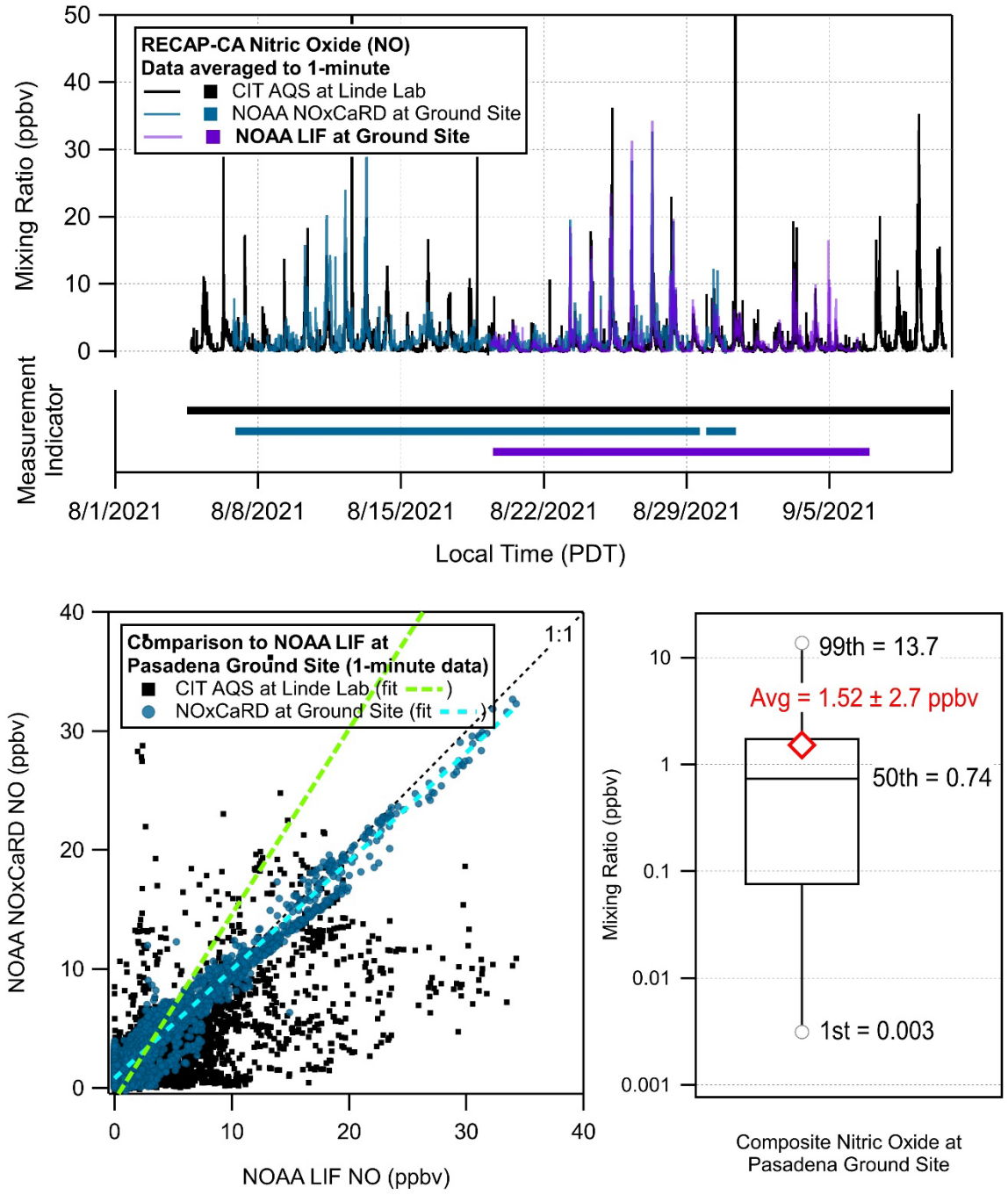


Figure A3. Observations and comparison of nitrogen oxide (NO) measurements during RECAP-CA.

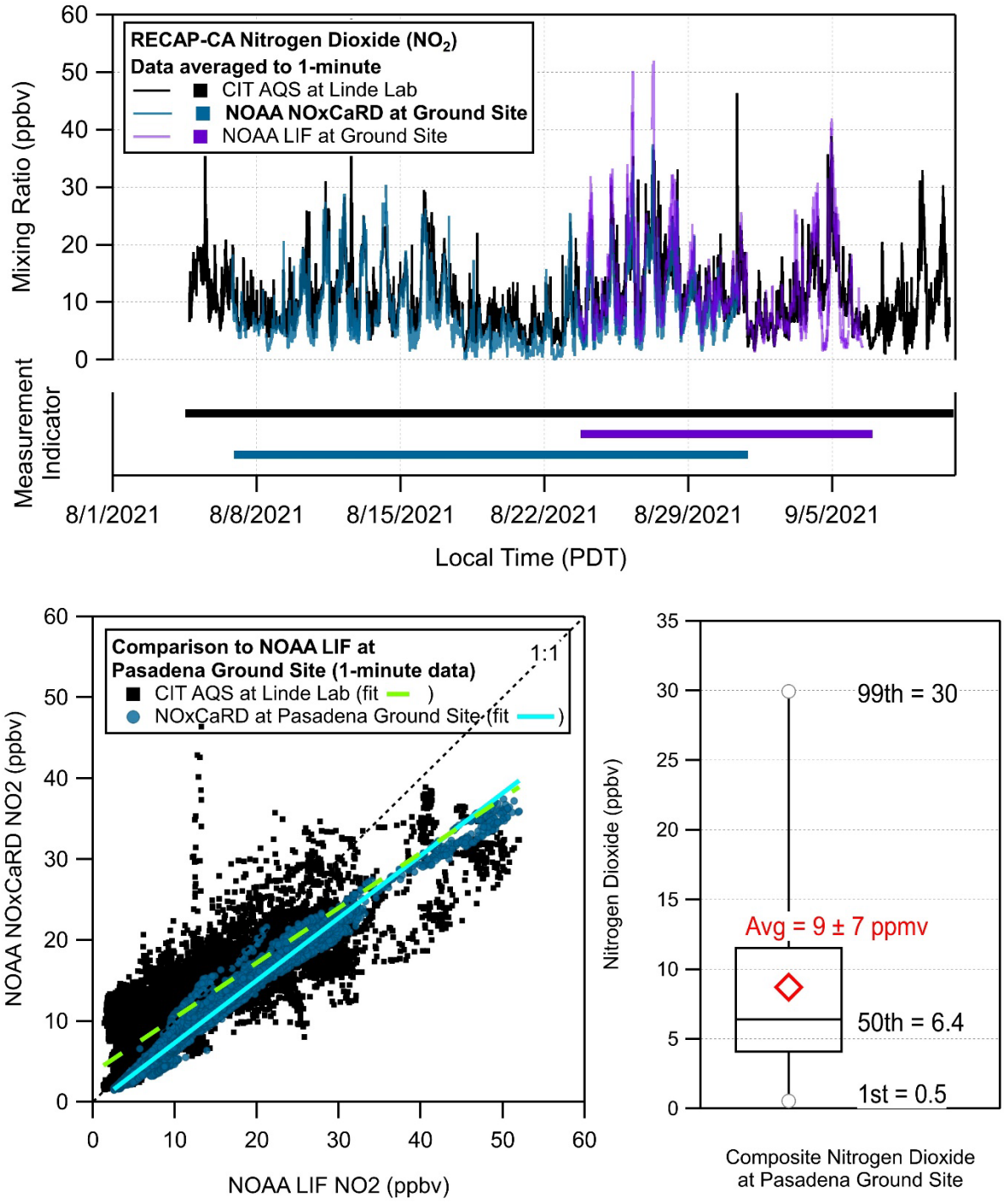


Figure A4. Observations and comparison of nitrogen dioxide ($NO_2$) measurements during RECAP-CA.

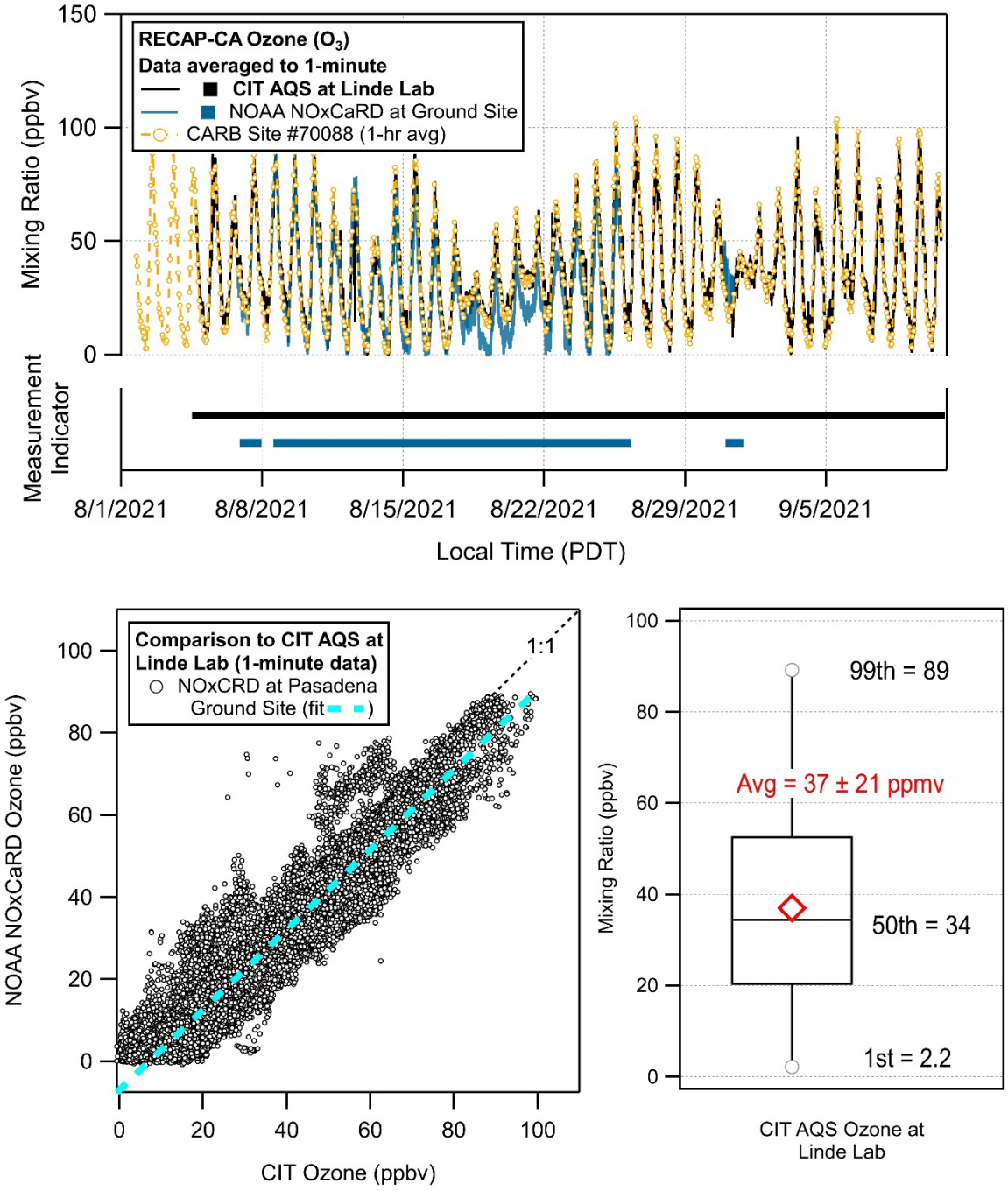


Figure A5. Observations and comparison of ozone ($O_3$) measurements during RECAP-CA.

**Appendix Table 1. RECAP-CA statistics and metrics used in analysis.**

| Line # | Measurement Identification | | Mixing Ratio Statistics | | | | | | | | Metrics Used for Analysis | | | | | | | | | |
|---|---|---|---|---|---|---|---|---|---|---|---|---|---|---|---|---|---|---|---|---|
| | metric: | | Mean | *Std. Dev.* | Median | Max | Min | Num | Mean | Median | *Used in calc* | C# | MW | MIR | kOH | kO3 | kNO3 | LogC* | SOA Yield | SOAP |
| | *Units:* | | *ppbv* | *1 sigma* | *ppbv* | *ppbv* | *ppbv* | | *ppbC* | *ppbC* | | | *g mol $^{-1}$* | *gVOC/gO $_3$* | *(cm $^3$ molec $^{-1}$ s $^{-1}$)* | | | *µ g/cm $^3$* | *g/g* | *g/g* |
| | ***Alkanes*** | | | | | | | | | | | | | | | | | | | |
| 1 | Ethane | GC-MS | 5.819 | *3.63* | 4.728 | 22.43 | 1.137 | 1746 | 11.64 | 9.46 | 1 | 2 | 30 | 0.28 | 2.48E-13 | | 4.00E-18 | 10.1 | 0 | 0 |
| 2 | Propane | GC-MS | 2.082 | *1.21* | 1.747 | 8.02 | 0.239 | 1748 | 6.25 | 5.24 | 1 | 3 | 44 | 0.49 | 1.09E-12 | | 9.20E-18 | 9.8 | 0 | 0 |
| 3 | iso-Butane | GC-MS | 0.432 | *0.23* | 0.382 | 1.94 | 0.043 | 1748 | 1.73 | 1.53 | 1 | 4 | 58 | 1.23 | 2.12E-12 | | 9.80E-17 | 9.5 | 0 | 0 |
| 4 | n-Butane | GC-MS | 0.712 | *0.43* | 0.593 | 3.47 | 0.065 | 1748 | 2.85 | 2.37 | 1 | 4 | 58 | 1.15 | 2.36E-12 | | 6.59E-17 | 9.5 | 0 | 0 |
| 5 | 2,2-dimethylpropane | GC-MS | 0.011 | *0.01* | 0.010 | 0.06 | 0.001 | 1747 | 0.05 | 0.05 | 1 | 5 | 72 | 0.67 | 8.30E-13 | | | 9.2 | 0 | 0 |
| 6 | iso-Pentane | GC-MS | 0.683 | *0.45* | 0.564 | 4.17 | 0.077 | 1748 | 3.42 | 2.82 | 1 | 5 | 72 | 1.45 | 3.60E-12 | | 1.56E-16 | 9.2 | 0 | 0 |
| 7 | n-Pentane | GC-MS | 0.356 | *0.21* | 0.308 | 3.05 | 0.038 | 1748 | 1.78 | 1.54 | 1 | 5 | 72 | 1.31 | 3.80E-12 | | 8.10E-17 | 9.2 | 0 | 0 |
| 8 | 2,2-Dimethylbutane | GC-MS | 0.034 | *0.02* | 0.029 | 0.21 | 0.003 | 1748 | 0.21 | 0.18 | 1 | 6 | 86 | 1.17 | 2.20E-12 | | | 8.8 | 0 | 0 |
| 9 | 2-Methylpentane | GC-MS | 0.147 | *0.08* | 0.134 | 0.63 | 0.013 | 1744 | 0.88 | 0.80 | 1 | 6 | 86 | 1.5 | 5.20E-12 | | 1.71E-16 | 8.8 | 0 | 0 |
| 10 | 3-Methylpentane | GC-MS | 0.156 | *0.10* | 0.133 | 1.01 | 0.010 | 1743 | 0.94 | 0.80 | 1 | 6 | 86 | 1.8 | 5.20E-12 | | 2.04E-16 | 8.8 | 0 | 0 |
| 11 | n-Hexane | GC-MS | 0.339 | *0.39* | 0.228 | 4.44 | 0.011 | 1745 | 2.03 | 1.37 | 1 | 6 | 86 | 1.24 | 5.20E-12 | | 1.05E-16 | 8.8 | 0.0028 | 0 |
| 12 | 2,4-Dimethylpentane | GC-MS | 0.068 | *0.04* | 0.056 | 0.34 | 0.005 | 1748 | 0.47 | 0.40 | 1 | 7 | 100 | 1.55 | 5.26E-12 | | 1.44E-16 | 8.5 | 0 | 0 |
| 13 | n-Heptane | GC-MS | 0.075 | *0.04* | 0.063 | 0.25 | 0.006 | 1738 | 0.53 | 0.44 | 1 | 7 | 100 | 1.07 | 6.80E-12 | | 1.37E-16 | 8.5 | 0.0066 | 0.05 |
| 14 | 2,2,4-Trimethylpentane | GC-MS | 0.152 | *0.09* | 0.135 | 0.56 | 0.012 | 1750 | 1.22 | 1.08 | 1 | 8 | 114 | 1.26 | 3.34E-12 | | 7.51E-17 | 8.1 | 0.003 | 0.05 |
| 15 | 2,3,4-Trimethylpentane | GC-MS | 0.052 | *0.04* | 0.041 | 0.27 | 0.003 | 1750 | 0.42 | 0.33 | 1 | 8 | 114 | 1.03 | 6.80E-12 | | | 8.1 | 0.003 | 0.05 |
| 16 | 2-Methylheptane | GC-MS | 0.057 | *0.04* | 0.046 | 0.25 | 0.003 | 1745 | 0.46 | 0.37 | 1 | 8 | 114 | 1.07 | 1.22E-11 | | | 8.1 | 0.003 | 0.05 |
| 17 | 3-Methylheptane | GC-MS | 0.037 | *0.03* | 0.029 | 0.19 | 0.002 | 1745 | 0.30 | 0.24 | 1 | 8 | 114 | 1.24 | 1.40E-11 | | | 8.1 | 0.003 | 0.05 |
| 18 | n-Octane | GC-MS | 0.058 | *0.04* | 0.044 | 0.23 | 0.003 | 1750 | 0.46 | 0.35 | 1 | 8 | 114 | 0.9 | 8.10E-12 | | 1.83E-16 | 8.1 | 0.013 | 0.06 |
| 19 | n-Nonane | GC-MS | 0.040 | *0.03* | 0.032 | 0.17 | 0.002 | 1740 | 0.36 | 0.29 | 1 | 9 | 128 | 0.78 | 9.70E-12 | | 1.93E-16 | 7.7 | 0.021 | 0.14 |
| 20 | n-Decane | GC-MS | 0.078 | *0.05* | 0.067 | 0.25 | 0.009 | 1750 | 0.78 | 0.67 | 1 | 10 | 142 | 0.68 | 1.10E-11 | | 2.59E-16 | 7.4 | 0.033 | 0.22 |
| 21 | Cyclopentane | GC-MS | 0.035 | *0.02* | 0.029 | 0.19 | 0.003 | 1748 | 0.17 | 0.15 | 1 | 5 | 70 | 2.39 | 4.80E-12 | | 1.50E-16 | 8.8 | 0 | 0.04 |
| 22 | Cyclohexane | GC-MS | 0.063 | *0.04* | 0.054 | 0.34 | 0.004 | 1728 | 0.38 | 0.32 | 1 | 6 | 84 | 1.25 | 7.00E-12 | | 1.35E-16 | 8.8 | 0.022 | 0 |
| 23 | Methylcyclopentane | GC-MS | 0.227 | *0.15* | 0.192 | 1.27 | 0.012 | 1748 | 1.36 | 1.15 | 1 | 6 | 84 | 2.19 | 8.60E-12 | | | 8.8 | 0.022 | 0 |
| 24 | Methylcyclohexane | GC-MS | 0.062 | *0.04* | 0.051 | 0.29 | 0.004 | 1750 | 0.44 | 0.36 | 1 | 7 | 98 | 1.7 | 9.60E-12 | | | 8.5 | 0.035 | 0.22 |
| | ***Alkenes*** | | | | | | | | | | | | | | | | | | | |
| 24 | Ethene | GC-MS | 0.992 | *0.61* | 0.819 | 3.45 | 0.080 | 1748 | 1.98 | 1.64 | 1 | 2 | 28 | 9 | 8.50E-12 | 1.59E-18 | 2.02E-16 | 10 | 0 | 0 |
| 25 | Propene | GC-MS | 0.211 | *0.14* | 0.174 | 0.91 | 0.021 | 1748 | 0.63 | 0.52 | 1 | 3 | 42 | 11.66 | 2.60E-11 | 1.00E-17 | 9.45E-15 | 9.7 | 0 | 0 |
| 26 | 1-Butene | GC-MS | 0.035 | *0.02* | 0.028 | 0.17 | 0.003 | 1748 | 0.14 | 0.11 | 1 | 4 | 56 | 9.73 | 3.10E-11 | 1.09E-17 | 1.25E-14 | 9.4 | 0 | 0 |
| 27 | cis-2-Butene | GC-MS | 0.008 | *0.01* | 0.005 | 0.10 | 0.000 | 1486 | 0.03 | 0.02 | 1 | 4 | 56 | 14.24 | 5.60E-11 | 1.27E-16 | 3.50E-13 | 9.4 | 0 | 0 |
| 28 | trans-2-Butene | GC-MS | 0.008 | *0.01* | 0.005 | 0.11 | 0.000 | 1547 | 0.03 | 0.02 | 1 | 4 | 56 | 15.16 | 6.40E-11 | 1.82E-16 | 3.90E-13 | 9.4 | 0 | 0 |
| 29 | 1-Pentene | GC-MS | 0.015 | *0.01* | 0.012 | 0.07 | 0.002 | 1748 | 0.08 | 0.06 | 1 | 5 | 70 | 7.21 | 3.10E-11 | 8.70E-18 | | 9.1 | 0.026 | 0 |
| 30 | 2-Methyl-1-butene | GC-MS | 0.014 | *0.01* | 0.011 | 0.10 | 0.001 | 1748 | 0.07 | 0.05 | 1 | 5 | 70 | 6.4 | 6.10E-11 | 1.40E-17 | | 9.1 | 0 | 0 |
| 31 | 3-Methyl-1-butene | GC-MS | 0.008 | *0.01* | 0.006 | 0.04 | 0.001 | 1747 | 0.04 | 0.03 | 1 | 5 | 70 | 6.99 | 3.20E-11 | 9.50E-18 | 1.39E-14 | 9.1 | 0 | 0 |
| 32 | cis-2-Pentene | GC-MS | 0.005 | *0.01* | 0.003 | 0.05 | 0.000 | 1723 | 0.02 | 0.01 | 1 | 5 | 70 | 10.38 | 6.50E-11 | 1.30E-16 | | 9.1 | 0.026 | 0 |
| 33 | trans-2-Pentene | GC-MS | 0.009 | *0.01* | 0.005 | 0.10 | 0.000 | 1745 | 0.04 | 0.02 | 1 | 5 | 70 | 10.56 | 6.70E-11 | 1.62E-16 | | 9.1 | 0.026 | 0 |
| | ***Alkynes and Dienes*** | | | | | | | | | | | | | | | | | | | |
| 34 | Ethyne (Acetylene) | GC-MS | 0.702 | *0.33* | 0.618 | 2.48 | 0.111 | 1748 | 1.40 | 1.24 | 1 | 2 | 26 | 0.95 | 9.00E-13 | 1.00E-20 | 5.00E-17 | 10 | 0 | 0 |
| 35 | 1,3-Butadiene | GC-MS | 0.028 | *0.03* | 0.020 | 0.17 | 0.001 | 1744 | 0.11 | 0.08 | 1 | 4 | 54 | 12.61 | 6.70E-11 | 6.30E-18 | 1.00E-13 | 9.4 | 0 | 0.13 |
| | ***Biogenics*** | | | | | | | | | | | | | | | | | | | |
| 36 | Isoprene | GC-MS | 0.903 | *1.17* | 0.278 | 6.77 | 0.004 | 1746 | 4.51 | 1.39 | 1 | 5 | 68 | 10.61 | 1.00E-10 | 1.17E-17 | 6.77E-13 | 9.1 | 0.026 | 0.01 |
| 37 | alpha-Pinene | GC-MS | 0.035 | *0.06* | 0.015 | 0.38 | 0.000 | 1540 | 0.35 | 0.15 | 1 | 10 | 136 | 4.51 | 5.20E-11 | 8.40E-17 | 3.40E-12 | 7.1 | 0.13 | 0.13 |
| 38 | beta-Pinene | GC-MS | 0.012 | *0.01* | 0.007 | 0.12 | 0.000 | 1684 | 0.12 | 0.07 | 1 | 10 | 136 | 3.52 | 7.40E-11 | 2.10E-17 | 1.40E-12 | 7.1 | 0.13 | 0.13 |
| 39 | Sum Monoterpenes* | PTR-MS | 0.186 | *0.15* | 0.140 | 1.09 | 0.018 | 1840 | 1.86 | 1.40 | 0 | 10 | 136 | 4.04 | 6.00E-11 | *5.00E-17* | *2.00E-12* | 0 | 0 | 0.19 |

| Line # | Measurement Identification | | Mixing Ratio Statistics | | | | | | | | Metrics Used for Analysis | | | | | | | | | |
|---|---|---|---|---|---|---|---|---|---|---|---|---|---|---|---|---|---|---|---|---|
| | metric: | | Mean | *Std. Dev.* | Median | Max | Min | Num | Mean | Median | *Used in calc* | C# | MW | MIR | kOH | kO3 | kNO3 | LogC* | SOA Yield | SOAP |
| | *Units:* | | *ppbv* | *1 sigma* | *ppbv* | *ppbv* | *ppbv* | | *ppbC* | *ppbC* | | | *g mol$^{-1}$* | *gVOC/gO$_3$* | *(cm$^3$ molec$^{-1}$ s$^{-1}$)* | | | *µ g/cm$^3$* | *g/g* | *g/g* |
| | ***Aromatics*** | | | | | | | | | | | | | | | | | | | |
| 40 | Benzene | GC-MS | 0.227 | *0.09* | 0.209 | 0.61 | 0.045 | 1750 | 1.36 | 1.25 | 1 | 6 | 78 | 0.72 | 1.20E-12 | | 3.01E-17 | 8 | 0.02 | 0.24 |
| 41 | Benzene* | PTR-MS | 0.220 | *0.11* | 0.193 | 0.76 | -0.017 | 1836 | 1.32 | 1.16 | 0 | 6 | 78 | 0.72 | 1.20E-12 | | 3.01E-17 | 8 | 0.02 | 0.24 |
| 42 | Toluene | GC-MS | 0.391 | *0.24* | 0.326 | 1.71 | 0.028 | 1750 | 2.74 | 2.28 | 1 | 7 | 92 | 4 | 5.60E-12 | | 6.79E-17 | 7.8 | 0.09 | 0.36 |
| 43 | Toluene* | PTR-MS | 0.477 | *0.32* | 0.373 | 2.62 | 0.048 | 1836 | 3.34 | 2.61 | 0 | 7 | 92 | 4 | 5.60E-12 | | 6.79E-17 | 7.8 | 0.09 | 0.36 |
| 44 | Sum C8-Aromatics* | PTR-MS | 0.305 | *0.22* | 0.235 | 1.28 | 0.032 | 1836 | 2.44 | 1.88 | 1 | 8 | 106 | 7.64 | 1.55E-11 | | 3.77E-16 | 7.4 | 0.049 | 0.08 |
| 45 | Sum C9-Aromatics* | PTR-MS | 0.154 | *0.12* | 0.116 | 0.74 | 0.014 | 1836 | 1.39 | 1.04 | 1 | 9 | 120 | 7.99 | 1.83E-11 | | 2.00E-15 | 7 | 0.73 | 0.04 |
| | ***Nitrogen and Sulfur Organics*** | | | | | | | | | | | | | | | | | | | |
| 46 | Acetonitrile* | PTR-MS | 0.355 | *0.36* | 0.269 | 6.25 | 0.110 | 1836 | 0.71 | 0.54 | 1 | 2 | 41 | 0.02 | 2.00E-13 | | 5.00E-19 | | 0 | 0 |
| 47 | Benzenenitrile* | PTR-MS | 0.005 | *0.00* | 0.004 | 0.02 | 0.001 | 1840 | 0.03 | 0.02 | 1 | 7 | 103 | 0.7 | 1.00E-12 | | | 8 | 0.02 | 0 |
| 48 | Nitromethane | GC-MS | 0.052 | *0.02* | 0.047 | 0.16 | 0.010 | 1745 | 0.05 | 0.05 | 1 | 1 | 61 | 0.07 | 2.00E-13 | | | | 0 | 0 |
| 49 | Methyl Nitrate | GC-MS | 0.049 | *0.02* | 0.045 | 0.16 | 0.018 | 1749 | 0.05 | 0.05 | 1 | 1 | 77 | 1 | 4.00E-13 | | | | 0 | 0 |
| 50 | Ethyl Nitrate | GC-MS | 0.014 | *0.01* | 0.012 | 0.04 | 0.004 | 1748 | 0.03 | 0.02 | 1 | 2 | 91 | 1 | 4.90E-13 | | | | 0 | 0 |
| 51 | iso-Propyl Nitrate | GC-MS | 0.018 | *0.01* | 0.015 | 0.08 | 0.003 | 1748 | 0.05 | 0.04 | 1 | 3 | 105 | 1 | 4.90E-13 | | | | 0 | 0 |
| 52 | n-Propyl Nitrate | GC-MS | 0.007 | *0.00* | 0.006 | 0.03 | 0.002 | 1300 | 0.02 | 0.02 | 1 | 3 | 105 | 1 | 4.90E-13 | | | | 0 | 0 |
| 53 | PAN* | I-CIMS | 1.674 | *1.21* | 1.362 | 7.16 | 0.135 | 997 | 1.67 | 1.36 | 0 | 1 | 121 | 0 | | | | 0 | 0 | 0 |
| 54 | SumPANs* | I-CIMS | 1.869 | *1.35* | 1.526 | 7.96 | 0.148 | 997 | 1.87 | 1.53 | 1 | 1 | 121 | 0 | | | | 0 | 0 | 0 |
| 55 | Isoprene Nitrates* | I-CIMS | 0.009 | *0.01* | 0.004 | 0.08 | 0.000 | 1713 | 0.04 | 0.02 | 1 | 5 | | 0 | | | | 0 | 0 | 0 |
| 56 | C4H7NO5* | I-CIMS | 0.011 | *0.01* | 0.006 | 0.07 | 0.000 | 1706 | 0.04 | 0.02 | 1 | 4 | 149 | 0 | | | | 0 | 0 | 0 |
| 57 | C5H9NO5* | I-CIMS | 0.021 | *0.01* | 0.017 | 0.09 | 0.002 | 1705 | 0.11 | 0.09 | 1 | 5 | 163 | 0 | | | | 0 | 0 | 0 |
| 58 | C10H17NO4* | I-CIMS | 0.005 | *0.00* | 0.003 | 0.03 | 0.001 | 1699 | 0.05 | 0.03 | 1 | 10 | 215 | | | | | | | 0 |
| 59 | Carbon Disulfide ($CS_2$) | GC-MS | 0.009 | *0.01* | 0.008 | 0.05 | 0.002 | 1746 | 0.01 | 0.01 | 1 | 1 | 76 | 0.25 | 1.00E-13 | | | | 0 | 0 |
| | ***Oxygenated VOCs, saturated (OVOC_sat)*** | | | | | | | | | | | | | | | | | | | |
| 60 | Formaldehyde | CARB | 3.016 | *2.13* | 2.326 | 11.35 | 0.119 | 2103 | 3.02 | 2.33 | 1 | 1 | 30 | 9.46 | 9.40E-12 | | 5.80E-16 | 9.2 | 0 | 0 |
| 61 | Acetaldehyde | GC-MS | 1.187 | *0.53* | 1.099 | 3.46 | 0.264 | 1358 | 2.37 | 2.20 | 1 | 2 | 44 | 6.54 | 1.60E-11 | | | 8.4 | 0 | 0 |
| 62 | Acetaldehyde* | PTR-MS | 3.221 | *1.71* | 2.759 | 10.74 | 0.492 | 1840 | 6.44 | 5.52 | 0 | 2 | 44 | 6.54 | 1.60E-11 | | | 8.4 | 0 | 0 |
| 63 | Octanal* | PTR-MS | 0.086 | *0.05* | 0.073 | 0.27 | 0.013 | 1840 | 0.69 | 0.58 | 1 | 8 | 128 | 3.16 | 1.00E-11 | | | 7 | 0.029 | 0.09 |
| 64 | Nonanal* | PTR-MS | 0.102 | *0.07* | 0.081 | 0.41 | -0.004 | 1840 | 0.92 | 0.73 | 1 | 9 | 142 | 3 | 1.10E-11 | | | 6.5 | 0.029 | 0.09 |
| 65 | Methanol | GC-MS | 4.032 | *1.68* | 3.619 | 17.15 | 1.403 | 1750 | 4.03 | 3.62 | 1 | 1 | 32 | 0.67 | 9.00E-13 | | 9.51E-18 | 8.4 | 0 | 0 |
| 66 | Methanol* | PTR-MS | 5.454 | *3.06* | 4.642 | 45.11 | 1.579 | 1840 | 5.45 | 4.64 | 0 | 1 | 32 | 0.67 | 9.00E-13 | | 9.51E-18 | 8.4 | 0 | 0 |
| 67 | Ethanol | GC-MS | 6.655 | *3.47* | 5.716 | 28.31 | 1.037 | 1750 | 13.31 | 11.43 | 1 | 2 | 46 | 1.53 | 3.20E-12 | | | 8.1 | 0 | 0 |
| 68 | Ethanol* | PTR-MS | 11.82 | *6.92* | 9.981 | 42.68 | 1.606 | 1840 | 23.63 | 19.96 | 0 | 2 | 46 | 1.53 | 3.40E-12 | | | 8.1 | 0 | 0 |
| 69 | iso-Propanol | GC-MS | 0.874 | *0.84* | 0.720 | 16.41 | 0.169 | 1530 | 2.62 | 2.16 | 1 | 3 | 60 | 0.61 | 4.20E-12 | | | 7.8 | 0 | 0 |
| | ***Oxygenated VOCs, usaturated (OVOC_unsat)*** | | | | | | | | | | | | | | | | | | | |
| 70 | Acetone | GC-MS | 5.40 | *2.64* | 4.829 | 20.27 | 1.403 | 1750 | 16.20 | 14.49 | 1 | 3 | 58 | 0.36 | 1.90E-13 | | | 9 | 0 | 0.01 |
| 71 | Sum Acetone+Propanal* | PTR-MS | 6.116 | *3.13* | 5.400 | 22.61 | 1.864 | 1840 | 18.35 | 16.20 | 0 | 3 | 58 | 1 | 2.00E-13 | | | 9 | 0 | 0.01 |
| 72 | 2-Butanone (MEK) | GC-MS | 0.353 | *0.21* | 0.309 | 1.55 | 0.051 | 1750 | 1.41 | 1.24 | 1 | 4 | 72 | 1.48 | 1.20E-12 | | | 8.7 | 0 | 0.01 |
| 73 | Formic acid* | I-CIMS | 3.468 | *1.82* | 3.094 | 13.47 | 0.350 | 1816 | 3.47 | 3.09 | 1 | 1 | 46 | 0.06 | 4.50E-13 | | | 7 | 0 | 0 |
| 74 | C5H10O3* | I-CIMS | 0.020 | *0.02* | 0.016 | 0.14 | 0.002 | 1718 | 0.10 | 0.08 | 1 | 5 | 118 | 0 | | | | 0 | 0 | 0 |
| 75 | Methyl acetate | GC-MS | 0.152 | *0.09* | 0.128 | 1.18 | 0.034 | 1745 | 0.45 | 0.38 | 1 | 3 | 74 | 0.07 | 3.50E-13 | | | 8.9 | 0 | 0 |
| 76 | Ethyl acetate | GC-MS | 0.058 | *0.04* | 0.047 | 0.29 | 0.009 | 593 | 0.23 | 0.19 | 1 | 4 | 88 | 0.63 | 8.80E-13 | | | 8.5 | 0 | 0 |
| 77 | Methacrolein (MACR) | GC-MS | 0.203 | *0.26* | 0.073 | 2.00 | 0.002 | 1746 | 0.81 | 0.29 | 1 | 4 | 70 | 6.01 | 3.10E-11 | | | | | 0 |
| 78 | Methylvinylketone (MVK) | GC-MS | 0.238 | *0.31* | 0.090 | 2.86 | 0.006 | 1631 | 0.95 | 0.36 | 1 | 4 | 70 | 9.65 | 1.90E-11 | | | | | 0.01 |
| 79 | Sum MVK+MACR* | PTR-MS | 0.484 | *0.49* | 0.292 | 4.77 | 0.032 | 1840 | 1.93 | 1.17 | 0 | 4 | 70 | 8 | 2.50E-11 | | | 0 | 0 | 0.005 |
| 80 | Benzenealdehyde* | PTR-MS | 0.052 | *0.03* | 0.043 | 0.29 | -0.054 | 1840 | 0.36 | 0.30 | 1 | 7 | 106 | 0 | 1.30E-11 | | 2.54E-15 | | | 0 |

| Line # | Measurement Identification | | Mixing Ratio Statistics | | | | | | | | Metrics Used for Analysis | | | | | | | | | |
|---|---|---|---|---|---|---|---|---|---|---|---|---|---|---|---|---|---|---|---|---|
| | metric: | | Mean | Std. Dev. | Median | Max | Min | Num | Mean | Median | Used in calc | C# | MW | MIR | kOH | kO3 | kNO3 | LogC* | SOA Yield | SOAP |
| | Units: | | ppbv | 1 sigma | ppbv | ppbv | ppbv | | ppbC | ppbC | | | g mol$^{-1}$ | gVOC/gO$_3$ | (cm$^3$ molec$^{-1}$ s$^{-1}$) | | | μg/cm$^3$ | g/g | g/g |
| | ***Oxygenated VOCs, usaturated (OVOC_unsat), continuted*** | | | | | | | | | | | | | | | | | | | |
| 81 | Furan* | PTR-MS | 0.061 | *0.03* | 0.054 | 0.58 | 0.008 | 1840 | 0.25 | 0.22 | 1 | 4 | 68 | 9.15 | 4.00E-11 | | | 0 | 0 | 0 |
| 82 | Methylfurans* | PTR-MS | 0.101 | *0.06* | 0.083 | 0.40 | 0.015 | 1840 | 0.50 | 0.42 | 1 | 5 | 82 | 8 | 6.20E-11 | | | | | 0 |
| 83 | C5H4O2* | PTR-MS | 0.055 | *0.04* | 0.045 | 0.46 | -0.018 | 1840 | 0.28 | 0.23 | 1 | 5 | 96 | 0 | | | | 0 | 0 | 0 |
| 84 | D5-Siloxane* | PTR-MS | 0.040 | *0.03* | 0.030 | 0.19 | 0.005 | 1840 | 0.40 | 0.30 | 1 | 10 | 371 | 0 | 2.00E-12 | | | 4.4 | 0.095 | 0 |
| 85 | Texanol* | PTR-MS | 0.049 | *0.03* | 0.040 | 0.23 | 0.005 | 1840 | 0.59 | 0.48 | 1 | 12 | 216 | 0 | 1.20E-11 | | | 3.3 | 0.0048 | 0 |
| | ***Halocarbons*** | | | | | | | | | | | | | | | | | | | |
| 86 | PCBTF* | PTR-MS | 0.088 | *0.07* | 0.070 | 1.45 | 0.007 | 1840 | 0.62 | 0.49 | 1 | 7 | 180 | 0.7 | 1.00E-12 | | 0 | 8.7 | 0 | 0 |
| 87 | CFCl3 | GC-MS | 0.217 | *0.05* | 0.213 | 0.56 | 0.114 | 1748 | 0.22 | 0.21 | 1 | 1 | 36 | 0 | 1.00E-13 | | 0 | 0 | 0 | 0 |
| 88 | CH2Cl2 | GC-MS | 0.441 | *0.76* | 0.224 | 16.63 | 0.022 | 1746 | 0.44 | 0.22 | 1 | 1 | 84 | 0.04 | 1.00E-13 | | 0 | 0 | 0 | 0 |
| 89 | CH2_CCl2 | GC-MS | 0.000 | *0.00* | 0.000 | 0.00 | 0.000 | 1585 | 0.00 | 0.00 | 1 | 2 | 96 | 1.79 | 1.70E-13 | 7.20E-21 | 0 | 0 | 0 | 0 |
| 90 | CH2Cl_CH2Cl | GC-MS | 0.017 | *0.00* | 0.016 | 0.08 | 0.011 | 583 | 0.03 | 0.03 | 1 | 2 | 98 | 1.7 | 1.00E-13 | | 0 | 0 | 0 | 0 |
| 91 | Chloroform (CHCl3) | GC-MS | 0.057 | *0.04* | 0.046 | 0.74 | 0.017 | 1750 | 0.06 | 0.05 | 1 | 1 | 118 | 0.02 | 1.70E-13 | | 0 | 0 | 0 | 0 |
| 92 | CF2Cl2 | GC-MS | 0.490 | *0.06* | 0.487 | 0.73 | 0.273 | 1748 | 0.49 | 0.49 | 1 | 1 | 120 | 0 | 1.00E-13 | | 0 | 0 | 0 | 0 |
| 93 | CHCl_CCl2 | GC-MS | 0.005 | *0.01* | 0.003 | 0.07 | 0.000 | 1737 | 0.01 | 0.01 | 1 | 2 | 130 | 0.64 | 2.20E-12 | | 0 | 0 | 0 | 0 |
| 94 | CCl2_CCl2 | GC-MS | 0.022 | *0.02* | 0.017 | 0.29 | 0.004 | 1750 | 0.04 | 0.03 | 1 | 2 | 164 | 0.03 | 1.00E-13 | | 0 | 0 | 0 | 0 |
| 95 | CF2Cl_CF2Cl | GC-MS | 0.018 | *0.00* | 0.017 | 0.03 | 0.008 | 1739 | 0.04 | 0.03 | 1 | 2 | 170 | 0 | 1.00E-13 | | 0 | 0 | 0 | 0 |
| 96 | CFCl2_CF2Cl | GC-MS | 0.076 | *0.02* | 0.072 | 0.16 | 0.029 | 1747 | 0.15 | 0.14 | 1 | 2 | 186 | 0 | 1.00E-13 | | 0 | 0 | 0 | 0 |
| | ***Methane and Inorganic Carbon*** | | | | | | | | | | | | | | | | | | | |
| 97 | Methane (CH4) | NOAA | 2091 | *104* | 2063 | 2528 | 1923 | 2215 | 2091 | 2063 | 1 | 1 | 16 | 0.014 | 6.00E-15 | | 1.00E-18 | | | |
| 98 | Carbon monoxide (CO) | NOAA | 275 | *82* | 256 | 692 | 132 | 2292 | 275 | 256 | 1 | 1 | 28 | 0.05 | 1.50E-13 | | | | | |
| 99 | Carbon dioxide (CO2) | NOAA | 439383 | *16568* | 435610 | 515542 | 414875 | 2215 | 439383 | 435610 | 1 | 1 | 44 | 0 | | | | | | |
| | ***Inorganic Nitrogen*** | | | | | | | | | | 1 | | | | | | | | | |
| 100 | Nitrogen oxide (NO) | NOAA | 1.541 | *2.73* | 0.763 | 31.83 | -0.002 | 1927 | | | 1 | 0 | 30 | | | | | | | |
| 101 | Nitrogen dioxide (NO2) | NOAA | 8.445 | *6.26* | 6.426 | 42.26 | 0.006 | 2021 | | | 1 | 0 | 46 | | 8.70E-12 | | | | | |
| 102 | Nitrogen oxides (NOx) | NOAA | 9.851 | *7.92* | 7.245 | 66.64 | 0.250 | 1916 | | | 1 | 0 | | | | | | | | |
| 103 | Sum N2O5+HPMTF* | I-CIMS | 0.005 | *0.01* | 0.001 | 0.21 | 0.000 | 1773 | | | 1 | | 108 | | | | | | | |
| 104 | HONO* | I-CIMS | 0.429 | *0.49* | 0.232 | 3.23 | -0.033 | 1806 | | | 1 | 0 | 47 | | 6.00E-12 | | | | | |
| 105 | Nitric acid (HNO3)* | I-CIMS | 1.428 | *1.33* | 0.874 | 8.16 | -0.163 | 1855 | | | 1 | 0 | 63 | | | | | | | |
| 106 | Ammonia (NH3) | CARB | 7.610 | *3.20* | 6.528 | 19.35 | 2.537 | 2103 | | | 1 | 0 | 17 | | 1.50E-13 | | | | | |
| 107 | Dinitrogen oxide (N2O) | NOAA | 337 | *2* | 337 | 377 | 334 | 2292 | | | 1 | 0 | 44 | | | | | | | |
| | ***Inorganic chlorine*** | | | | | | | | | | 1 | | | | | | | | | |
| 108 | Hydrochloric acid (HCl) | TILDAS | 0.806 | *0.91* | 0.470 | 5.11 | -0.298 | 1187 | | | 1 | 0 | 36 | | 8.00E-14 | | | | | |
| 109 | Nitryl chloride (ClNO2)* | I-CIMS | 0.059 | *0.09* | 0.017 | 0.62 | -0.001 | 1853 | | | 1 | 0 | 81 | | | | | | | |

*Appendix Table 2. Emission ratios for RECAP-CA. Bolded numbers denote recommend values based on best practice methods.*

| | | | | | | | | | | **Method 1:** OH-corr, Primary Only | | | | **Method 2:** O3-corr | | **Method 3:** OH corr, includes secondary | | | |
|---|---|---|---|---|---|---|---|---|---|---|---|---|---|---|---|---|---|---|---|
| **Line #** | **Measurement Identification** | | **Night ER: [x]/[CO]** | | | **Night ER: [x]/[Ethyne]** | | | | **ER: [Δx]/[ΔCO]** | | | | **ER: [Δx]/[ΔCO]** | | **ER: [Δx]/[ΔCO]** | | | |
| | | **units:** | ***ppbv ppmv*** $^{-1}$ | ***uncert.*** | ***fit (r)*** | ***ppbv ppmv*** $^{-1}$ | ***uncert.*** | ***fit (r)*** | ***ppbv ppmv*** $^{-1}$ | ***ER uncert.*** | ***VOC*** $_{bknd}$ ***(ppbv)*** | ***VOC*** $_{bknd}$ ***uncert.*** | ***ppbv ppmv*** $^{-1}$ | ***1 sigma*** | ***ppbv ppmv*** $^{-1}$ | ***1 sigma*** | ***VOC*** $_{bknd}$ ***(ppbv)*** | ***VOC*** $_{bknd}$ ***uncert.*** |
| | ***Alkanes*** | | | | | | | | | | | | | | | | | |
| 1 | Ethane | GC-MS | 30.3 | *1.8* | 0.67 | 6.75 | *0.44* | 0.63 | **32.02** | ***0.80*** | 1.63 | *0.13* | | | | | | |
| 2 | Propane | GC-MS | 12.1 | *0.48* | 0.80 | 2.76 | *0.12* | 0.77 | **11.40** | ***0.26*** | 0.64 | *0.04* | | | | | | |
| 3 | iso-Butane | GC-MS | 2.38 | *0.095* | 0.80 | 0.526 | *0.025* | 0.75 | **2.21** | ***0.05*** | 0.17 | *0.01* | | | | | | |
| 4 | n-Butane | GC-MS | 3.70 | *0.219* | 0.67 | 0.824 | *0.054* | 0.63 | **3.43** | ***0.11*** | 0.30 | *0.02* | | | | | | |
| 5 | 2,2-dimethylpropane | GC-MS | 0.052 | *0.002* | 0.77 | 0.011 | *0.001* | 0.71 | **0.051** | ***0.001*** | 0.00 | *0.00* | | | | | | |
| 6 | iso-Pentane | GC-MS | 4.10 | *0.151* | 0.82 | 0.858 | *0.043* | 0.73 | **4.41** | ***0.10*** | 0.18 | *0.01* | | | | | | |
| 7 | n-Pentane | GC-MS | 1.98 | *0.112* | 0.69 | 0.420 | *0.029* | 0.62 | **1.85** | ***0.06*** | 0.15 | *0.01* | | | | | | |
| 8 | 2,2-Dimethylbutane | GC-MS | 0.193 | *0.007* | 0.85 | 0.040 | *0.002* | 0.74 | **0.204** | ***0.004*** | 0.01 | *0.00* | | | | | | |
| 9 | 2-Methylpentane | GC-MS | 0.819 | *0.026* | 0.86 | 0.171 | *0.008* | 0.76 | **1.041** | ***0.015*** | 0 | *0* | | | | | | |
| 10 | 3-Methylpentane | GC-MS | 0.818 | *0.053* | 0.64 | 0.177 | *0.013* | 0.58 | **1.010** | ***0.024*** | 0 | *0* | | | | | | |
| 11 | 2,4-Dimethylpentane | GC-MS | 0.519 | *0.012* | 0.91 | 0.105 | *0.004* | 0.79 | **0.606** | ***0.006*** | 0 | *0* | | | | | | |
| 12 | n-Heptane | GC-MS | 0.516 | *0.016* | 0.87 | 0.107 | *0.005* | 0.76 | **0.654** | ***0.007*** | 0 | *0* | | | | | | |
| 13 | 2,2,4-Trimethylpentane | GC-MS | 1.07 | *0.026* | 0.91 | 0.219 | *0.009* | 0.79 | **1.026** | ***0.013*** | 0.03 | *0.00* | | | | | | |
| 14 | 2,3,4-Trimethylpentane | GC-MS | 0.510 | *0.011* | 0.93 | 0.106 | *0.004* | 0.82 | **0.555** | ***0.006*** | 0 | *0* | | | | | | |
| 15 | 2-Methylheptane | GC-MS | 0.490 | *0.013* | 0.90 | 0.099 | *0.004* | 0.77 | **0.594** | ***0.006*** | 0 | *0* | | | | | | |
| 16 | 3-Methylheptane | GC-MS | 0.329 | *0.009* | 0.90 | 0.066 | *0.003* | 0.76 | **0.408** | ***0.004*** | 0 | *0* | | | | | | |
| 17 | n-Octane | GC-MS | 0.539 | *0.017* | 0.86 | 0.113 | *0.005* | 0.76 | **0.606** | ***0.007*** | 0 | *0* | | | | | | |
| 18 | n-Nonane | GC-MS | 0.381 | *0.010* | 0.89 | 0.078 | *0.003* | 0.77 | **0.420** | ***0.005*** | 0 | *0* | | | | | | |
| 19 | n-Decane | GC-MS | 0.505 | *0.020* | 0.80 | 0.107 | *0.006* | 0.72 | **0.668** | ***0.010*** | 0 | *0* | | | | | | |
| 20 | Cyclopentane | GC-MS | 0.201 | *0.009* | 0.78 | 0.043 | *0.002* | 0.71 | **0.215** | ***0.005*** | 0.011 | *0.001* | | | | | | |
| 21 | Cyclohexane | GC-MS | 0.370 | *0.017* | 0.76 | 0.079 | *0.004* | 0.69 | **0.482** | ***0.008*** | 0 | *0* | | | | | | |
| 22 | Methylcyclopentane | GC-MS | 1.11 | *0.074* | 0.63 | 0.239 | *0.018* | 0.57 | **1.460** | ***0.036*** | 0 | *0* | | | | | | |
| 23 | Methylcyclohexane | GC-MS | 0.482 | *0.016* | 0.85 | 0.099 | *0.005* | 0.74 | **0.609** | ***0.007*** | 0 | *0* | | | | | | |
| | ***Alkenes*** | | | | | | | | | | | | | | | | | |
| 24 | Ethene | GC-MS | 7.16 | *0.141* | 0.94 | 1.58 | *0.047* | 0.88 | 8.144 | *0.084* | 0.201 | 0.010 | **8.457** | ***0.156*** | | | | |
| 25 | Propene | GC-MS | 1.58 | *0.041* | 0.90 | 0.342 | *0.013* | 0.83 | 2.235 | *0.028* | 0 | *0* | **2.069** | ***0.047*** | | | | |
| 26 | 1-Butene | GC-MS | 0.282 | *0.008* | 0.89 | 0.062 | *0.002* | 0.83 | 0.379 | *0.005* | 0 | *0* | **0.360** | ***0.008*** | | | | |
| 27 | cis-2-Butene | GC-MS | 0.063 | *0.005* | 0.59 | 0.014 | *0.001* | 0.53 | 0.098 | *0.003* | 0 | *0* | **0.167** | ***0.002*** | | | | |
| 28 | trans-2-Butene | GC-MS | 0.070 | *0.005* | 0.60 | 0.017 | *0.001* | 0.57 | 0.114 | *0.003* | 0 | *0* | **0.179** | ***0.003*** | | | | |
| 29 | 1-Pentene | GC-MS | 0.126 | *0.004* | 0.88 | 0.026 | *0.001* | 0.78 | 0.170 | *0.002* | 0 | *0* | **0.164** | ***0.004*** | | | | |
| 30 | 2-Methyl-1-butene | GC-MS | 0.102 | *0.007* | 0.60 | 0.020 | *0.002* | 0.50 | 0.153 | *0.003* | 0 | *0* | **0.232** | ***0.006*** | | | | |
| 31 | 3-Methyl-1-butene | GC-MS | 0.068 | *0.002* | 0.85 | 0.014 | *0.001* | 0.76 | 0.098 | *0.001* | 0 | *0* | **0.095** | ***0.002*** | | | | |
| 32 | cis-2-Pentene | GC-MS | 0.046 | *0.003* | 0.58 | 0.009 | *0.001* | 0.48 | 0.080 | *0.002* | 0 | *0* | **0.102** | ***0.003*** | | | | |
| 33 | trans-2-Pentene | GC-MS | 0.091 | *0.007* | 0.58 | 0.018 | *0.002* | 0.49 | 0.163 | *0.005* | 0 | *0* | **0.200** | ***0.006*** | | | | |
| | ***Alkynes and Dienes*** | | | | | | | | | | | | | | | | | |
| 34 | Ethyne (Acetylene) | GC-MS | 3.75 | *0.106* | 0.89 | 1 | *0.000* | 1 | **3.46** | ***0.06*** | 0.254 | 0.009 | | | | | | |
| 35 | 1,3-Butadiene | GC-MS | 0.257 | *0.012* | 0.75 | 0.052 | *0.003* | 0.64 | 0.39 | *0.01* | 0 | *0* | **0.383** | ***0.013*** | | | | |

| | | | Night ER: [x]/[CO] | | | Night ER: [x]/[Ethyne] | | | Method 1: OH-corr, Primary Only ER: [Δx]/[ΔCO] | | | | Method 2: O3-corr ER: [Δx]/[ΔCO] | | Method 3: OH corr, includes secondary ER: [Δx]/[ΔCO] | | | |
|---|---|---|---|---|---|---|---|---|---|---|---|---|---|---|---|---|---|---|
| **Line #** | **Measurement Identification** | **units:** | ***ppbv ppmv$^{-1}$*** | ***uncert.*** | ***fit (r)*** | ***ppbv ppmv$^{-1}$*** | ***uncert.*** | ***fit (r)*** | ***ppbv ppmv$^{-1}$*** | ***ER uncert.*** | ***VOC$_{bknd}$ (ppbv)*** | ***VOC$_{bknd}$ uncert.*** | ***ppbv ppmv$^{-1}$*** | ***1 sigma*** | ***ppbv ppmv$^{-1}$*** | ***1 sigma*** | ***VOC$_{bknd}$ (ppbv)*** | ***VOC$_{bknd}$ uncert.*** |
| | ***Aromatics*** | | | | | | | | | | | | | | | | | |
| 36 | Benzene | GC-MS | 1.11 | *0.023* | 0.93 | 0.246 | *0.007* | 0.88 | **1.08** | ***0.01*** | 0.09 | *0.00* | | | | | | |
| 37 | Benzene* | PTR-MS | 1.19 | *0.028* | 0.91 | 0.239 | *0.009* | 0.83 | **1.21** | ***0.01*** | 0.06 | *0.00* | | | | | | |
| 38 | Toluene | GC-MS | 3.02 | *0.080* | 0.90 | 0.645 | *0.025* | 0.81 | **3.48** | ***0.04*** | 0.00 | *0.00* | | | | | | |
| 39 | Toluene* | PTR-MS | 3.49 | *0.105* | 0.86 | 0.689 | *0.033* | 0.76 | **4.35** | ***0.05*** | 0.00 | *0.00* | | | | | | |
| 40 | Sum C8-Aromatics* | PTR-MS | 2.41 | *0.066* | 0.88 | 0.462 | *0.022* | 0.77 | **3.34** | ***0.03*** | 0.00 | *0.00* | | | | | | |
| 41 | Sum C9-Aromatics* | PTR-MS | 1.29 | *0.033* | 0.89 | 0.251 | *0.012* | 0.77 | **1.90** | ***0.02*** | 0.00 | *0.00* | | | | | | |
| | ***Nitrogen and Sulfur Organics*** | | | | | | | | | | | | | | | | | |
| 42 | Nitromethane | GC-MS | 0.218 | *0.009* | 0.79 | 0.050 | *0.002* | 0.78 | **0.22** | ***0.00*** | 0.02 | *0.00* | | | | | | |
| | ***Oxygenated VOCs, saturated (OVOC_sat)*** | | | | | | | | | | | | | | | | | |
| 43 | Acetaldehyde | GC-MS | 5.50 | *0.178* | 0.89 | 1.30 | *0.050* | 0.86 | | | | | | | **2.11** | ***0.25*** | **0.45** | ***0.02*** |
| 44 | Acetaldehyde* | PTR-MS | 18.7 | *0.646* | 0.82 | 3.35 | *0.169* | 0.74 | | | | | | | 14.96 | *0.49* | 0.82 | *0.04* |
| 45 | Octanal* | PTR-MS | 0.529 | *0.023* | 0.75 | 0.102 | *0.006* | 0.69 | **0.57** | ***0.01*** | **0.03** | ***0.00*** | | | | | | |
| 46 | Nonanal* | PTR-MS | 0.775 | *0.030* | 0.79 | 0.144 | *0.008* | 0.73 | **0.83** | ***0.01*** | **0.02** | ***0.00*** | | | | | | |
| 47 | Methanol | GC-MS | 17.2 | *0.816* | 0.75 | 3.55 | *0.219* | 0.65 | **16.40** | ***0.35*** | **1.94** | ***0.05*** | | | | | | |
| 48 | Methanol* | PTR-MS | 29.4 | *1.602* | 0.68 | 4.54 | *0.330* | 0.61 | 27.21 | *0.59* | 1.85 | *0.09* | | | | | | |
| 49 | Ethanol | GC-MS | 43.4 | *1.306* | 0.87 | 9.18 | *0.392* | 0.78 | **37.89** | ***0.68*** | **2.20** | ***0.10*** | | | | | | |
| 50 | Ethanol* | PTR-MS | 82.3 | *2.688* | 0.84 | 14.9 | *0.741* | 0.75 | 73.96 | *1.10* | 2.85 | *0.16* | | | | | | |
| 51 | iso-Propanol | GC-MS | 4.25 | *0.284* | 0.65 | 0.935 | *0.069* | 0.61 | **3.93** | ***0.29*** | **0.42** | ***0.04*** | | | | | | |
| 52 | Acetone | GC-MS | 20.2 | *0.982* | 0.74 | 4.73 | *0.235* | 0.73 | 18.27 | *0.65* | 2.88 | *0.10* | | | **10.41** | ***1.07*** | **2.52** | ***0.09*** |
| 53 | Sum Acetone+Propanal* | PTR-MS | 27.9 | *1.455* | 0.69 | 4.85 | *0.310* | 0.66 | 23.17 | *0.67* | 2.95 | *0.11* | | | 14.73 | *1.23* | 2.57 | *0.11* |
| 54 | 2-Butanone (MEK) | GC-MS | 1.45 | *0.048* | 0.85 | 0.319 | *0.013* | 0.79 | 1.50 | *0.06* | 0.16 | *0.01* | | | **0.55** | ***0.08*** | **0.10** | ***0.01*** |
| 55 | Methyl acetate | GC-MS | 0.634 | *0.029* | 0.76 | 0.142 | *0.007* | 0.72 | 0.61 | *0.02* | 0.07 | *0.00* | | | **0.39** | ***0.04*** | **0.06** | ***0.00*** |
| 56 | Ethyl acetate | GC-MS | | | | | | | | | | | | | | | | |
| | ***Oxygenated VOCs, usaturated (OVOC_unsat)*** | | | | | | | | | | | | | | | | | |
| 57 | Methacrolein (MACR) | GC-MS | 0.275 | *0.015* | 0.70 | 0.056 | *0.004* | 0.61 | | | | | | | | | | |
| 58 | Methylvinylketone (MVK) | GC-MS | 0.238 | *0.019* | 0.59 | 0.050 | *0.005* | 0.53 | | | | | | | | | | |
| 59 | Sum MVK+MACR* | PTR-MS | 1.42 | *0.074* | 0.69 | 0.218 | *0.013* | 0.68 | | | | | | | | | | |
| 60 | Furan* | PTR-MS | 0.349 | *0.011* | 0.84 | 0.065 | *0.003* | 0.75 | 0.41 | *0.01* | 0.00 | *0.00* | | | **0.26** | ***0.02*** | **0.02** | ***0.00*** |
| 61 | Methylfurans* | PTR-MS | 0.647 | *0.031* | 0.73 | 0.102 | *0.007* | 0.65 | 0.68 | *0.01* | 0.00 | *0.00* | | | **0.31** | ***0.04*** | **0.03** | ***0.00*** |
| 62 | C5H4O2* | PTR-MS | 0.376 | *0.018* | 0.73 | 0.064 | *0.004* | 0.67 | 0.49 | *0.01* | 0.00 | *0.00* | | | **0.37** | ***0.01*** | **0.02** | ***0.00*** |
| 63 | D5-Siloxane* | PTR-MS | 0.291 | *0.013* | 0.74 | 0.053 | *0.004* | 0.65 | **0.30** | ***0.01*** | **0.00** | ***0.00*** | | | | | | |
| 64 | Texanol* | PTR-MS | 0.328 | *0.016* | 0.72 | 0.064 | *0.004* | 0.64 | **0.38** | ***0.01*** | **0.01** | ***0.00*** | | | | | | |
| | ***Halocarbons*** | | | | | | | | | | | | | | | | | |
| 65 | PCBTF* | PTR-MS | 0.631 | *0.0323* | 0.70 | 0.112 | *0.0063* | 0.70 | **0.48** | ***0.02*** | **0.02** | ***0.00*** | | | | | | |
| 66 | CH2Cl_CH2Cl | GC-MS | 0.036 | *0.0025* | 0.83 | 0.009 | *0.0007* | 0.78 | | | | | | | | | | |
| | ***Methane and Inorganic Carbon*** | | | | | | | | | | | | | | | | | |
| 67 | Methane (CH4) | NOAA | 937 | *45* | 0.71 | 186 | *12.263* | 0.63 | | | | | | | | | | |
| 68 | Carbon dioxide (CO2) | NOAA | 161723 | *6342* | 0.77 | 32286 | *1887* | 0.68 | | | | | | | | | | |
| | ***Inorganic Nitrogen*** | | | | | | | | | | | | | | | | | |
| 69 | Nitrogen dioxide (NO2) | NOAA | 69.1 | *1.877* | 0.87 | 14.7 | *0.638* | 0.78 | | | | | | | | | | |
| 70 | Nitrogen oxides (NOx) | NOAA | 70.0 | *2.265* | 0.84 | 15.1 | *0.797* | 0.72 | | | | | | | | | | |